CHEMICAL REVIEWS

pubs.acs.org/CR

Review

Bioprinting: From Tissue and Organ Development to *in Vitro* Models

Carlos Mota,* Sandra Camarero-Espinosa, Matthew B. Baker, Paul Wieringa, and Lorenzo Moroni*

Cite This: *Chem. Rev.* 2020, 120, 11032–11092

Read Online

ACCESS | Metrics & More | Article Recommendations

ABSTRACT: Bioprinting techniques have been flourishing in the field of biofabrication with pronounced and exponential developments in the past years. Novel biomaterial inks used for the formation of bioinks have been developed, allowing the manufacturing of *in vitro* models and implants tested preclinically with a certain degree of success. Furthermore, incredible advances in cell biology, namely, in pluripotent stem cells, have also contributed to the latest milestones where more relevant tissues or organ-like constructs with a certain degree of functionality can already be obtained. These incredible strides have been possible with a multitude of multidisciplinary teams around the world, working to make bioprinted tissues and organs more relevant and functional. Yet, there is still a long way to go until these biofabricated constructs will be able to reach the clinics. In this review, we summarize the main bioprinting activities linking them to tissue and organ development and physiology. Most bioprinting approaches focus on mimicking fully matured tissues. Future bioprinting strategies might pursue earlier developmental stages of tissues and organs. The continuous convergence of the experts in the fields of material sciences, cell biology, engineering, and many other disciplines will gradually allow us to overcome the barriers identified on the demanding path toward manufacturing and adoption of tissue and organ replacements.

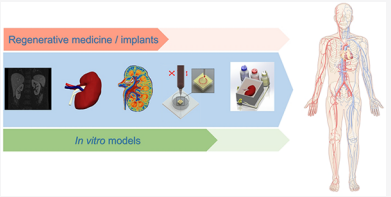

CONTENTS

Special Issue: 3D Printing for Biomaterials

Received: December 8, 2019
Published: May 14, 2020

https://dx.doi.org/10.1021/acs.chemrev.9b00789
Chem. Rev. 2020, 120, 11032–11092

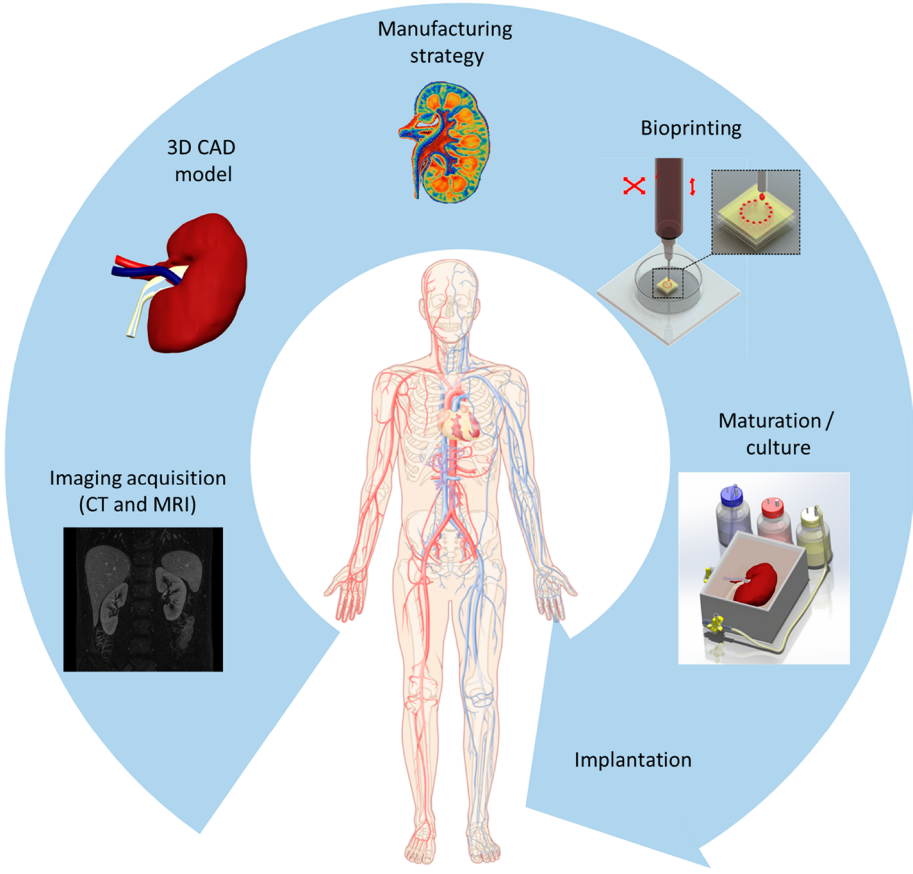

Figure 1. Schematic representation of the steps necessary to produce bioprinted tissues and organ-like constructs.

1. INTRODUCTION

With the advent of tissue engineering and regenerative medicine (TERM), new therapeutic approaches for the regeneration or replacement of tissues and organs have been investigated over the past decades.[1−3]

Biomaterials (naturally derived or synthetic)[4−7] and suitable stem cells[8−10] hold great potential to be used to regenerate or repair and, eventually, as a suitable replacement for tissues and organs. Despite the increasing complexity of the tissue and organ units developed so far, either generating acellular or cellular constructs, an insufficient degree of functionality is achieved when evaluated *in vitro* and ultimately *in vivo*. Novel approaches aim to mimic to a certain extent the embryonically developed counterparts but still fall short on the degree of complexity that can be achieved.

All organs arise from the three germ layers—ectoderm, endoderm, and mesoderm—that we briefly discuss below to guide the reader throughout the complexity of the different tissues and organs. We will cover the spatiotemporal arrangement and cellular organization of these layers, termed gastrulation, and highlight their extreme complexity that is still not totally understood. The complexity of several organs and tissues is dictated not only by different specialized cells but also by a complex and dynamic extracellular matrix (ECM) composition. For example, in the case of the kidney, more than 20 differentiated cell types are harbored to a complex ECM composed of proteins, glycoproteins, and glycosaminoglycans (GAGs). Stem cells could facilitate the generation of the different cells required if properly maintained in culture and expanded in a large scale. Both human embryonic and induced pluripotent stem cells (iPSCs), in particular, have the potential to fit this purpose. Pluripotent stem cells (PSCs) have an indefinite self-renewal ability and plasticity, which allow *in vitro* generation of an unlimited number of distinct cell types. PSCs have thus opened new avenues for TERM.

In this review, we highlight the bioprinting of tissue and organ units to achieve regenerative alternatives. We briefly describe the most commonly used bioprinting techniques and biomaterials. Furthermore, we cover the importance of understanding tissue and organ development in order to obtain representative *in vitro* models. This understanding can facilitate the development of future approaches, which can help in building functional organ units and pave the way for full organ bioprinting. After briefly introducing PSCs, we present the general steps in embryonic development and tissue morphogenesis. We elaborate on the current state-of-the-art in tissue and organ bioprinting, with a particular attention to the skin, nervous system, cartilage, bone, blood vessels, heart, kidney, liver, pancreas, glands, cornea, and muscle. In doing so, we will discuss the cell source used and the maturity of the bioprinted constructs achieved.

https://dx.doi.org/10.1021/acs.chemrev.9b00789
Chem. Rev. 2020, 120, 11032−11092

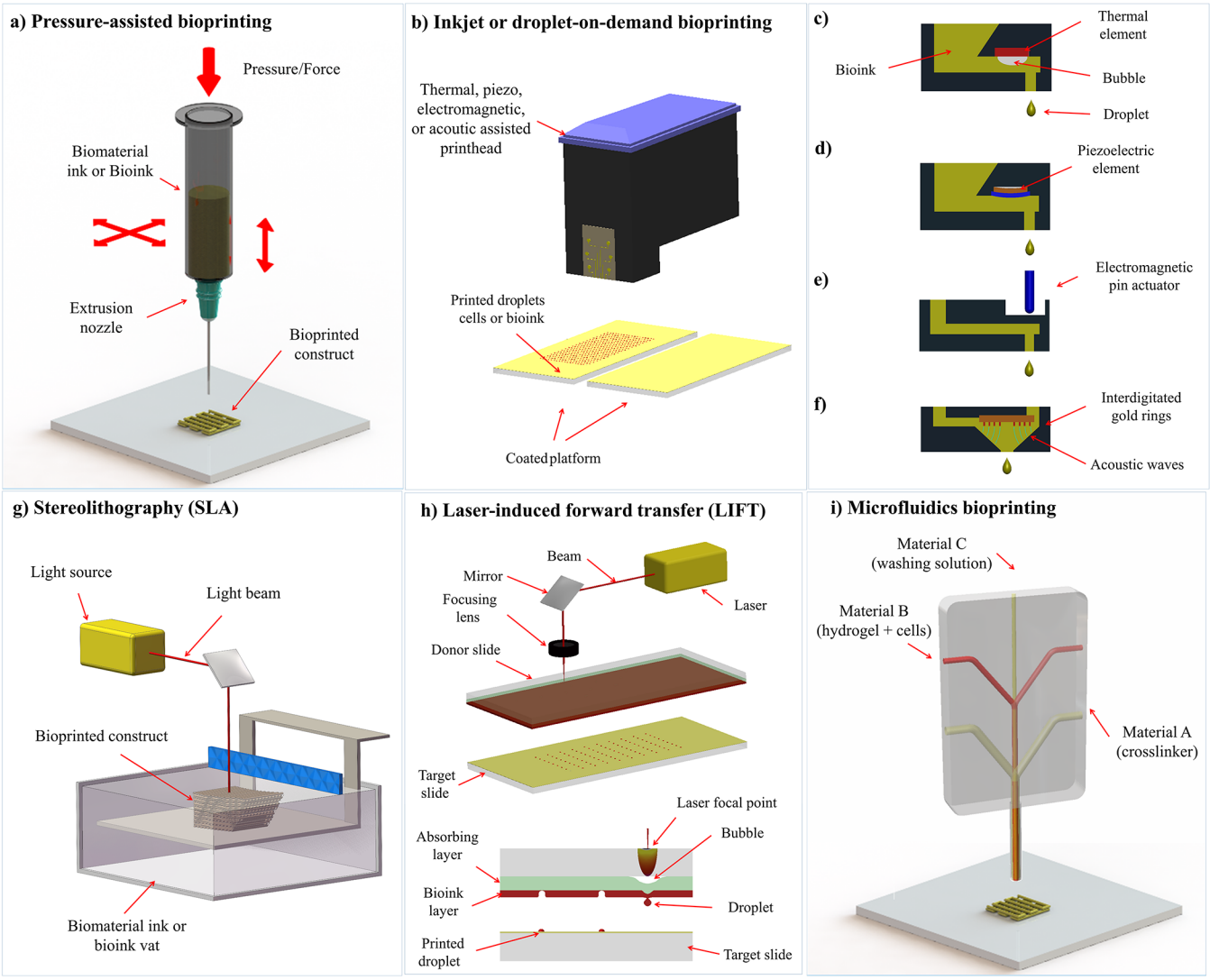

Figure 2. Schematics of the bioprinting techniques commonly used to produce tissue and organ constructs: (a) pressure-assisted; (b) inkjet or droplet-on-demand where droplets are formed by (c) thermal, (d) piezo, (e) electromagnetic, or (f) acoustic waves; (g) stereolithography; (h) laser-induced forward transfer; and (i) microfluidic bioprinting. Adapted with permission from refs 12 and 24. Copyrights 2015 Elsevier Inc. and 2012 John Wiley & Sons, Ltd.

2. BIOPRINTING

Bioprinting is a group of additive manufacturing (AM) technologies that allow the selective distribution of cells, biomaterials, growth factors, or combinations thereof, to manufacture living tissues and organs in three dimensions.[11] Bioprinting encompasses the fabrication of both acellular constructs characterized by hierarchical structural properties or smart surface properties that can steer cell activity and cell-laden biological constructs.[11] For bioprinting, the process workflow typically starts from the data acquisition of magnetic resonance imaging (MRI) or computed tomography (CT) scans of the affected tissue or organ to be manufactured (Figure 1). These medical image data sets provide essential information about the macrostructure of tissues and organs, but information at the microstructure or even at a cellular level is still not possible with these techniques. Alternatively, advanced microscopy (fluorescent, confocal, or two-photon) could provide further detail at the cellular level; however, the structures that can be imaged are normally limited in size, and primary tissue needs to be sacrificed. Currently, MRI or CT data sets are mainly used to design the overall volume to be manufactured, while the information about the infill is normally designed through open-source or proprietary bioprinter software. This is still a limiting factor for more innovative bioprinting strategies, hence the true power of the technology is yet to be unveiled.

Over the past decade, several bioprinting technologies have been developed and adapted to manufacture tissues or organs by selectively dispensing cells, hydrogels, or combinations of these. These technologies are classified in several groups where the nomenclature is normally associated with the mechanism behind the bioprinting technique. The most predominant class of bioprinting techniques is pressure-assisted systems, as these are available at low costs. Other systems such as piezo-, thermal-, laser-, acoustic, and microfluidic-driven bioprinting are less popular due to their relatively higher cost. Here, we briefly review these systems, while we refer readers to other recent reviews for a more comprehensive report of bioprinting technologies.[12−21]

https://dx.doi.org/10.1021/acs.chemrev.9b00789
Chem. Rev. 2020, 120, 11032−11092

2.1. Pressure-Assisted Bioprinting

Pressure-assisted systems are largely used among different research groups working on bioprinting as more and more low-cost systems are becoming commercially available.[22,23] These systems are normally equipped with one or more cartridges that allow the dispensing of different combinations of cells and biomaterials.[23] Plastic or glass cartridges are filled with the selected biomaterial inks or bioinks. By applying gas pressure, the material is ejected in the form of a filament through a needle or nozzle (Figure 2a). In this case, the type of material, the gas pressure, nozzle diameter, and deposition speed normally define the resolution. High resolution is difficult to achieve as the shear stress increases with decreasing nozzle diameter, which usually affects cell viability. The average strand diameter produced with these systems varies from 200 μm to millimeter size.

2.2. Thermal-Assisted Bioprinting

The first bioprinting studies reported in the literature were performed with thermal-assisted bioprinting where an office inkjet printer was modified to allow the dispensing of cells and biomaterials (Figure 2b,c).[25,26] In this droplet-on-demand (DOD) technology, an electrical element is used to generate heat that vaporizes the material near the element, forming a droplet (Figure 2c). This vaporization induces a sudden expansion of the material in a small capillary channel, prompting the formation and ejection of the droplet of material. The application of heat influences cell viability during and post bioprinting. Another disadvantage of this technique is the limited range of viscosities that can be processed. Furthermore, when cells are included, sedimentation and nozzle clogging are also observed.[27] The resolution of thermal bioprinting is generally related to the volume ejected from each nozzle and varies from the picoliter to nanoliter range, with a resolution as low as 100 μm for bioprinted strands containing cells.

2.3. Piezo-Assisted Bioprinting

Piezoelectric materials normally change shape or size when stimulated electrically. The piezo-assisted bioprinting technique uses piezoelectric elements that upon deformation induce the ejection of small volumes of materials in a droplet form (Figure 2d). Similar to thermal-assisted bioprinting, it is possible to dispense droplets of picoliter to nanoliter volumes. With the capability of dispensing very accurately nanoliter to picoliter droplets, this bioprinting technique is normally used for the fabrication of microarrays and similar screening platforms and was used recently to deposit glia and retinal ganglion cells without influencing cell viability.[28] Other systems such as the ones based on electromagnetic actuators have also been used for bioprinting (Figure 2e). In these systems, the displacement of a mechanical element induces the droplet formation, and this element can be actuated in direct contact with the bioink or indirectly with the deformation of an elastomeric membrane.

2.4. Acoustic Bioprinting

One of the few nozzle-free techniques is acoustic bioprinting, where acoustic waves are applied to a liquid to generate the ejection of a droplet (Figure 2f). This technique allows accurate dispensing of individual cells encapsulated in picoliter droplets.[29] Acoustic waves or acoustic tweezers have been used to organize cells accurately in specific configurations and even deposit cells on top of previously positioned cells.[30] The speed of displacement is relatively slow, and further improvements are necessary to position the large amounts of cells that compose a tissue. Accurate control to position the cells might be possible with acoustic wave technologies, but the application of these to produce 3D constructs is yet to be achieved.

2.5. Magnetic-Assisted Bioprinting

The application of permanent magnets or Bitter electromagnets to create magnetic fields has been extensively used for the patterning of cells in controlled arrays or locations where the magnetic field is stronger. For the control of the cells or cell spheroids through the application of magnetic fields, a previous labeling of cells with magnetic nanoparticles or the application of paramagnetic fluids is required. With magnetic-assisted biofabrication assembly, it is already possible to create 3D structures[31] or single-cell patterning[32] (according to the method and magnetic field used). As these technologies mature, a similar approach could be envisioned by the combination of magnetic fields to pattern cells during a bioprinting process or postbioprinting. This is still not investigated, but it could open the possibility to control cells throughout the bioprinting process and even promote the possibility of post manufacturing stimulation (e.g., by applying magnetic fields to control stem cell fate[33]).

2.6. Light-Assisted Bioprinting

Some of the initial systems based on light-assisted bioprinting are also termed as stereolithography (SLA). Within SLA techniques, two distinctive types are used: laser or light source systems such as digital light processing (DLP).[12,34] The laser systems induce selective cross-linking of a photosensitive material point by point (Figure 2g), while DLP systems use a dynamic mirror array that selectively projects light into areas to cross-link all points assigned for each layer. Several other light-based systems have been developed by, for instance, combining pressure-based bioprinting with light-emitting diodes (LEDs) that cross-link the material upon extrusion.[35]

Other laser-assisted bioprinting systems are used to selectively dispense bioinks similar to DOD instead of selectively cross-linking materials. These laser techniques are termed laser-induced forward transfer (LIFT) where a fast-pulse laser beam is focused on a point of a glass slide previously coated with an absorbed layer that vaporizes and induces a droplet formation (Figure 2h). The absorption layer also contains a layer of cell-laden hydrogels.[36] The bioink droplet that is formed is ejected toward a collection glass slide previously coated with a hydrogel layer to minimize impact. The bioprinted construct is formed by the deposition of droplets with predesigned patterns layer-by-layer until the 3D construct is obtained. Laser-assisted bioprinting is another nozzle-free technique, which avoids shear stress on cells normally observed in other techniques.

Two-photon polymerization (2PP) is also a light-assisted bioprinting technique that allows a high-accuracy cross-linking by selectively irradiating a voxel.[37] 2PP systems cross-link the voxels of interest successively until a 3D structure is obtained. Due to the high resolutions possible with 2PP, the build time is rather long, and the size of the constructs normally obtained ranges between a few hundreds of microns to a few millimeters. 2PP has been mainly used to produce 3D scaffolds that are postseeded with cells, and only recent studies report cells directly embedded in the resin.[38]

New SLA systems, also termed volumetric SLA, are capable of cross-linking in a fast way a volume or 3D object by combining the rotation of a resin vat and a DLP projector or laser light source that selectively projects light in a synchronized way.[39,40] This technique has been recently used to demonstrate the capabilities of this new approach to produce bioprinted

https://dx.doi.org/10.1021/acs.chemrev.9b00789
Chem. Rev. 2020, 120, 11032−11092

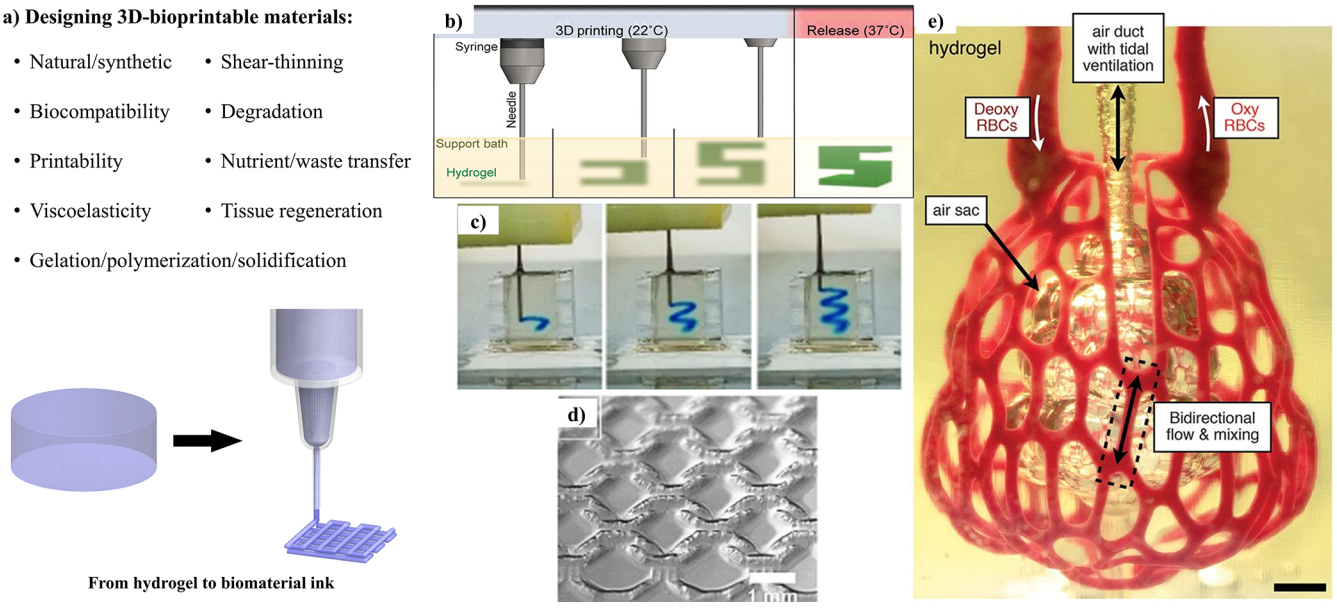

Figure 3. New material development and advanced strategies can lead to breakthroughs in bioprinting of complex organ and tissue constructs. (a) Bioink development requires moving from hydrogels to bioinks with a number of requirements for successful organ formation. Gel in gel printing techniques like (b) FRESH and (c) jammed microgels allow the free-form printing of softer gels into more complex structures. (d) New developments in multitechnique hydrogels like thiol−ene gelatin expand the ink toolbox significantly. (e) Large-scale complex manufacturing of organ-like objects is possible with advances in light-polymerization techniques. Adapted with permission for refs 51−53 and 55. Copyrights 2015 Hinton et al. (published by The American Association for the Advancement of Science), 2018 Highley et al. (published by WILEY-VCH Verlag GmbH & Co. KGaA), 2019 Grigoryan et al. (published by The American Association for the Advancement of Science), and 2017 WILEY-VCH Verlag GmbH & Co. KGaA.

Table 1. Examples of Natural and Synthetic Polymers and Materials Used for Bioprinting

material class	polymer/material	common name	techniques	bioink use	ref
	Thermoplastic polymers				
poly(esters)	poly(caprolactone)	PCL	FDM, SLS	N	69−71
	poly(lactic acid)	PLA	FDM	N	72
	poly(lactic-*co*-glycolic acid)	PLGA	FDM	N	73
	poly(ethylene oxide terephthalate-*co*-butylene terephthalate)	PEO/PBT polyactive	FDM	N	74
poly(urethanes)	thermoplastic poly(urethane)	PU, TPU	FDM	N	75
	Hydrogels				
synthetic	poly(ethylene oxide-*co*-propylene oxide)	pluronic	extrusion	Y	76
	poly(vinyl alcohol)	PVA	extrusion		77, 78
	self-assembling peptides		extrusion	Y	79, 80
	poly-*N*-isopropylacrylamide	NIPAM	extrusion, DLP	Y	81
natural	alginate		extrusion, jet	Y	82
	hyaluronic acid	HA	extrusion, jet	Y	83
	decellularized extracellular matrix	dECM	extrusion	Y	84
	gelatin		extrusion, DLP, jet	Y	85
	agarose			Y/N	86, 87
	nanocellulose			Y	88
	Resins				
UV cross-linking	poly(ester) acrylates		DLP, 2PP, extrusion	N	89
	gelatin methacrylate	GelMA	2PP, extrusion	Y	90
	poly(ethylene glycol) (meth)acrylate	PEGDA, PEGMA	2PP, DLP, extrusion	Y	91
	poly(carbonate) acrylates		2PP, DLP	N	92
	Composites				
composite additives	nanocellulose		extrusion	Y	93
	bioglass		extrusion	N	94
	hydroxyapatite	HAp	extrusion/SLA	Y	95
	graphene oxide, reduced graphene oxide	GO, rGO	extrusion, DLP	Y	96
	carbon nanotubes		extrusion	Y	97

https://dx.doi.org/10.1021/acs.chemrev.9b00789
Chem. Rev. 2020, 120, 11032−11092

constructs by including cells within the liquid resin that was cross-linked with a total light exposure time below 1 min.[39] While this technique allows a faster volume manufacturing, no control of the cell spatial distribution can be achieved so far.

2.7. Microfluidics Bioprinting

Microfluidics is a long-established technology initiated in the 50's[41,42] that has been widely adopted by several fields, in particular by TERM, where cells and biomaterials can be cultured in highly defined and controlled conditions.[43] The possibility to control accurately fluid flow ensuring laminar regimes has allowed researchers to investigate cellular environments with high accuracy while reducing the volume of reagents necessary. Lately, bioprinting has adapted microfluidics chip concepts as dispensing heads (Figure 2i). With this, it has been possible to design new types of bioprinting systems that allow accurate processing and dispensing of low viscosity materials combined with cells.[44−47] One of the advantages of microfluidics bioprinting is that it is based on well-established technology, and the development of different heads is simple. Furthermore, creating disposable microfluidic print heads is possible by preparing the printing chambers with polydimethylsiloxane (PDMS). Some commercially available bioprinters have already adopted microfluidic dispensing technology.[48,49]

3. BIOMATERIALS, BIOMATERIAL INKS, AND BIOINKS

One of the initial limiting factors of bioprinting was the availability of suitable biomaterials to be used as inks (biomaterials only) or bioinks (biomaterials with cells).[50] These biomaterials have to be selected, designed, and prepared according to the chosen bioprinting technique and the target tissue or organ (Figure 3a). New techniques including supporting baths like FRESH[51] and jammed microgels[52] (Figure 3b and 3c) have expanded the printability of soft bioinks, while broadly usable ink platforms[53] (Figure 3d) expand the generality of fabrication bioinks. Recent technological breakthroughs like FRESH[54] and SLATE[55] (Figure 3e) allow the bioprinting of complex organ-like structures. Numerous natural and synthetic biomaterials, discussed below, have been explored. Despite the large number of hydrogel formulations for bioprinting, it is still difficult to generate the optimal material that is both printable and capable of mimicking the cell microenvironment. Here, we briefly summarize the most commonly used natural and synthetic polymers, while we encourage the readers to refer to recent exhaustive reports on materials for bioprinting.[17,50,56−59]

The materials used in bioprinting can be broken down into thermoplastic polymers, hydrogels, light cross-linkable resins, and composites (Table 1). While AM of thermoplastic polymers and ultraviolet (UV) cross-linkable resins have a longer history and mainly have been used to build scaffolds that are seeded with cells post manufacturing, the bioprinting of hydrogels and composites where cells are directly included in the manufacturing process has a more recent emergence. Each material class has separate requirements for the various 3D bioprinting techniques (i.e., a gel for extrusion printing and a gel for DLP printing have different requirements) and is beyond the scope of this review; consequently, a brief overview of the classes of materials will be given here. More comprehensive reviews can be found for bioprinting materials, in general,[13,14,60] for hydrogels[61−63] and composites.[64] For technique-specific material requirements, SLA,[65] extrusion based bioprinting,[66] selective laser sintering (SLS),[12,67] 2PP,[68] and inkjet or droplet-on-demand[18,66] have also been reviewed.

3.1. Thermoplastic Polymers

The application of hybrid approaches where hybrid AM/bioprinting systems are used to manufacture a thermoplastic scaffold in combination with less mechanically stable bioinks has been explored for skeletal and in some cases organ constructs.[70,71,84] These scaffolds are manufactured utilizing more classic methods of AM such as fused deposition modeling (FDM) or SLS. In these multitechnique manufacturing systems, the combination of both techniques is possible, although the selection of thermoplastic polymers is limited to materials with low melting temperatures. In general, most thermoplastic polymers are melted at elevated temperature and extruded through a nozzle, and upon cooling, chain entanglement and polymer crystallization combine to create the 3D defined solid polymer construct. Thermoplastic polymers for complex tissue fabrication must perform both during fabrication [melting, extrusion, solidification] and during tissue regeneration [biocompatibility, degradation, tissue ingrowth]. Widely used thermoplastic polymers for AM are limited to poly(esters), poly(urethanes), and various copolymers based on these small libraries.

Current materials-based research in this area focuses around two main efforts. On one hand, the optimization of the printability of commercial polymers,[98] uniquely structured copolymers, and blends can extend the application of currently known polymer classes. On the other hand, the polymer library is also being expanded into new backbones, like poly(ester amides),[99] to provide new classes of materials for thermoplastic printing.

3.2. Hydrogels

The use of hydrogels in bioprinting, slow to make progress at first, has emerged as an energetic area of research in the past five years. Hydrogels are ideal materials for cell culture and encapsulation, yet their softer mechanical properties and hydrated state provide challenges for translation to high fidelity printed constructs; this notable trade-off is well-known to the community.[62] The first uses of hydrogels in bioprinting were agarose or collagen being used as a "3D paper" or support in which to print 3D cell spheroids[100,101] and poly(ethylene glycol) (PEG) diacrylate (PEGDA) to print cell-encapsulated gels via SLA.[102] Currently, the Ca^{2+}-induced gelation of alginate has become one of the most widely used bioinks in 3D printing, with photopolymerizable gels (resins, see below) like gelatin methacrylate (GelMa) and PEGDA also being popular choices.

Despite these added challenges of fabricating with soft materials, hydrogels provide an excellent scaffold for stimuli responsiveness, integration of complex biochemical/biomechanical signals, and recapitulation of the soft tissue's natural environment. Recently, numerous bioprintable hydrogels have emerged in the literature, each with decided benefits and features, with a trend toward multifunctional systems. On one hand, (modified) natural polymers like alginate,[35,103] chitosan,[104] hyaluronic acid (HA),[105,106] and gelatin[53,107] have shown good printability, yet limited tailorability. Synthetic hydrogels like poly(glicidol)[108] and PEG[109] have excellent chemical and mechanical tailorability, yet often require significant optimization to print. The chemical modification of naturally occurring polymers (e.g., HA, alginate, gelatin) to produce hydrogels, which a chemist can tailor, has provided a powerful approach to overcome the limitations of the synthetic vs natural dichotomy. The recent trend toward creating multicomponent inks (often from combinations of synthetic/

https://dx.doi.org/10.1021/acs.chemrev.9b00789
Chem. Rev. 2020, 120, 11032−11092

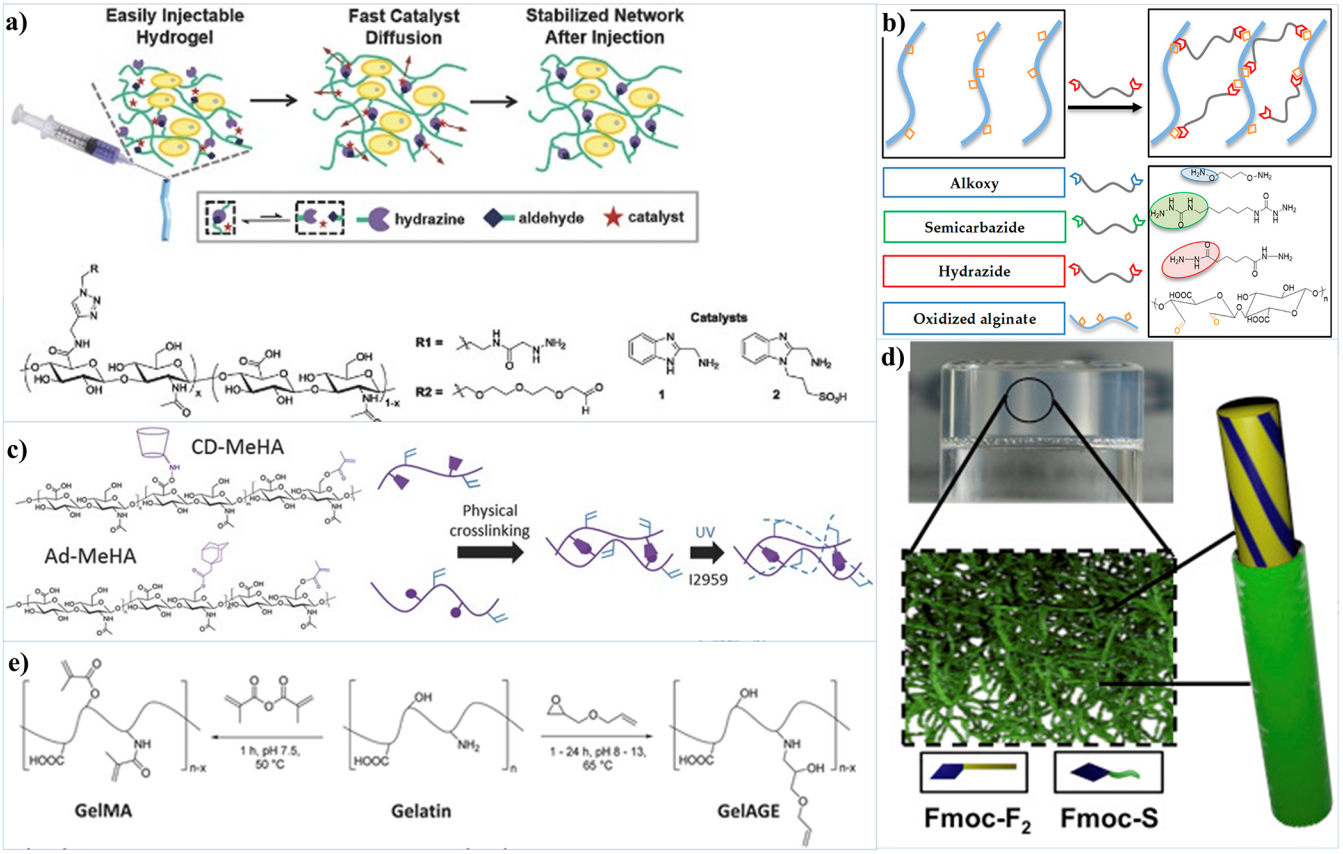

Figure 4. Recent trends in materials development, including dynamic and reversibly cross-linked systems like (a), (b) dynamic covalent systems and (c), (d) supramolecular hydrogels and (e) advanced cross-linking strategies. Adapted with permission from refs 53, 80, 103, 105, and 127. Copyrights 2017 WILEY-VCH Verlag GmbH & Co. KGaA, 2016 Elsevier Inc., 2015 WILEY-VCH Verlag GmbH & Co. KGaA, 2018 Hafeez et al. (published by MDPI AG), and 2018 WILEY-VCH Verlag GmbH & Co. KGaA.

natural/modified materials) attempts to circumvent some limitations of individual compositions. The native ECM relies on complex networks for function and may be a good design principle moving forward; however, many of these new multicomponent ink studies are combinatorial and empirical, with few systems being rationally designed or generating widely usable concepts.

Hydrogels generally require a cross-linking step post or during bioprinting and can rely on light polymerization (akin to a resin) and ionic cross-linking; however, self-healing and shear-thinning hydrogels have also emerged which do not need a subsequent cross-linking step.[103,105,110] Cross-linking and the biofunctionalization of hydrogels via new reactions have been a recent flourishing area of research with novel strategies like thiol−ene,[35,53,108,111] supramolecular,[105,112] light-responsive,[113] and dynamic covalent[72,103,111] chemistry all being leveraged to create new hydrogels with decided benefits in tailorability and functionality over their parent materials.

3.3. Resins

The class of biomaterial inks that can be cross-linked with light and used with SLA, DLP, and 2PP techniques are commonly termed as resins. Light cross-linkable resins are a widely used class of polymers for the creation of 3D constructs for biofabrication and span from hard thermoset-like materials to soft and hydrated hydrogels. Since they are such a widely used class of materials for biofabrication, they are reviewed separately in this section—the overlap with photopolymerizable hydrogels (see above) should be apparent and appreciated. Such resins traditionally form a 3D network upon irradiation with sufficient UV light, via induced photochemical polymerization. Within this area, (meth)acrylate resins have been the most widely used chemistry, including GelMA and PEG methacrylate (PEGMA) for printing of hydrogels and poly(ester) acrylates for printing of thermosets. However, any light-initiated polymerization or cross-linking is amenable. As recent examples, DLP resins allow large-scale fabrication, and light-induced thiol−ene resins,[35,53,108] poly(ester) urethane acrylates,[114] and poly(propylene fumarate) resins[115,116] have emerged as versatile and promising strategies. UV cross-linkable resins have a wide range of properties, as their formulations can be optimized with respect to the type of UV-polymerizable monomers (or macromers), network density, photoinitiator, and secondary cross-linking steps taking the ultimate form of a cross-linked polymer networks ranging from soft hydrated hydrogels to high performance resins.

A more recent trend within light-polymerizable materials is the use of visible light for the fabrication. The use of visible-light photoinitiators like Eosin Y[117] and ruthenium redox couples[118] allows fabrication to be performed with lower-energy light sources, minimizing the harmful effects of UV light. While UV light is traditionally cytotoxic and mutagenic, recent proteome-wide studies show that cells in the presence of some UV-cross-linkable materials show no discernible damage to their proteome.[119]

https://dx.doi.org/10.1021/acs.chemrev.9b00789
Chem. Rev. 2020, 120, 11032−11092

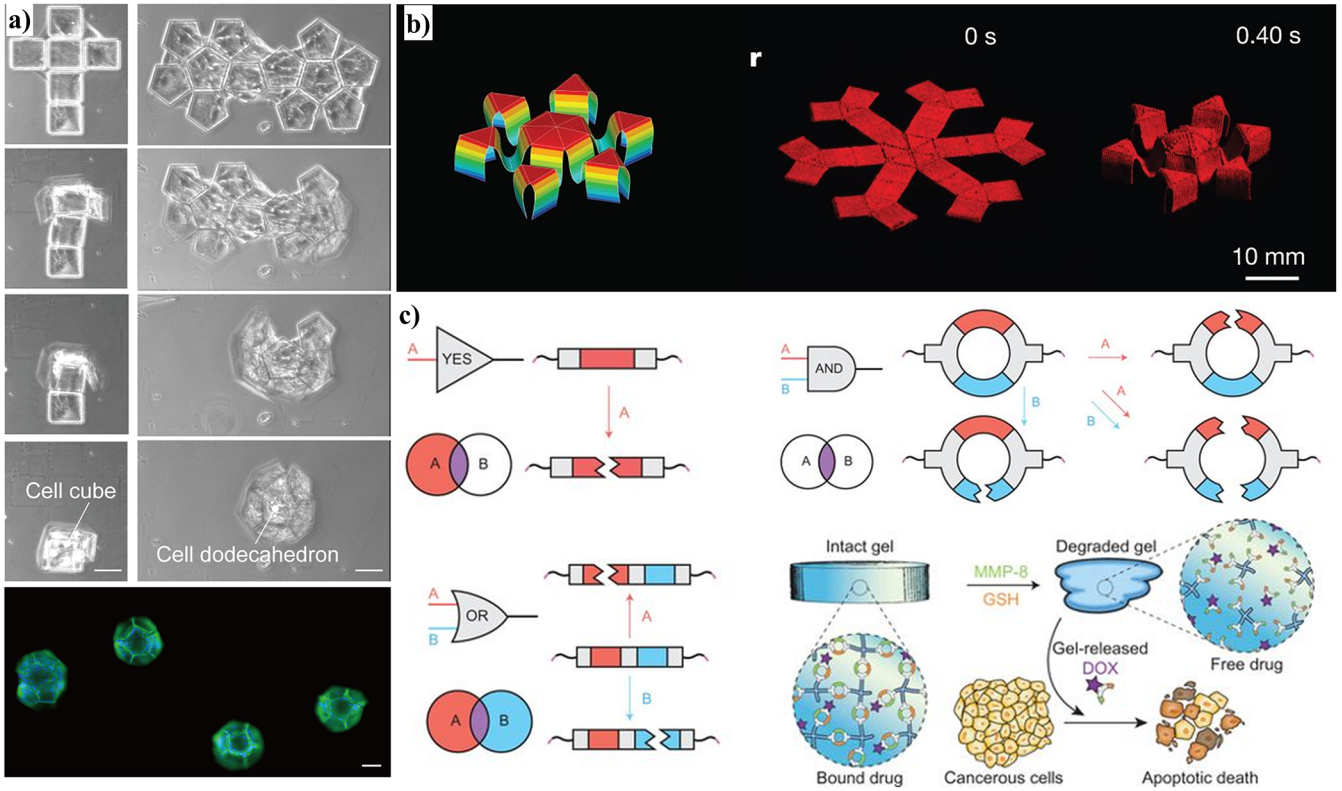

Figure 5. Future direction of bioprinted constructs where the materials can morph and change shape in response to (a) cellular forces or (b) external stimuli such as magnetic fields and (c) the development of complex stimuli-responsive materials, like logic gate systems. Adapted with permission from refs 133, 140, and 141. Copyright 2012 Kuribayashi-Shigetomi et al. (published by Public Library of Science), 2018 Springer Nature.

3.4. Composites

Composite bioprinting comprises the blending of a polymeric matrix and particulate reinforcements for added mechanical strength and/or functionality.[64,120] These blends combine the processability of the polymeric matrix with the mechanical or chemical identity of the particulate matter. For TERM application, the most common example is the use of calcium phosphate or ceramics combined with thermoplastic polymers for 3D extrusion printing.[94,95] The polymeric matrix enables the processability of the composite, while the calcium phosphate provides the instructive biochemical cues for enhanced bone formation.[121] While tricalcium phosphate and hydroxyapatite (HAp) have largely dominated the composite bioprinting, graphene oxide,[96] carbon nanotubes,[97] nanocellulose,[93,122] iron oxide nanoparticles,[123] alumina platelets,[124] and silver nanoparticles[125] have all been explored in conjunction with solid polymers and hydrogels alike.

3.5. Current Trends and Next-Generation Biomaterials

Current and future developments on bioprintable materials focus on two main areas: (1) chemical complexity and biomimicry and (2) stimuli-responsive and dynamic materials. While many studies are beginning to blend the areas above, complexity and tailorability in materials for biofabrication will inevitably lead to greater use and adoption of this technique across laboratories and into the marketplace. A single material that can address all the challenges associated with fabricating living tissue appears unlikely, in light of the fact that our own body uses a palette of materials and their blending for hierarchical material formation. Future research should focus on the combinations of systems to recapitulate this instructive, responsive, and dynamic natural environment.

Traditionally, materials for bioprinting have been poorly tailorable, with biocompatibility being achieved via nonspecific protein absorption or nonspecific covalent conjugation, mechanical properties via concentration or molecular weight, and little chemical space for material diversity. Across the different materials classes, at large, there are significant movements to create biomaterial platforms which can be easily tailored with respect to the introduction of chemical functionality. Examples include functionalizable DLP resins[115] and hydrogels (Figure 4e)[53] and gels for extrusion,[35,103] with click-type reactions coming to the forefront for bioconjugation strategies.[126]

Furthermore, chemical complexity is still introduced into the range of polymers that are 3D printable. Notably, few hydrogels are widely bioprintable, thus hydrogel ink and bioink formulations are becoming extremely active areas of research.[114] Within hydrogels, novel cross-linking strategies and materials formulations including supramolecular (Figure 4c and 4d),[105,112,120] dynamic covalent (Figure 4a and 4b),[103,111] jammed microgels,[52] and gel-in-gel[51] have emerged as promising areas of research, often imparting improved printabilty and dynamic responsiveness of the gels (Figure 4). DLP printing suffers from a lack of biodegradable and biocompatible resins for bioprinting; this gap is starting to be addressed by several research groups[115,116] and promises to be an active area of research in the near future.

A second major effort within biopriting is the movement toward stimuli-reponsive and dynamic materials for fabrication. Stimuli-responsive materials are often summated in the moniker

https://dx.doi.org/10.1021/acs.chemrev.9b00789
Chem. Rev. 2020, 120, 11032−11092

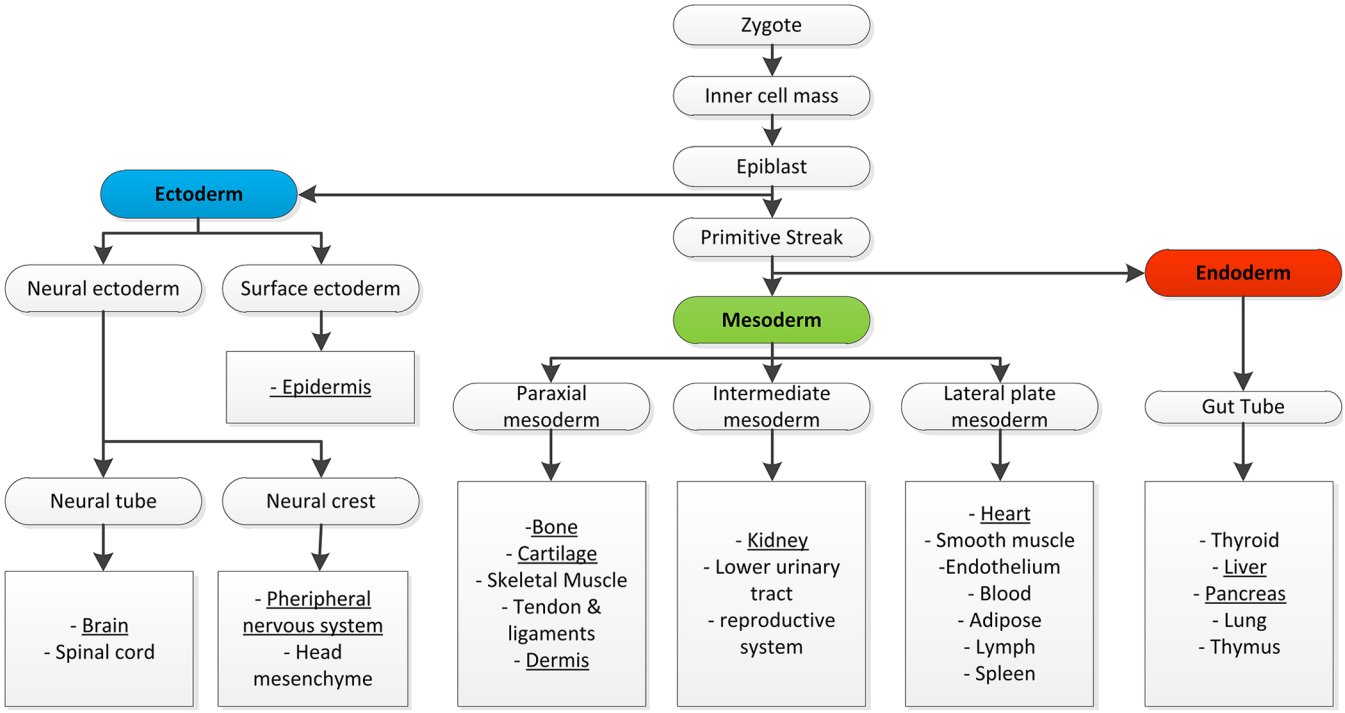

Figure 6. Ontology tree of the embryonic development presenting the three germ layers and an overview of some organ/tissue development for each layer. Organs or tissues that have been a topic of bioprinting research and covered in this review are underlined. Adapted with permission from ref 168. Copyright 2013 Edgar et al. (published by Public Library of Science).

4D printing,[20,128] yet the idea that 3D-fabricated constructs can change over time has become predominant. Stimuli responsiveness with respect to enzymatic activity,[110] temperature,[129] pH,[130] and magnetic fields (Figure 5b)[131] has been demonstrated, while complex mechanisms and feedback loops can be extrapolated from current generation biomaterial developments like cell-responsive elements (Figure 5a),[132] logic gates (Figure 5c),[133] and out-of-equilibrium materials.[134] In addition, dynamic hydrogels as cell culture environments have seen vigorous investigation over the past few years,[135,136] with some dynamic inks moving into bioprinting.[103,105,137] With the extensive work done within dynamic covalent and supramolecular biomaterials,[138] this remains a rich area for bioprinting materials development.

Finally, a current trend toward more complex bioprinting materials and combinations of techniques and materials is more recently occurring.[139] These complex techniques need not be complicated, but via the smart combination of simple elements, one can build up functional units. This trend of hierarchical structure formation, blending of materials, and gradient formation mimics some of the features of the biological microenvironment and is a welcome improvement over single-material approaches. Admittedly, there is much work to be done in this area, and the number of combinations and design space becomes extremely large.

4. CELL SOURCES AND SELECTION

Most of the reported bioprinting studies have used commercially available cell lines from animal or human sources. This can be attributed to the fact that cell lines are readily available, with relatively easy and established protocols for culture and expansion. Primary cells normally isolated from animal tissues and organs are another alternative of choice. In this case, the required steps to isolate the cells from the tissue are normally complex, and normally a mixed population is obtained, which might require further steps for the isolation of the cells of interest. Furthermore, the expansion of these cells *in vitro* without losing phenotype can be a limitation. Human primary cells from donors that have undergone surgery, where a specific tissue or organ is removed, are also an alternative despite being less frequent. Furthermore, in this case the resected tissue might suffer from a pathological condition, which can limit the use for regeneration strategies. On the other hand, mature and specialized cells do not seem to be the best choice since they are often characterized by a limited proliferation capacity and dedifferentiation when expanded in conventional cell culture systems.

Most studies were reported where cell lines and primary cells have been selected and aimed at the validation of the technology and biomaterials used; only *in vitro* models or proof-of-concept studies are normally achieved. In some proof-of-concept studies, primary cells from the same animal species are used for the manufacturing of regenerative constructs and tested *in vivo* in healthy models or specially developed disease models where the regeneration potential of the developed construct can be better validated.

PSCs, either embryonic or induced, can contribute largely to the advances in the field and can be the ideal biological cell source for bioprinted approaches for multiple tissue regeneration and organ replacement strategies. PSCs have an indefinite self-renewal ability and plasticity, which allow *in vitro* generation of an unlimited number of distinct cell types and have opened new avenues for regenerative medicine. Embryonic stem cells (ESCs) allow the generation of all the cells in the body, but research with these cells is limited in most countries due to several ethical concerns, which limit their application for

https://dx.doi.org/10.1021/acs.chemrev.9b00789
Chem. Rev. 2020, 120, 11032−11092

Table 2. Main Bioprinting Studies Aiming at Skin Development

cells	composition	structure	mechanical properties	method	sequence	comments	ref
fibroblasts (mouse, NIH 3T3)	gelatin/alginate/ fibrinogen blend	fibroblast/gel layers + keratinocyte layer	n/a	piston-driven	fibrobalst/gel layers deposited, then immersed in $CaCl_2$/thrombin to cross-link	rapid 5 mm thick	205
primary dermal fibroblasts (human)					keratinocytes deposited on top	scaffold-free construct	
primary epidermal keratinocytes (human)							
primary fibroblasts (human)	plasma-derived fibrin matrix	fibroblast/gel layers + keratinocyte layer	n/a	piston-driven	fibroblast/fibrinogen/$CaCl_2$ mixed and deposited	in situ mixing	206
primary keratinocytes (human)					keratinocytes in medium deposited on top	rapid keratinocyte/fibroblast assembly	
fibroblast cell line (human)	collagen type I	collagen layer + fibroblast cell layer + keratinocyte cell layer	n/a	drop on demand	print acidic collagen (pH 4.5) nebulize neutralizer to cross-link	gels and cells printed separately	203
immortalized keratinocytes (human)					deposit cells in medium	comparison of printed vs manual layer assembly	
NIH 3t3 fibroblast (mouse)	collagen type I	matriderm substrate + fibroblast/gel layers + keratinocyte/gel layers	n/a	laser-assisted	cell-laden collagen pre-cross-linked	*in vivo* wound bed integration	36
immortalized keratinocyte (human)					20 layers of each cell/gel combination		
NIH 3t3 fibroblast (mouse)	collagen type I	matriderm substrate + fibroblast/gel layers + keratinocyte/gel layers	n/a	laser-assisted	cell-laden collagen pre-cross-linked	laminin staining shows beginning of basal membrane formation	204
immortalized keratinocyte (human)	alginate/human plasma blend				20 layers of each cell/gel combination		
amniotic fluid-derived PSCs (human)	fibrin/collagen type I	amniotic PSCs/fibrin/collagen	n/a	pressure-assisted	cross-linking by thrombin solution sequential application before and after cell/gell layers	cell/gel deposition directly *in vivo*	208
bone mesenchymal stromal cells (MSCs) (human)		MSCs/fibrin/collagen					
amniotic PSCs	hyaluronic acid (HA)/gelatin/PEG	single-layer amniotic PSCs/HA/ gelatin/PEG	0.2 to 2 kPa (Shear)	pressure-assisted	simultaneous deposition/thiolene-thiol + Irgacure 2959	in situ *in vivo* deposition	209
					UV cross-linking	protective bandage during healing	
keratinocytes (human)	PVP ink	keratinocyte/PVP + melanocyte/PVP layer on	n/a	drop on demand	fibroblast/collagen/PVP dermal construct	melanocyte incorporation	212, 226
melanocytes (human)	PVP ink/collagen type I	fibroblast/PVP/collagen			keratinocytes + melanocytes printed on top	structurally graded dermal layer	
fibroblasts (human)							
neonatal dermal fibroblasts (human)	gelatin, fibrinogen, collagen I, elastin	dermal fibroblasts + hydrogel (dermis)		piston-assisted	multiple layers printer for the dermis	constructs with low stability when printed in well plates	207
neonatal epithelial keratinocytes (human)		laminin/entactin (basement membrane)		droplet on demand	coating of the dermis with DoD with basement membrane	permeability test shows that tight junctions are formed	
		keratinocytes (epidermis)			automatic dispensing of epidermis cells in the central region of construct		

https://dx.doi.org/10.1021/acs.chemrev.9b00789
Chem. Rev. 2020, 120, 11032−11092

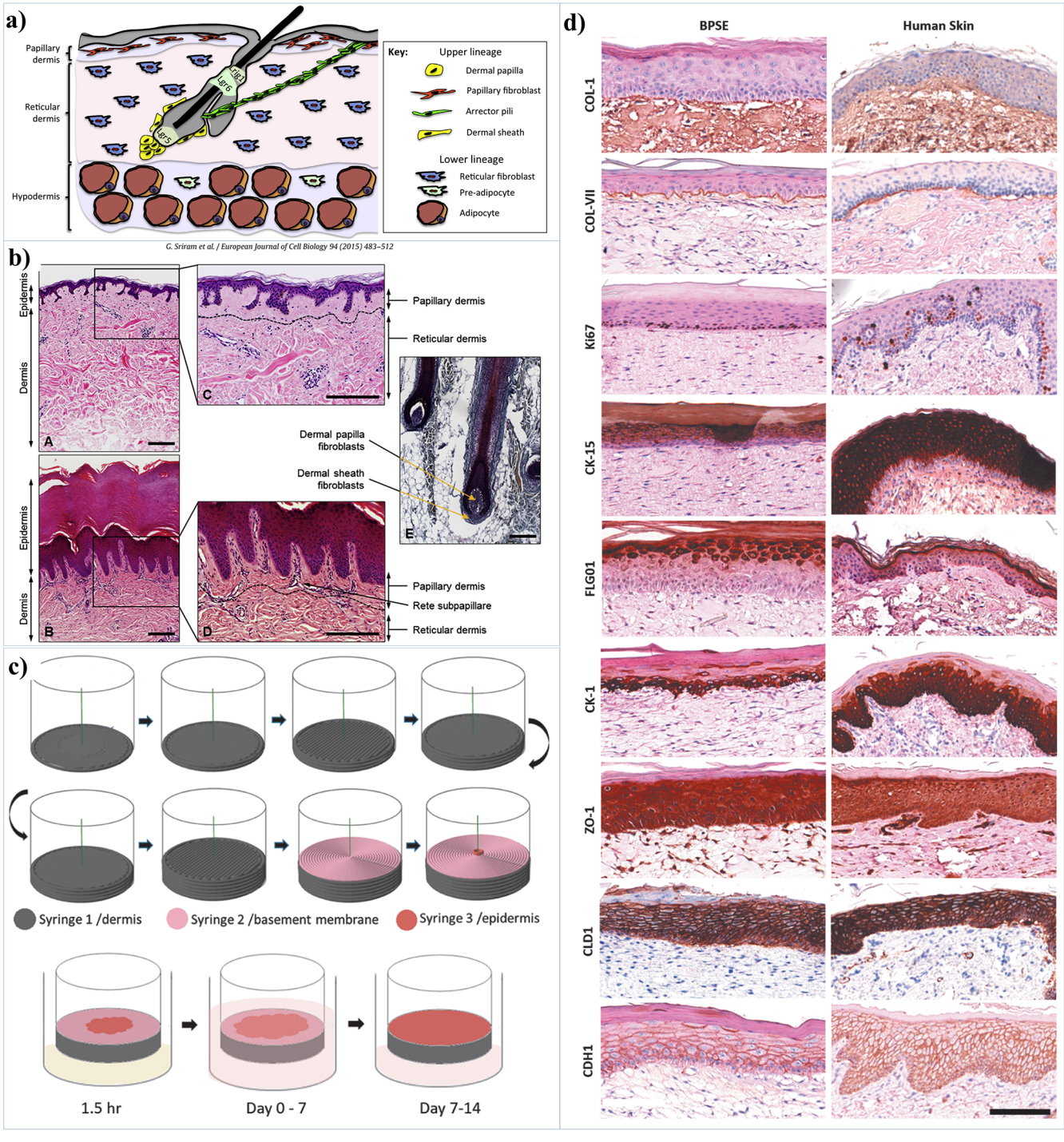

Figure 7. Skin physiology and its bioprinted counterparts: (a) schematic representation of the skin, (b) histological sections of adult human skin with different layers and constituents, (c) example of bioprinted skin with layers for dermis, basement membrane, and epidermis, and (d) histological characterization of the bioprinted and human skin. Adapted with permission from refs 182, 183, and 207. Copyright 2014 Elsevier Ltd., 2015 Sriram et al. (published by Elsevier GmbH), and 2019 Mary Ann Liebert Inc.

regenerative therapy purposes. An alternative source of PSCs with less ethical restrictions are iPSCs. Takahashi and Yamanaka generated the first iPSCs from mice in 2006. This was achieved using embryonic and adult somatic fibroblasts by introducing the master regulatory transcription factors Oct3/4, Sox2, c-Myc, and Klf4, under ESC culture conditions.[142] In a follow up work, the same researchers generated the first human iPSCs (hiPSCs) using fibroblasts by applying the factors previously described, currently known as the Yamanaka factors.[143]

Multiple protocols have been established for the differentiation of iPSCs and ESCs toward specific lineages such as cardiomyocytes (CMs),[144−146] insulin-producing cells,[147] kidney progenitor cells,[148−152] nerve progenitors,[153−155] and many others. Furthermore, most of these cells have been cultured with specially developed *in vitro* protocols to create organoid structures, with different cell stages during culture being able to create complex structures with multiple cells types normally identified in the native tissue or organ. These promising

https://dx.doi.org/10.1021/acs.chemrev.9b00789
Chem. Rev. 2020, 120, 11032−11092

differentiation protocols are constantly evolving, but further work is still necessary to ensure that the differentiated cells are of the intended tissues.[156]

For the aforementioned reasons, iPSCs seem to be the most logical choice for the future advances of bioprinted tissues and ultimately organs. Furthermore, these cells can be expanded in sufficient amounts to be bioprinted, although the stage of differentiation that should occur before bioprinting is still unknown. The main limitations of using such cells and associated differentiation protocols are the high costs associated with the cell culture medium and all the growth factors required. Furthermore, these PSCs require intricate differentiation protocols, which will require hydrogels that do not affect the diffusion of growth factors necessary to drive these cells toward specific lineages. In cases where complex tissues and organs are the objective, several cells would be needed, and the combination of multiple cells will certainly require elaborated protocols with multiple growth factors, which might pose extra hurdles. For example, in the case of the kidney, more than 20 differentiated cells are harbored in an organ. Even when cell culture techniques would be developed to maintain and expand specialized cells in sufficient numbers for bioprinting, such biological complexity would still pose limits in their use. Mature cells derived from PSCs could solve these issues if properly maintained in culture and expanded in a large scale.

Initial PSC bioprinting trials have been recently reported.[157−159] Similarly, bioprinting of a specific tissue or organ with PSC-derived cells has also started to be reported.[34,160−167]

5. ECTODERM

Developmental biology has helped to understand the delicate formation process of several organs, which arise from the three germ layers (ectoderm, endoderm, and mesoderm). Each of these layers will give rise to several tissues and organs individually, but in some cases cross interconnections are also known to contribute with several tissue and organ complexes (Figure 6).

The skin and the nervous system are both derived from the ectoderm, the outermost germ layer of the developing embryo.[169,170] A brief description of the related developmental process of these tissues provides context for tissue organization and composition, tissue mechanical properties, and related repair mechanisms. Overall, this gives tissue-specific insight relevant for current and prospective bioprinting activities.

5.1. Skin

The skin has the important function of protecting the body from the surrounding environment, including radiation, dehydration, temperature extremes, and injury.[171] This is achieved through its well-defined stratified structure and specialized appendages, such as sebaceous glands and hair follicles. Many of the skin formation processes observed during development are conserved in skin repair, allowing a return of function after injury. However, wound repair can be compromised in cases of extreme injury (e.g., deep lacerations, burns)[172,173] or because of extenuating factors such as diseases, demographic, or life style.[174] The relative accessibility and seemingly simple layered composition make skin an attractive proof-of-principle for bioprinting applications, with examples over the past decade of *in vitro* and *in vivo* skin replacements (Table 2). While this technology presents many advantages over other biofabrication techniques, current approaches do not emulate the structural and compositional heterogeneity of this dynamic tissue and, therefore, fail to achieve a completely functional mimic. Improvements will rely on technical and material developments to harness mechanisms of skin self-assembly and repair.

5.1.1. Skin Structure. Skin has an outer epidermis and an underlying dermis, separated by a basal membrane, a layer of collagens, laminins, and glycoproteins (e.g., perlecan, nodigens). This membrane is a key component of skin and initially separates the ectoderm layer from the mesoderm, the germ layers which give rise to the epidermal keratinocytes and dermal fibroblasts, respectively.[175] The basement membrane itself is produced by the keratinocytes and fibroblasts through the complementary expression of ECM molecules.[175] During development, ectoderm stratification is initiated by signals from the underlying mesoderm,[169,176] triggering the division of basal keratinocyte stem cells. These migrate upward, differentiating to form the granular layer and then the cornified layer. The final outer stratum of dead cornified keratinocytes provides the body with the final barrier that is continually renewed through the same stratification process, with complete epidermal renewal occurring over 48 days.[177] The basement membrane is essential to this renewal process by forming a niche for epidermal stem cells, regulating the epithelial stratification process by controlling growth factor diffusion and providing cell adhesion cues.[178] As the epidermis is primarily held together by cell−cell junctions,[179,180] it is assumed that the dermis provides most of the structural integrity of the skin.[181]

The major cellular constituent of the dermis is the dermal fibroblast, with an interplay of signaling between the dermis and epidermis driving epidermal stratification, the formation of appendages (e.g., hair follicles, sweat glands), and the regulation of dermal homeostasis (Figure 7a,b).[178,182,183] The upper dermal layer adjacent to the basal membrane, known as the papillary dermis, is comprised of densely packed 10 μm collagen fibrils within an interpenetrating network of elastin that is populated by papillary dermal fibroblasts. Below this is the reticular dermis, exhibiting an ECM of loosely organized, larger 50 μm collagen fibrils with the limited presence of elastin and with the presence of distinct reticular dermal fibroblasts.[181−183] A determining factor of collagen fibril size within the skin is the presence of decorin, a proteoglycan which is known to produce smaller collagen fibrils *in vivo*[184] and *in vitro*[185] and is more highly expressed within the papillary dermis by resident papillary fibroblasts.[186]

As a result of structural and compositional differences, these layers exhibit distinct mechanical properties, with the highly fibrillar papillary dermis having a stiffness an order of magnitude higher compared to the loosely packed reticular dermis.[181] Differences in mechanical properties are also suggested to depend on proteoglycan distribution within these layers, imparting a viscoelastic behavior based on the supramolecular assembly of these molecules. The mechanical properties of skin also differ at different locations of the body[187] and have in-plane anisotropy at different locations,[188] which correlates to changes in collagen and elastin content and overall ECM orientation.[189] This variety in tissue and different methods of evaluation produce measurements ranging from 0.02 to 58 MPa.[190] In addition to skin integrity, tissue stiffness also has implications for the cells residing within these layers, which are reported to respond to mechanical cues.[191−193] This reported heterogeneity of skin, in terms of tissue stratum and tissue location, and the impact this can have on mechanical and mechanobiological

https://dx.doi.org/10.1021/acs.chemrev.9b00789
Chem. Rev. 2020, 120, 11032−11092

aspects provide criteria as well as inspiration for the development of tissue-engineered constructs to facilitate skin repair.

After injury, a rigid fibrin-based ECM structure (a blood clot) forms, and fibroblasts migrate to the location, producing collagen to create a wound bed.[172] The mechanical properties of the wound bed also play a role in the healing process, where tension stimulates fibroblasts to proliferate[194] and differentiate into myofibroblasts,[195] a contractile phenotype that facilitates wound closure.[196] During this time, the wound bed increases in stiffness[197] in a matter of days, from approximately 18 kPa to greater than 40 kPa. This has a subsequent impact on epithelial cells, which are known to proliferate more on stiff substrates and require a substrate stiffness greater than 40 kPa to effectively close a breach in the epithelial barrier.[198−200] However, excessive tension applied during a critical time window in the healing process can trigger abnormal fibrotic ECM deposition and leads to excessive (hypertrophic) scar formation.[195,201]

With a market value of approximately $6.7 billion,[172] interest in skin wound healing continues to grow. These efforts have been driven by academic research into skin dynamics, the search for improved clinical wound healing applications, and the search by the cosmetic industry for an ethical alternative to animal testing of cosmetics.[202]

5.1.2. Skin Bioprinting. One of the earliest examples of skin bioprinting applied DOD printing to manufacture layered skin.[203] Layers of collagen were dispensed initially followed by intercalated layers of fibroblasts and collagen followed by layers of keratinocytes. Constructs were cultured using an air−liquid interface, and substantial shrinkage was observed.

Laser-assisted bioprinting has also been used, where laser irradiation transfers encapsulated cells to a target slide with high precision and resolution to generate printed skin with a biomimetic layered arrangement.[36,204] Initial studies by Koch et al.[204] showed the capability of using laser-assisted bioprinting to manufacture layered constructs of fibroblasts and immortalized keratinocytes. Michael et al. bioprinted on top of an acellular dermal matrix, depositing 20 collagen layers that incorporate fibroblasts and another 20 layers containing keratinocytes.[36] The constructs were implanted in nude mice with a dorsal skin chamber, and histological results showed an integration of the constructs with the surrounding tissue. Neovascularization was also observed.

Full thickness skin with dermis and epidermis layers was recently achieved by Pourchet et al. via a piston-driven extrusion approach.[205] After an initial validation with mouse fibroblasts, primary human dermal fibroblasts were used to create the dermis layer, and a layer of human epidermal keratinocytes was seeded on top to mimic the skin structure. A comparison with healthy skin showed similarities; however, after 26 days in culture, differences were noted including cellular organization and the thicknesses of both epidermis and dermis. A similar approach was followed by Cubo et al.,[206] again with fibroblasts deposited within fibrin as the dermal layer and keratinocytes dispensed on the construct surface. The bioprinted skin was implanted in immunodeficient mice and sutured in place. After 8 weeks, explants stained positively for human skin markers, and histological characterization showed similar stratified architecture when compared with human skin.

Increasingly complex methods include creating multimaterial stratified structures, as recently described by Derr et al.[207] This multilayered approach of sequentially bioprinted cell/hydrogel compositions resulted in a stable skin-like construct (Figure 7c). While the composition of the layered structure does not directly reflect native skin, the resulting skin mimic was mechanically stable, produced analogous cellular and ECM distribution, and achieved appreciable barrier function (Figure 7d).

Bioprinting directly onto the wound has also been tested in small- and large-size animal models.[208−210] The easy access of skin-related wounds has facilitated these early examples of direct *in situ* bioprinting, providing a proof-of-principle of future possibilities such as the application of bioprinting in a clinical setting.

5.1.3. Skin Biofabrication Considerations. The bioprinting examples discussed so far provide a robust proof-of-concept application, due in part to the intrinsic ability of bioprinting to recreate the layered architecture of skin. The manual creation of hydrogel layers was the original approach and is technically simpler, but this lacks control in terms of composition and cellular resolution and has also been shown to be less mechanically stable.[211,212] Electrospinning has also been used to create a layer of nonwoven nanofibers as a mimic of the basement membrane layer; however, the resulting layers are large compared to the native dermal/epidermal transition and may impede the intimate crosstalk between the two layers.[213,214] In contrast, examples of skin bioprinting have shown that it is possible to have accurate planar (XY) deposition of different cell types within a skin construct, such as the controlled inclusion of melanocytes to provide the skin with pigment.[212] Further control over the heterogeneity throughout the depth of the construct is also possible, resulting in a skin mimic that closely reflects the native tissue organization in terms of cell populations, composition, and structure.[212]

As the technology continues to develop, attempts should continue to focus on improving the level of mimicry. The majority of current approaches employ collagen type I, with a few exceptions including fibrin. While both are present in the native ECM and wound bed, respectively, additional components are often ignored. Further, there have been limited attempts to recreate the different fibrillar regions within the dermis. Looking at the process of skin development described above, these two aspects are not mutually exclusive. The concentration of decorin, a proteoglycan, changes throughout these layers, and its presence influences the assembly dynamics and, therefore, the size range of collagen fibrils. Thus, incorporating this molecule might address both the compositional and structural heterogeneity of the tissue.

Mechanics of bioprinted skin is also often overlooked, with a few reports dedicated to measuring the mechanics of these replacement tissues.[215,216] The mechanical properties of skin are important for two reasons: the replacement skin must ultimately provide a physical barrier with suitable strength, and the biomechanics of the tissue directly affect the quality of wound healing. As discussed above, both fibroblasts and keratinocytes are influenced by the elasticity of their surrounding environment, and it is this aspect where bioprinting and the development of new and novel bioinks can excel. The ability to create different layers with mechanics specifically tuned to the resident cell type provides a powerful mechanism to influence wound healing. This could be even further harnessed by creating materials that respond appropriately over time and promote the different stages of wound healing, such as migration, proliferation, and differentiation.

In terms of "raw materials" for bioprinting, a wide number of cell sources have been employed for the manufacturing of skin constructs. Initial approaches described above mainly used immortalized cell lines from humans, animals, or a combination

https://dx.doi.org/10.1021/acs.chemrev.9b00789
Chem. Rev. 2020, 120, 11032−11092

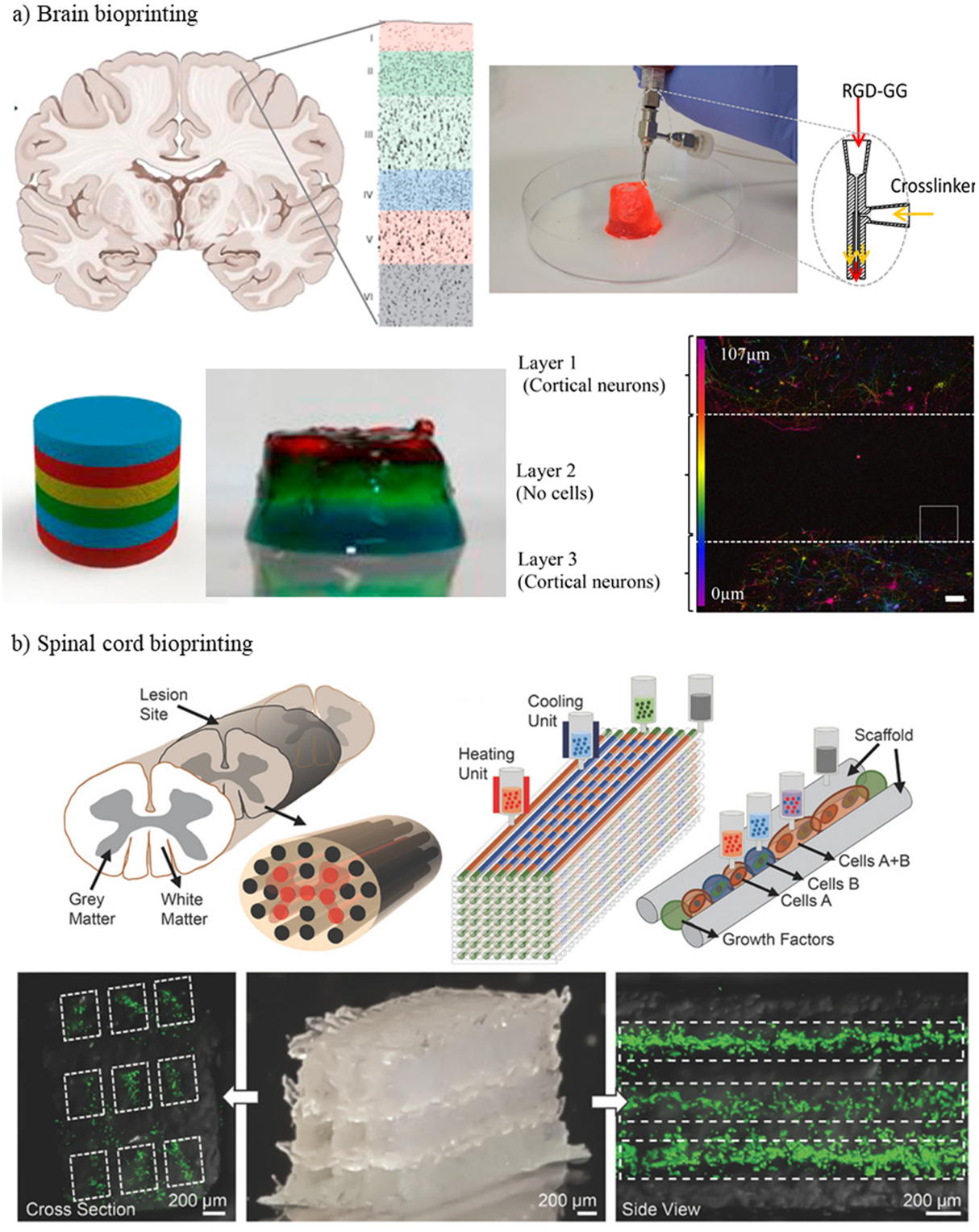

Figure 8. (a) Cortex is the outermost region of the brain and is part of the CNS that is most susceptible to bioprinting because of its stratified structure comprising different neuron types. This has been emulated by printing neurons within a multilayered hydrogel, with initial indications showing the initial formation of interlayer connections. (b) The spinal column is a more challenging structure within the CNS to recreate. Shown is a combination of hydrogel bioplotting, used to create structural support, and bioink containing various neural progenitors. Deposited in a manner to reflect the anisotropic arrangement of the spine, deposited cells showed good viability and directional growth along the axis of the printed spinal cord. Adapted with permission from refs 166 and 252. Copyright 2015 Elsevier Ltd. and 2018 WILEY-VCH Verlag GmbH & Co. KGaA.

therein to generate proof-of-concept approaches.[36,203,204] Primary cells have also been used, and a number of stem cell sources have been identified, some with clinical relevance.[208,217−219]

https://dx.doi.org/10.1021/acs.chemrev.9b00789
Chem. Rev. 2020, 120, 11032−11092

5.1.4. Skin Future Outlook. The most attractive clinical application for skin bioprinting is to treat partial and full thickness burn wounds, based on a clear medical need to quickly replace large swathes of skin and the current lack of wholly effective treatment options. However, a number of obstacles exist before such technology will be present in the operating theater, including regulatory restrictions. Bioprinting is still an emerging technology, and as such, the regulations for safety compliance in clinical applications are still being written.[220] Furthermore, current approaches, such as skin grafts and spray-on cell encapsulations, are already established and are comparatively less technically demanding and, therefore, less expensive.[217,221,222] Promoting the adoption of a bioprinting technique requires that a clear advantage is presented, including medical performance and financial benefit.

Despite the promising *in vivo* results obtained in some studies, current bioprinted skin substitutes remain an oversimplification of the complexity of native skin. The skin also includes appendages, such as hair follicles and sweat glands, and is highly innervated, both of which improve skin function and the quality of skin repair.[223,224] Furthermore, while healthy skin is a highly vascularized tissue, providing resident cells with sufficient nutrients, recent reports suggest that excessive formation of new blood vessels within the wound bed can impede healing and contribute to scar formation.[225] With the overall aim of incorporating different cell types in specifically designed spatial configurations throughout a 3D construct, bioprinting alone is capable of reconstituting in a meaningful and functional way these different tissue components. Although not currently taken into account, the impact of incorporating these elements on the success of wound healing will present bioprinting with a unique advantage over other techniques.

5.2. Nervous System

The nervous system is divided into the central nervous system (CNS) and the peripheral nervous system (PNS), two neural networks that work in concert to regulate homeostasis and sense and respond to external stimuli. The CNS refers to the brain and the spinal cord, while the PNS comprises the neurons distributed throughout the body. The key functional unit of both systems is the neuron, a specialized cell with long extensions (axons and dendrites) that connect to other neurons or tissues to transmit neuroelectric signals throughout the body. In addition, both systems contain specialized glial cells that provide critical support for neural function and impact nerve tissue repair.

During development, neural progenitors of both the CNS and PNS undergo a spatiotemporally orchestrated migration throughout the fetus and differentiate upon reaching respective destinations. At this time, axons and dendrites extend from the neural cell bodies and follow haptotactic and chemotactic cues to create connections with other neurons or with tissues and organs.

The PNS has an intrinsic regenerative capacity that relies on conserved pathfinding mechanisms in combination with a conducive ECM and trophic support from glial cells.[227,228] In contrast, glial and non-neuronal cells of the injured CNS form scar tissue that impedes regeneration.[229] Owing to the restricted access and delicate nature of CNS tissue *in vivo*, bioprinting has focused on developing *in vitro* CNS models. By comparison, the PNS is more accessible for an intervention when tissue damage is too extensive; recent bioprinting examples aim to emulate the supportive ECM and glial cell organization of the PNS to improve regeneration in these extreme cases (Figure 9a).[230] To advance the application of bioprinting to recreate or repair the CNS and PNS, the tissue composition and structure must be appreciated along with an understanding of conserved and distinct mechanisms of these tissues during development or after injury.

5.2.1. Central Nervous System (CNS). The CNS is often described as tightly packed neural and glial cells, with the majority of self-organization driven by spatiotemporal gradients and cell−cell interaction.[231−233] There are approximately 86 billion neurons in the brain and an almost equal number of glial/non-neural cells.[234] A neuron forms a synapse with another neuron to create a connection, and one neuron is capable of contacting up to 1000 other neurons, resulting in over 60 trillion synapses within the brain.[232] These connections bridge activity across different regions, from the outer cerebrum, where learning and other higher functions occur, to the cerebellum, responsible for muscle coordination, to the brain stem, which controls primary functions (e.g., heart rate, breathing). Finally, the spine serves to transmit signals to and from the body.[235] The majority of CNS bioprinting activities has focused on recreating the outermost cortical layer of the cerebellum and its well-defined multilayered structure, which underpins the majority of complex higher functions (Figure 8a).

In addition to neurons, there are also CNS glial cells that regulate and maintain neural function, including oligodendrocytes and astrocytes. In particular, oligodendrocytes myelinate axons (wrap them in an insulated fatty layer) to help signal conduction; many neurodegenerative diseases, such as multiple sclerosis (MS), are the result of pathological demyelination of neurons.[236] Throughout the CNS, there is an expansive blood vessel network to supply nutrients with astrocytes regulating nutrient flow and moderating the blood−brain barrier (BBB) to ensure that noxious molecules do not enter the brain via the bloodstream.

The ECM of the CNS is the perineuronal net (PNN),[237] which distinctively lacks an ECM ultrastructure compared to other organs and has limited amounts of collagen type I and fibronectin. Instead, the PNN is comprised of the membrane-forming collagen IV and hyaluronan that wrap around the individual dendrites and neural cell bodies. The PNN incorporates glycoproteins tenascin-R, tenascin-C, a number of proteoglycans, and proteins such as Semaporin 3A.[238] Because many of these molecules inhibit axon growth, this inhibitory PNN sheath is suggested to direct synaptic formations and maintenance during learning.[231,239] This milieu of cells, myelin, and ECM creates a relatively soft tissue, with elastic modulus measures ranging from 0.689 to 2.51 kPa depending on where and how the measurement is performed.[240] The mechanical properties of this tissue are also suggested to play a critical role in creating the distinctive ridges (gyri) and valleys (sulci) of the developing brain.[233]

Astrocytes form a scar around the site of a CNS injury, creating a mechanically soft boundary that protects healthy brain tissue from immune cells coming from the disrupted BBB.[227,236] The center of the lesion contains fibrinogen and collagen type I, which trigger astrocytes to adopt a reactive phenotype, producing collagen type IV and proteoglycans.[229,233,241−243] While collagen type IV promotes neurite growth, it also sequesters the other biomolecules to inhibit nerve growth through the barrier. Attempts to prevent scar formation delay BBB repair and result in more damage to healthy CNS tissue.[244,245] However, a degree of neural repair across the

https://dx.doi.org/10.1021/acs.chemrev.9b00789
Chem. Rev. 2020, 120, 11032−11092

injury is achieved when the astrocyte interaction with collagen type I is blocked.[241]

5.2.1.1. CNS Bioprinting. The delicate nature of the CNS has focused therapeutic developments on injectable hydrogel systems for *in vivo* applications.[246−248] However, CNS bioprinting has attracted interest for *in vitro* models that emulate the distinct layered structure of the cerebral cortex, owing to the intrinsic layering ability of the technology. While earlier work established general feasibility, a number of examples have emerged which showcase the promise of this approach.

An initial example of feasibility was generated by Tao et al. in 2006,[249] using a modified HP inkjet printer to deposit sequential layers of fibrin, thrombin (for cross-linking), and rat primary cortical neurons in suspension. Generating a layer thickness of around 60 μm, this fibrin construct achieved an estimated elastic modulus of 2.9 MPa. However, the low viscosity of the cell suspension led to a relatively diffuse distribution of cells, precluding any fine determination of neural cell placement; the stated theoretical 85 μm resolution droplet placement was not observed in the final pattern. However, electrophysiological assessment revealed that these cells not only survived the process but also generated a functional neural network.

Work from the Yoo lab[250,251] also performed a sequential deposition process, this time collagen type I at a pH of 4.5 (pre-cross-linking) and a nebulized spray of calcium carbonate (to increase pH and initiate cross-linking), followed by deposition of embryonic astrocytes and cortical neurons in suspension. While no assessment of cell function, printing resolution, or mechanical properties was reported, this proof of principle verified that the brief exposure to acidic conditions was not detrimental to cell viability and made it possible to maintain distinct hydrogel regions or layers of different cell types in specific patterns.

Recent work has focused on the deposition of neural cells within a hydrogel carrier. Lozano et al. created a multilayer hydrogel with distinct cell populations via the in-line mixing of a gellan gum hydrogel and ionic cross-linking solutions during the bioprinting process (Figure 8a).[252] While this relatively manual process resulted in low-resolution patterns, it provides a nice example of recreating the lamellae of the cerebral cortex and initial indications of forming a neural network between distinct layers.

With the aim of improving pattern fidelity and resolution, others have focused on developing approaches where the hydrogel maintains both printability and sufficient cross-linking upon deposition. This has been achieved with either thermally induced cross-linking, where bioprinting and deposition collection occur at different temperatures,[247] or sequential thermal cross-linking during the initial deposition followed by a secondary cross-linking solution to further stabilize the resulting structure.[253] These approaches created cell-laden gel filaments with a resolution ranging from 200 to 250 μm which could be stacked during printing to form an open, porous 3D structure.

As with other bioprinting endeavors, the challenge of achieving a construct with a material composition and mechanical properties that are appropriate for the biological application while being constrained by processability is a mainstay. This is represented well by Joung et al., as shown in Figure 8b, who performed an extensive study on various material combinations to create a CNS spinal graft.[166] While initial attempts to bioprint fibroblasts were successful using GelMA or gelatin/fibrin gels, spinal neural progenitors (sNPCs) derived from human iPCSs did not survive this process. Instead, Matrigel as an alternative bioink resulted in successful bioprinting of both sNPCs and oligodendrocyte precursor cells (OPCs). Meanwhile, the structural component of the scaffold was realized by bioprinting an alginate and methylcellulose (MC) blend to form an oriented array of microchannels; different AG/MC compositions and different ionic cross-linking solutions (calcium chloride, barium chloride) were trialed. During bioprinting, the channels were filled with a cell-laden Matrigel to create a composite hydrogel structure. The final AG/MC composition used was capable of creating 150 μm channels and had an elastic modulus of 55 kPa; while this is stiffer than the native spinal tissue, it was found that softer compositions were not mechanically stable enough to realize the final structure.

5.2.1.2. CNS Fabrication Considerations. Overall, Joung et al.[166] report a stiffness ranging from 40 to 200 kPa, while Dai et al.[253] report a range of properties from 0.8 kPa to almost 5 kPa, the latter being within the range of elasticity often reported in the brain. However, the mechanical properties of the healthy and injured brain can be different, and reports suggest that stiffer substrates are detrimental for CNS regeneration.[227,254,255] Ultimately, a timely shift in stiffness could achieve ultimate repair by promoting cell proliferation at one stage, followed by differentiation and, ultimately, maturation.[256,257] The development of a bioprintable material that undergoes appropriate temporal changes in mechanical properties while maintaining cell viability remains a challenge.

The biological epitopes within the hydrogel are also of critical importance. Until now, material selection has largely focused on printability and cell viability, with the majority of studies using collagen type I and fibrin as mainstays of the bioprinting domain. However, these two materials are only present during a state of injury and are known to promote a reactive astrocyte phenotype that produces inhibitory molecules. Therefore, the use of these materials is seemingly counterproductive when attempting to create an environment that promotes neural network formation or induce a repair. Other materials, such as Matrigel or other laminin-rich substitutes, are better at emulating the native environment though present challenges in terms of printability. Other possible materials include more bioinert options, such as alginate or gellan gum; however, these typically need to be modified through the addition of cell-adhesion peptides for appropriate cell response.[258] Hydrogel materials capable of sequestering endogenous CNS ECM components, thereby mimicking the formation of a functionally appropriate PNN microenvironment that promotes neural and glial cell self-organization, are currently unavailable.

Toward achieving a complex biomimetic construct, the inclusion of all appropriate cell types within the CNS is required to achieve appropriate ECM production and functional self-organization. The studies outlined above provide a number of examples of the many CNS cells sources currently available (as reviewed by Gage and Temple). Possibilities range from primary cells (typically embryonic to ensure viability), to adult NSCs, to reprogrammed iPSCs. Both NSCs and iPSCs require a more thorough validation of the phenotype attained, but hold the most promise in terms of a clinical application that is patient-specific and nonimmunogenic. When determining neural phenotype, morphological and marker expression alone are not sufficient to indicate a functional tissue. Instead, functionality in terms of conductive of neural signals is needed, as showcased by both Gu et al.[259] and Joung et al.[166] While attaining appropriate and functional cells is a considerable

https://dx.doi.org/10.1021/acs.chemrev.9b00789
Chem. Rev. 2020, 120, 11032−11092

challenge, the field of neuroscience has a number of toolsets available to this end.

5.2.1.3. CNS Future Outlook. For the moment, the application of CNS bioprinting is limited to *in vitro* model development, although the goal of repairing neural networks for *in vivo* applications represents a conspicuous challenge. The advent of the brain organoid, where stem cells are coaxed to form a "mini-brain" through self-organizing, has drawn attention to *in vitro* models for studying brain development.[260] While this might seemingly obviate the need for bioprinting, brain organoids still have a number of limitations such as throughput, control of cell diversity, and direction of appropriate cell patterning. In this sense, bioprinting can facilitate investigations by enabling the prepatterning of organoid composition to help direct and drive the self-assembly process.

As increasingly more representative 3D models develop, extending beyond the layered cerebral cortex to include the brain stem or cerebellum, improved monitoring will also be required to better understand the structure/function of the created tissues. In parallel progress, complementary fields of research will accelerate this development, making it possible to monitor activity in a printed brain via 3D electrodes[261,262] or through light sheet calcium imaging.[263,264]

5.2.2. Peripheral Nervous System (PNS). After the migration of neural crest cells and their subsequent differentiation into specific peripheral nerve lineages, neural cells are organized into clusters called ganglia located throughout the body.[265−268] These cell clusters extend axons to innervate specific tissues, classified as afferent (transmitting from the body) or efferent (transmitting to the body). As axons extend, glial progenitor cells migrate along the axons, proliferating and differentiating into mature Schwann cells (SCs) that support axonal function. Once an axon reaches its target tissue, some SC progenitors can also migrate past axons into the target tissue and differentiate into various specialized cells that act as innervation points within tissues, such as terminal SCs or even other neural ganglia.[266,269,270]

The PNS is functionally grouped as sensory, sympathetic, and parasympathetic. Efferent sympathetic ganglia are located along the exterior of the spinal column and extend into the body, passing on signals that regulate homeostasis while providing the "flight or fight" physiological response to a perceived threat (e.g., adrenaline release, increased heart rate). Efferent parasympathetic ganglia are uniquely located within various organs and extend throughout each respective tissue, transmitting signals coming directly from the CNS.[271]

Sensory ganglia (afferents) are located close to the spine and have axons which connect the spinal cord to tissue throughout the body, providing a path for sensory inputs, such as pain and temperature, as well as homeostatic feedback.[268] Though technically not considered a part of the PNS, somatic motor axons also extend from the spinal cord and bundle together with sensory axons to innervate muscle tissue. These bundle tracts of axons form nerve fibers with which we are familiar, such as the sciatic nerve or ulnar nerve (origin of the "funny bone" sensation). SCs are present throughout PNS nerve fibers, either myelinating axons or generally supporting neural function.[270]

A peripheral nerve fiber has a hierarchical organization, starting with the *endoneurium* that envelopes axons and SCs to form endoneurial tubes around each axon with tube diameters corresponding to the resident axons (2−20 μm).[272−274] Endoneurial tube boundaries are demarcated by ECM proteins synthesized by resident SCs, including type I and type III collagen fibrils,[275,276] and a basal lamina of collagen type IV and laminin molecules.[277] The ECM of the endoneurium between endoneurial tubes is comprised of hydroscopic GAGs and also includes fibroblasts.[278,279] This highly heterogeneous structure has an estimated elastic modulus of 55 kPa, and overall, axons occupy approximately 50% of the cross-sectional area.[280−283] A perineural epithelial cell layer, or *perineurium*, envelopes the endoneurium to form fascicles and serves as a blood−nerve barrier, similar to the CNS; groups of fascicles form the nerve fiber properly, enveloped by the *epineurium* and *mesoneurium* membranes.[284,285] The epineurium is comprised predominantly of collagen type I with an estimated elastic modulus of 22 kPa, whereas the perinerium has a modulus of 89 kPa and contains collagen type III.[275,280,286]

A severed peripheral nerve is separated into the viable fiber segment still connected to neuronal cell bodies (the proximal nerve segment) and the dead/dying segment that used to innervate target tissues (the distal nerve segment).[287] The distal segment experiences Wallerian degeneration that removes debris from any intact endoneurial tubes.[288,289] Distal SCs dedifferentiate into a regenerative phenotype, proliferate, line the endoneurial tubes to assume the distinctive bands of Büngner formation, and produce proteins to promote axon growth.[290−292] Meanwhile, axons sprout from the proximal stump and form growth cones, a specialized structure that responds to a combination of contact-mediated (haptotactic) and diffusible (chemotactic) cues to guide a regenerating axon to a target tissue.[288,293,294] The endoneurial tubes present laminins, oriented collagen fibrils, and a 3D microchannel architecture that directs neurite growth toward target tissue.[292] In some cases, a tube (or "nerve guide") can help to bridge the defect (entubulation), acting to concentrate the fibrin coming from the injured stumps. This forms a fibrin cable that acts as a scaffold for SC migration and axon growth, in contrast with the CNS where fibrin triggers a reactive glia phenotype that inhibits repair. The fibrin cable fails to form when the nerve defect is too long, and the current golden standard bridges the proximal and distal stumps with an autogenic or allogenic nerve graft. This approach is successful because of the native endoneurial microarchitecture and, for autografts, the native SCs which support efficient axon regeneration. However, the limitations of nerve grafts have driven the development of alternatives; the reader is directed to extensive reviews on other biofabrication approaches by Daly et al.,[295] Kehoe et al.,[296] and Wieringa et al.[297]

While the bioprinting of neural cell bodies in this context serves little purpose, the bioprinting of SC-laden constructs is a promising approach (Figure 9a). SCs provide neurotrophic growth factors and create essential ECM components, and incorporating them within a permissive anisotropic architecture is considered beneficial for long gap repair.

5.2.2.1. PNS Bioprinting. Recent bioprinting efforts have focused on achieving better PNS repair by creating nerve guides that incorporate SCs and other cell types known to improve nerve growth (Table 3). The most original is the formation of a nerve guide tube comprised entirely of cells, assembled via the Kensai bioprinting method of placing cell spheroids onto a needle array to form 3D shapes (in this case, a tube) (Figure 9d). Early attempts utilized fibroblasts (Figure 9c),[298] while later efforts applied a novel gingival mesenchymal stromal cell (MSC).[299] This approach relies on intrinsic fusion between cellular spheroids to maintain the tube structure, and both studies state that the tube mechanical properties need to be

https://dx.doi.org/10.1021/acs.chemrev.9b00789
Chem. Rev. 2020, 120, 11032−11092

Table 3. Main Bioprinting Studies of CNS and PNS

tissue	cells	composition	structure	mechanical properties	method	sequence	comments	ref
brain	hippocampal	cells in medium collagen "biopaper"	circle patterns on a biopaper membrane	fibrin: *E*: 2.92 MPa	inkjet	collagen hydrogel "biopaper" preformed	first example	249
	cortical (rat)	cells in medium (NT2)	NT2/fibrin layered structure			cells printed on to this substrate in a determined pattern	low resolution	
	NT2 neural precursors (human)	fibrin gel				fibrin deposition, follow by thrombin, then cells in suspension		
brain	embryonic astrocytes	coll I	layered	n/a	extrusion (droplet)	print acidic collagen (pH 4.5)	multilayered, multicellular	250
	embryonic neurons					deposit cells in medium	acidic exposure	
						nebulize neutralizer to cross-link		
brain	NSC line C17.2 (mouse)	coll I (for cells)	layered	n/a	extrusion (droplet)	print acidic collagen (pH 4.5)	multimaterial patteren	251
		fibrin (for VEGF)				deposit cells in medium	VEGF-induced migration	
						nebulize neutralizer to cross-link		
brain	embryoic primary cortical neurons (mouse)	gellam gum + RGD	layered	n/a	manual coaxial extrusion	coaxial deposition of GG-RGD and ionic solution (5× PBS or 1 M $CaCl_2$)	multilayer cortex-like with extending growth	252
brain	NSC (mouse)	PU nanoparticle dispersion	stacked filament structure	0.6−4 kPa (Shear)	extrusion (FDM)	extruded onto heated surface (thermal cross-linking)	used as injectable for Zebra fish *in vivo* model	247
brain	glioma cell line SU3	gelatin alginate fibrin	stacked filament structure	n/a	extrusion (FDM)	extruded on cooled surface; postprocess cross-linking with calcium chloride (alginate) and thrombin (fibrin)	3D brain tumor model	253
	glioma cell line U87 (human)							
brain	hNSC (human)	alginate carboxymethyl-chitosan agarose	stacked filament structure	4.75 kPa (start)	extrusion (FDM)	postprocess cross-linking calcium chloride	multicellular brain model; functional calcium signaling	259
				0.8 kPa (final)				
spine	neonatal dermal fibroblasts	matrigel gelatin/fibrin GelMA	oriented microchannel structure	40−200 kPa (range of materials)		thrombin/transglutaminase (TG) solution (fibrin/gelatin)	matrigel required for cell viability.	166
	hiPSC-derived ventral sNPCs (human)	PDMS	laden with cells			UV (GelMA, PEGDA)	functional calcium imaging	
	miPSC-derived OPCs (mouse)	PEGDA alginate/methycellulose				$BACl_2/CaCl_2$ (alginate)		
spine	iPSC-derived NPCs (human)	fibrinogen/alginate	multilayered cylinder spinal column mimic	n/a	pressure- assisted (microfluidic)	cross-linking by in-line mixing gel with $CaCl_2$/thrombin	microfluidic in-line mixing	49
							motor neuron differentiation	
PNS	bone MSCs (mouse), SCs (unknown species)	no gel, cells only	large parallel filaments	n/a	manual extrusion	cells in a capillary, manually extruded into a 3D-printed agarose mold	cell aggregates printed or manually assembled	301, 302
			fugitive agarose for support and microchannels formation			cross-linked by cell fusion	requires manual removal of agarose rods	
PNS	RSC96 SC line (rat)	alginate	log-cabin filament structure	n/a	extrusion (FDM)	PVA or glycerol bath	PVA in bath counters strand buoyancy, improves pattern fidelity	78
	primary SCs (rat)	hyaluronic acid				$CaCl_2$ + PEI for cross-linking		

https://dx.doi.org/10.1021/acs.chemrev.9b00789
Chem. Rev. 2020, 120, 11032−11092

Table 3. continued

tissue	cells	composition	structure	mechanical properties	method	sequence	comments	ref
PNS	primary SCs (rat)	fibrinogen/HA	parallel oriented filaments with 85/90/95 respective orientation and oriented pores between	n/a	extrusion (FDM)	layers of filaments extruded into PVA bath; thrombin cross-linking	structure with slight offset achieves stability and general orientation	77
							good viability, fibril and neurite orientation	
PNS	dermal fibroblasts using (human)	none	nerve guide tube	n/a	Kensai cell fusion	place cell aggregates on pin cushion array	5 mm defect *in vivo* trial	298
							no autograft control	
PNS	gingival MSCs (human, NCC origin)	none	nerve guide tube	n/a	cell fusion	place cell aggregates on pin cushion array	5 mm defect *in vivo* trial	299
							unique cell choice	

further explored. Regardless, both showed successful nerve repair, and the use of gingival MSCs in the latter example presents an interesting cell source since facial MSCs derive from a neural crest origin. As such, these cells represent a unique source of progenitors that generate SCs.[300]

A nerve guide design developed by Owens et al. was also comprised of only cells, but this time forming multiple oriented channels approximately 500 μm in diameter.[301] The approach relies on the assembly of oriented agarose filaments to define a support structure into which fused filaments of cell aggregates are placed to form a tube. While this has been performed in an automated fashion in previous reports,[302] the current work performs these steps manually. The multichannel structure was created by placing 500 μm diameter agarose filaments during device assembly, which in principle can be removed after cell fusion. Altering the cellular composition of the consecutive filament cellularly generated compositional heterogeneity by having MSCs in the filaments placed around the epineurial periphery and more SCs located within the central endoneurial compartment. The structure was supported by a traditional nerve guide during implantation and showed clear nerve regenerative capacity in a rat animal model. However, poor mechanical integrity of the construct required that the agarose filaments which defined the microchannels were left in place, effectively blocking axon growth in a major region of the guide cross section.

A series of reports from the Chen lab employ HA hydrogels as an SC carrier and the extrusion of the cell-laden gel to form an oriented array of filaments.[77,78] A key aspect of this strategy is the deposition of the filament structure into a polyvinyl alcohol (PVA) bath, which acts to counter the filament buoyancy and to stabilize the filament diameter at approximately 200 um; the bath also facilitates rapid cross-linking via thrombin or calcium for HA gels blended with fibrin or alginate, respectively. This results in exquisite formation of a self-supporting structure of fused filaments shown in Figure 9a, with consecutive layers oriented at 80, 90, or 100°. This strategy forms 100 μm diameter microchannels between the filaments, all with a general orientation to better direct nerve growth. While these are again larger than endoneurial tubes and no *in vivo* testing has so far been reported, *in vitro* evaluation of SC growth shows good viability, and filaments are shown to exhibit oriented fibrin fibrils that induce cell alignment reminiscent of the bands of Büngner.

5.2.2.2. PNS Fabrication Considerations. The majority of bioprinting efforts center on creating a supportive environment for nerve regeneration (Table 3). While none of the studies discussed here evaluate the mechanical properties of their bioprinted constructs, the elasticity of the environment is known to have an impact on axon extension. Many reports have shown that peripheral axons have optimal growth on substrates with an elasticity greater than 1 kPa, in contrast with 55 kPa of the endoneurium.[303,304] However, while the intact basal lamina and myelin component around a single axon also have an elasticity of 55 kPa,[305] the cytoskeleton of SCs grown on such substrates achieves an elasticity of approximately 1.3 kPa.[306] These findings in combination with observations that axons adhere to SCs during regeneration suggest that the complex combination of extracellular and cellular mechanics is required to create the optimal microenvironments for nerve repair.

Further practical restrictions must be considered for surgical implantation of a nerve guide. In this regard, the suitability of both cell-only and hydrogel-based nerve guides remains an open question. Given the target tissue elasticity of approximately 50

https://dx.doi.org/10.1021/acs.chemrev.9b00789
Chem. Rev. 2020, 120, 11032−11092

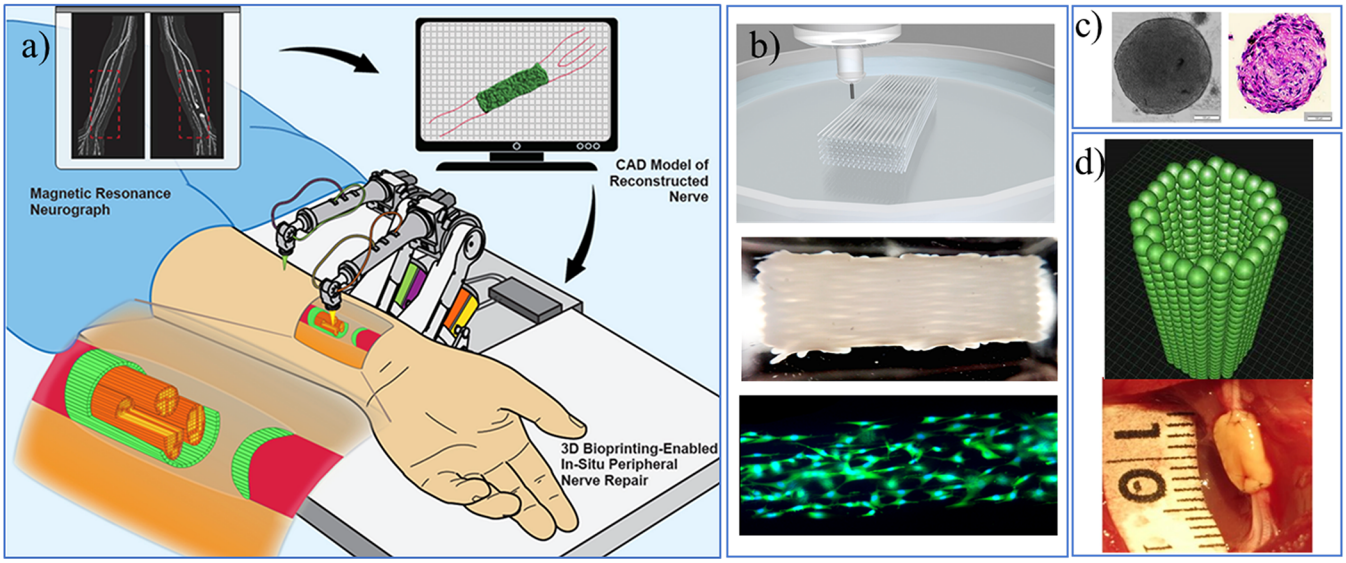

Figure 9. (a) Envisioned application of bioprinting to repair a peripheral nerve defect by directly depositing ECM and cells to recreate the characteristic anisotropic architecture. (b) A bioprinted anisotropic hydrogel structure containing SCs to provide trophic support for regenerating neurites and oriented open-pore structures to permit neurite growth across the nerve defect. (c) Cell aggregates carefully for Kensai method bioprinting and (d) aggregates arranged to form a scaffold-free nerve conduit, used to bridge a nerve defect to elicit repair. Adapted with permission from refs 77, 230, 298, and 299. Copyright 2018 Elsevier Ltd., 2016 Elsevier B.V., 2017 Yurie et al. (published by Public Library of Science), and 2018 Zhang et al. (published by Springer Nature).

kPa and the concurrent practical need to surgically immobilize a nerve guide in place, the most viable solution is to combine bioprinted structures with a traditional nerve guide or generate a multimaterial structure with a more resilient epineurium-mimicking outer layer.

The use of fibrin gel matches the composition of the natural PNS repair environment and provides a suitable substrate to stimulate repair, in contrast with the CNS. Further inclusion of additional factors, such as collagen type I, collagen type IV, and laminin, may also prove beneficial. However, many of these structural proteins can be produced and self-assembled by cells incorporated within the construct.[300,307]

A number of cell types have been shown to promote nerve repair, including adipose- or bone-derived MSCs. However, SCs remain the most likely candidate as they produce both ECM and growth factors suitable for nerve repair.[307−310] For research purposes, SCs are available as immortalized cell lines or isolated primary cells, though care must be taken regarding passage number and phenotype.[311−313] For more clinically relevant applications, it is possible to derive SCs from bone-derived MSCs, a readily available, patient-specific cell source.[314] The possibility of generating SCs from gingival MSCs, a neural crest derivative, also presents an interesting approach.[300]

With respect to nerve guide development, recreating an appropriate microarchitecture remains a challenge.[297] The oriented filament design presented by England et al.[77] provides an array of microchannels to direct nerve growth across a gap and emulates the aligned collagen fibrils of the native PNS ECM (Figure 9b). Presenting a regenerating nerve with a bulk hydrogel is known to impede nerve repair over long gaps; therefore, the incorporation of endoneurial-like anistropic porosity remains a critical objective.[315,316] Bioprinting fugitive structures within constructs could be a possible strategy to realize directed porosity after fabrication;[317,318] however, continued technical development is required to attain bioprinted structures of the same resolution as the endoneurial microstructure. Until then, a combination of bioprinting and FDM techniques represents a more accessible option to combine hydrogels with fugitive structures of an appropriate scale.[319,320]

5.2.2.3. PNS Future Outlook. Nerve guides are commercially available for clinical use, and research continues in this field, highlighting the immediate need for improved PNS nerve repair solutions.[296] Once bioprinting technology overcomes fabrication limitations, regulatory hurdles, and productions costs, the development of a bioprinted clinical solution for PNS repair is a realistic goal.

However, the bioprinting of neurons and neural integration within the context of complex tissue formation remains to be addressed. For example, parasympathetic ganglia exist within tissues, and this organization can be recreated via bioprinting. While a source for parasympathetic neurons still needs to be established, incorporating these cells would create more biologically representative tissues.[269,321,322] Concomitantly, the bioprinting of SCs or specific ECM components within an engineered tissue could be an interesting strategy to promote extrinsic innervation from the sympathetic and sensory populations. As the bioprinting and regenerative medicine fields at large move to create more functional tissues, the inclusion of the neural component, until now largely ignored, needs to be addressed, and the further development of bioprinting technologies and associated bioink materials will be essential to this process.

6. MESODERM

The mesoderm is the middle layer of the three germ layers developed from the inner cell mass during gastrulation. Gastrulation results in the formation of the primitive streak, which is divided along the anterior−posterior axis based on differential gene expression in cells. The anterior primitive streak gives rise to the definitive endoderm (discussed below), and its lineage-specific organs follow the formation of the gut tube along

https://dx.doi.org/10.1021/acs.chemrev.9b00789
Chem. Rev. 2020, 120, 11032−11092

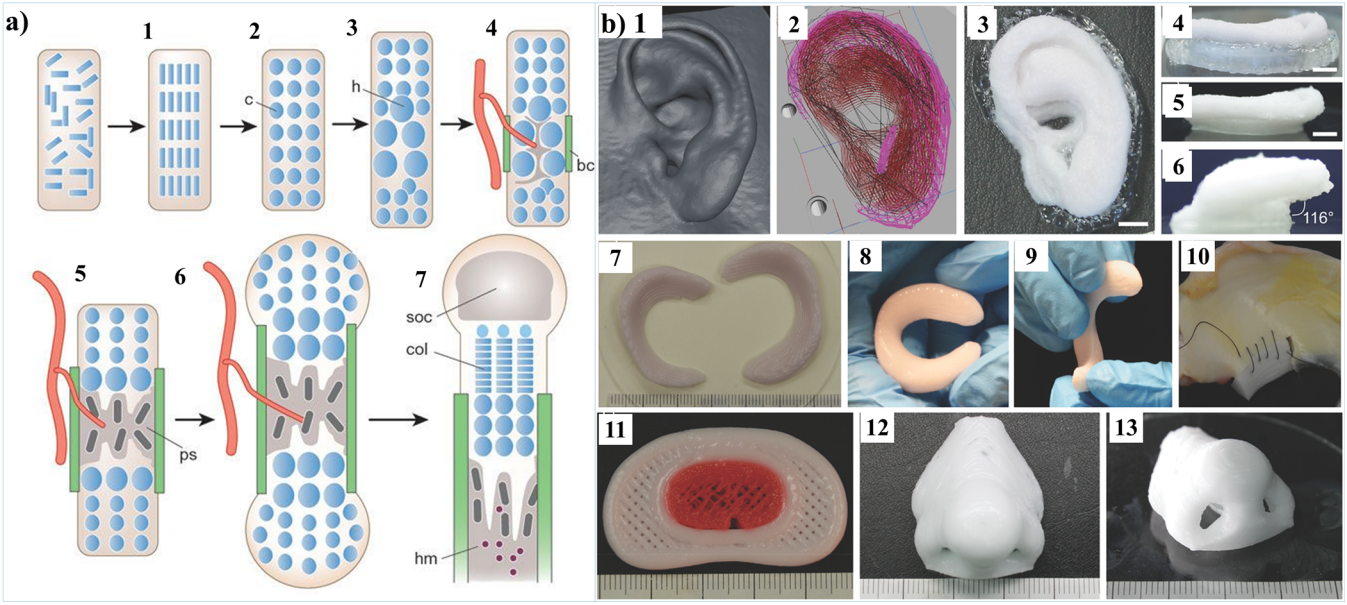

Figure 10. (a) Cartilage and endochondral bone formation. 1 - Mesenchymal cells condense, proliferate and 2 - differentiate onto chondrocytes (c). 3 - Chondrocytes at the center of condensation become hypertrophic (h). 4 - Perichondrial cells become osteoblasts and form the bone collar (bc). Hypertrophic chondrocytes direct the formation of mineralized matrix, attract blood vessels, and undergo apoptosis. 5 - Osteoblasts of primary spongiosa accompany vascular invasion, forming the primary spongiosa (ps). 6 - Chondrocytes continue to proliferate, lengthening the bone. Osteoblasts of primary spongiosa are precursors of eventual trabecular bone; osteoblasts of bone collar become cortical bone. 7 - At the end of the bone, the secondary ossification center (soc) forms through cycles of chondrocyte hypertrophy, vascular invasion, and osteoblast activity. The growth plate below the secondary center of ossification forms orderly columns of proliferating chondrocytes (col). Haematopoietic marrow (hm) expands in marrow space along with stromal cells. (b) Bioprinted cell laden hydrogels to create ear (1−6), meniscus (7−10), spinal disc (11), and nose (12, 13) grafts. Scale bars = 5 mm, and the smallest divisions on the ruler are 1 mm. Reprinted by permission from refs 353 and 354. Copyright 2003 Springer Nature and 2015 WILEY-VCH Verlag GmbH & Co. KGaA.

the growth factor gradient established along the dorso−ventral axis. Simultaneously, the posterior streak gives rise to a definitive mesoderm and the resulting tissues including musculoskeletal (cartilage and bone), cardiovascular and immune systems, kidneys, and gonads.

6.1. Cartilage

Cartilage is the elastic connective tissue formed in the early stages of embryonic development that serves as a template for bone growth and persists in some parts of the mature skeleton. It is present in the body in three main forms: elastic cartilage, fibrocartilage, and hyaline or articular cartilage, each accounting for specific functions.[323,324] While all the three cartilage types are characterized by a high water content (65−80 wt %) and a collagen II- and GAG-rich ECM supported and maintained by chondrocytes, there are substantial differences between them. Elastic cartilage, located at the outer ear and epiglottis for example, has an elastin-rich ECM that provides elasticity to the tissue, whose main function is to provide support while maintaining structure and shape upon repetitive bending.[323,325] Fibrocartilage, the toughest of the three, has a collagen I-rich ECM (as well as collagen II) that brings extra stiffness and reduced elasticity to the tissue. Fibrocartilage is thus located at high load-bearing areas such as the meniscus, the annulus fibrosus of the intervertebral discs, and the entheses.[323,325]

Hyaline or articular cartilage is present at the end of long bones, such as the knee, elbow, hip, and shoulder joints, serving as an interface that reduces the friction and allows rotational and translational movements while bearing and transferring the loads applied to the synovial joints during articulation.[326] Articular cartilage, isotropic in structure at birth, progressively develops into an anisotropic structure as a consequence of the continuous loading to which it is subjected and appears well-defined at skeletal maturity.[327,328] Adult hyaline cartilage is characterized by three distinct zones (superficial or persistent, intermediate or proliferating, and deep or hypertrophic zones), each with different ECM components, and the arcade-like collagen II organization along the depth of the tissue.[324,328−330]

The superficial zone (10−20% of the cartilage thickness) is responsible for minimizing friction and, thus, is covered by a thin layer (few hundreds of nanometers up to a micrometer) of accumulated proteins, such as lubricin or proteoglycan 4 (PRG4), known as the *lamina splendens*.[331,332] The superficial zone accounts for a densely packed collagen II fiber network that is organized in parallel to the articulating surface.[333,334] Cartilage of this zone has a low concentration of GAGs that allows for a higher fluid flow.[335−337] The intermediate zone (40−60% of the cartilage thickness), bearing and dissipating most of the load applied on cartilage, accounts for the characteristic arcade-like collagen II fiber orientation.[334] Here, the concentration of GAGs is higher with very little fluid flow. The deep zone of cartilage (20−50% of the cartilage thickness) is responsible for transferring the loads to subchondral bone. Collagen II fibers appear perpendicular to the underlying bone, and collagen X is also present.[334] The concentration of GAGs is maximal, allowing for very little or no fluid flow.[337] The ECM components (collagen II and GAG concentrations) and the structure of the different zones (arcade-like) are responsible for the strength and pressurization of the tissue via entrapment of water molecules, which together and in combination with permeability and viscoelasticity result in a tissue with anisotropic and poro-viscoelastic mechanical properties.[337,338] Thus, articular cartilage accounts for an aggregate modulus of 0.08−2 MPa and a

https://dx.doi.org/10.1021/acs.chemrev.9b00789
Chem. Rev. 2020, 120, 11032−11092

Young's modulus of 0.3−0.8 MPa in compression and 5−25 MPa in tension.[339−344] The dynamic compressive Young's modulus of bovine articular cartilage has been reported to be as high as 9.64 ± 1.81 MPa, as compared to the equilibrium Young's modulus of 0.64 ± 0.16 MPa.[74] Similarly, a dynamic compressive Young's modulus of human articular cartilage of around 4 MPa[337]has been reported as compared to approximately 0.6 MPa in equilibrium conditions.[345]

The formation of articular cartilage starts when the condensation of stem cells arising from the mesoderm subsequently comes closer on the center of the condensate and forms gap junctions and a dense structure parallel to the bone anlagen.[346] Here, the interzone develops as a morphogenetic process that will later give rise to the synovial joint. After complete formation of the joint, the cartilage appears at the end of still developing bones that together form the growth plate (Figure 10a).[347] The superficial zone is responsible for the appositional growth of the tissue with chondrocytes that are persistent and become only proliferative when they reach the middle zone. Finally, the deep zone is responsible for the formation of subchondral bone with chondrocytes that become hypertrophic.

Due to its avascular character, the low concentration of cells, and the intrinsic nonproliferative character, cartilage is unable to self-heal or regenerate onto a functional tissue.[324,329,348,349] Tissue engineering of non-load-bearing cartilage such as the nose and ear has been successfully achieved (Table 4). The first (and most visual) results appeared two decades ago by Cao et al., who created an artificial ear by seeding bovine chondrocytes on a nonwoven poly(glycolic acid) (PGA) mesh that was further embedded in PLA by solvent-casting processes with an alginate mold.[350] The constructs were subcutaneously implanted into athymic mice; after 12 weeks, they showed a gross histologic appearance of neocartilage. The main drawback of this study was the need of a support material to avoid sample collapse during *in vivo* implantation. Encouraged by these results, several groups have attempted to tissue-engineer ear cartilage via AM techniques. Poly(caprolactone) (PCL) provides good structural properties and has been the most used in FDM or SLS to create stable biodegradable scaffolds that were then seeded with cells (either chondrocytes or stem cells) with or without the aid of hydrogel materials such as collagen I.[70,351] Recently, FDM-generated PCL scaffolds have been exploited as the main substrate in the first clinical application for auricular reconstruction.[352]

Although these approaches are promising, the amount of cells that can be encapsulated within the fabricated constructs is limited to porosity and pore size. Thus, cell-based bioprinting appears as an ideal technique. As mentioned earlier, the main difficulties arise from the need of materials with good structural stability and sufficient elasticity to allow repeated bending or compression of the construct (Table 4). Alginate has been widely used as a cell-encapsulating hydrogel for bioprinting techniques. However, it lacks sufficient stability for this particular application. In order to overcome this issue, Markstedt et al. developed a novel bioink based on a nanofibrillated cellulose−alginate composite that was used in combination with human chondrocytes to produce ear-shaped and meniscus-shaped scaffolds.[93] These materials showed cell viability after 7 days of culture, good printability and structure, and mechanical properties that could be tuned from 50 to 250 kPa (compressive stiffness) depending on the cellulose weight (%) loading. However, it is noteworthy that nanofibrillated

Table 4. Bioprinted Approaches for Cartilage Tissue

tissue	cells	composition	structure	mechanical properties	method	sequence	comments	ref
elastic cartilage and fibrocartilage	primary human nososeptal chondrocytes	alginate matrix and nanofibrilated cellulose	90 deg grid pattern; ear and meniscus shape	commpressive stress of ≈60−240 kPa (depending on cellulose content)	pressure-based bioprinting	postprinting cross-linking in $CaCl_2$	*in vitro* preeliminary study; only cell viability was reported	93
elastic, hyaline, and firbocatilage	primary bovine articular chondrocytes	gellan and alginate mixed with human micronized biocartilage or HAp particles	stuck fibers to create ear, nose, menisci, and spinal disk	maximum storage modulus (shear) of 96 ± 1.0 kPa for biocartilage reinforced gels and 110 ± 2.0 kPa for HAp	pressure-based bioprinting	co-extrusion with support material providing cations for cross-linking	*in vitro* long-term cultures (8 weeks); deposition of GAGs and collagen II	354
elastic cartilage	primary rabbit ear chondrocyes	gelatin, fibrinogen, HA, glycerol	90 deg grid patter to create ear-shaped scaffolds	maximum normalized load of ≈20.000 N/m^2	ITOP, pressure-based, thermally assisted multimaterial printing	simultaneous printing of cell-laden hydrogels and support material	*in vivo* subcutaneaous implantation in athymic mice	377
articular cartilage	primary human articular chondrocytes	PCL and GelMa	disks with a 90 deg grid internal pattern	equilibrium compressive modulus of 130 ± 7.8 kPa	melt-electrospining writing of thermoplast and injection molding of hydrogel	fabrication of PCL scaffolds, etching, and injection molding of hydrogel	*in vitro* cultures needed the incorporation of HA; higher expression of collagen I and X than collagen II	369
articular cartilage	primary equine chondrocytes	PEG or HA cross-linked PEG-NIPAm-HPMACys and PCL	90 deg patterns to create discs, femoral condiles, or cones	compressive dynamic Young's modulus of 645 ± 12 kPa	extrusion-based and pressure-based bioprinting	FDM of PCL, addition of pre-cross-linked gel and photo-cross-linking	*in vitro* preliminary study; only cell viability was reported	371
osteochondral defect	hMSC	*N*-acryloyl glycinamide and *N*-[tris(hydroxymethyl)methyl] acrylamide copolymer with TGF-*β* on cartilage phase and *β*-tricalciumphosphate on the bony phase	90 deg grid patterns	compressive Young's modulus of 16 and 23 kPa for cartilage and bone phases	extrusion-based thermally assisted printing	printing and gelation via sol−gel transition of the supramolecular polymer	*in vitro* and *in vivo* regenerative potential	378

https://dx.doi.org/10.1021/acs.chemrev.9b00789
Chem. Rev. 2020, 120, 11032−11092

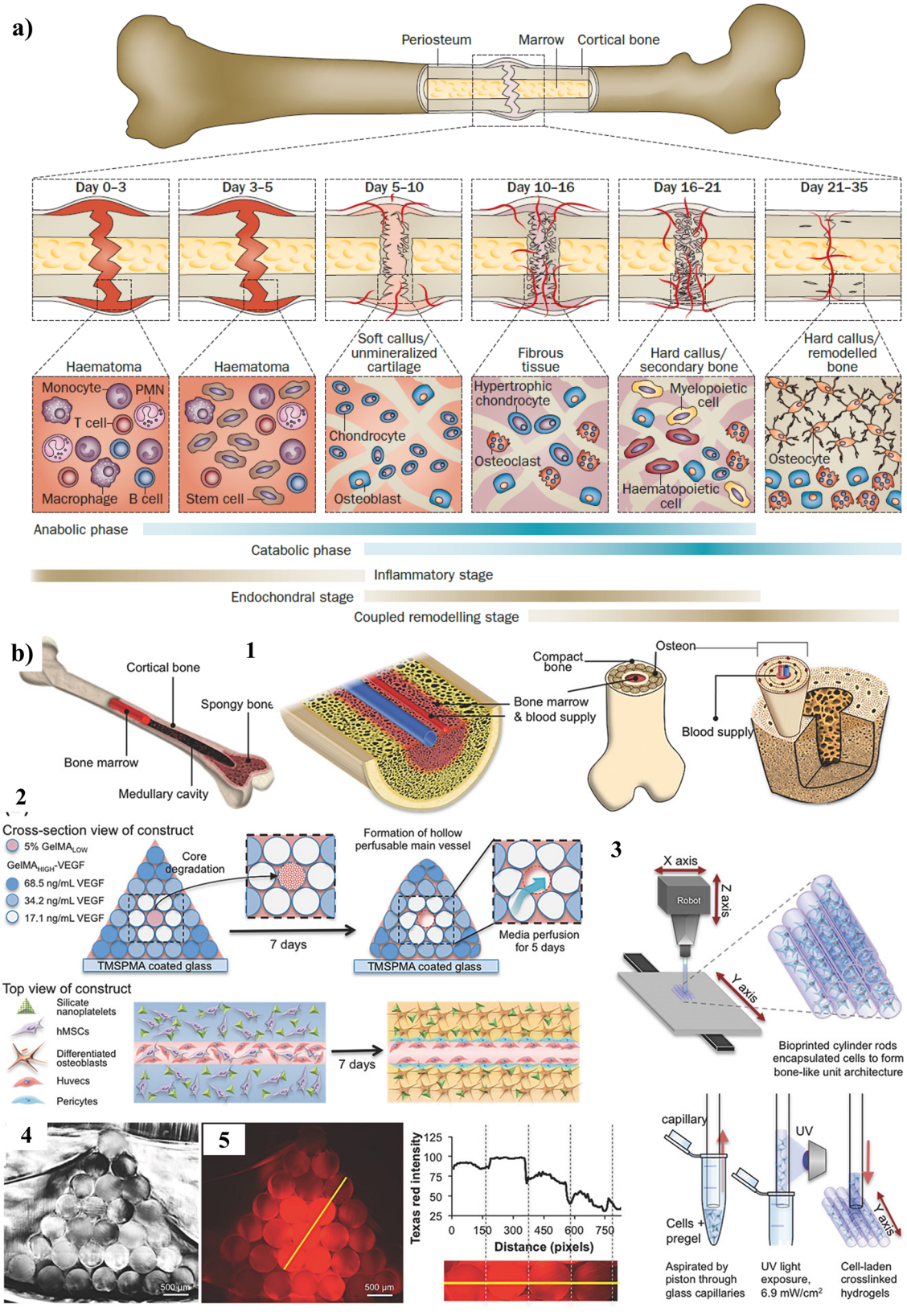

Figure 11. (a) Bone healing mechanism. The primary metabolic phases (anabolic and catabolic) of fracture healing are presented in the context of three major biological stages (inflammatory, endochondral bone formation, and coupled remodeling) that encompass these phases. The primary cell types that are found at each stage and the time span of their prevalence in each stage are denoted. Upon injury, specific-cell-mediated immune functions remove necrotic tissues, promote angiogenesis, and initiate repair (0−3 days). Stem cells are recruited from the skeletal and vascular tissue, forming an initial cartilaginous callus that is later vascularized (5−10 days). On the periphery of the callus, the periosteum swells initiating the primary bone formation. Chondrocytes within the newly formed callus proliferate and differentiate, reaching hypertrophy (10−16 days). Hypertrophic chondrocytes mineralize the existing matrix template and undergo apoptosis. After this initial phase, resorption and remodelling occur simultaneously,

https://dx.doi.org/10.1021/acs.chemrev.9b00789
Chem. Rev. 2020, 120, 11032−11092

Figure 11. continued

and secondary bone formation begins (16−21 days). Osteoclasts resorb the formed matrix template that, after being cleared by macrophages, is remodelled by a differentiated osteoblast that will form the osteoid (21−35 days). (b) Schematic bone structure (1) and fabrication of bone mimetic 3D architecture containing osteogenic and vasculogenic niches. (2) A perfusable vascular lumen lined with HUVECs can be fabricated within a pyramidal bioprinted construct by arranging individual rods of VEGF-functionalized GelMA bioinks with different mechanical strengths. The hMSC-laden three outer layers of cylinders were loaded with silicate nanoparticles to induce osteogenic differentiation of hMSCs into bone tissue. The VEGF was covalently conjugated into the three outer layers of the cylindrical hydrogels. The concentrations of conjugated VEGF were determined with ELISA as 17.1, 34.2, and 68.5 ng mL^{-1}. (3) Scheme of the 3D printing procedure of independent cell-laden cylinders using an automatized and computer-controlled bioprinter. (4) Cross-section image of the pyramidal bioprinted construct. (5) Chemical conjugation of a gradient sulforhodamine 101 (Texas Red) cadaverine onto −COOH-modified GelMA bioprinted fibers. The fluorescence intensity was directly proportional to the conjugated amount of the fluorescent dye. Adapted with permission from refs 387 and 388. Copyright 2014 Springer Nature and 2017 WILEY-VCH Verlag GmbH & Co. KGaA.

cellulose contains crystalline domains that require acidic environments (or enzymatic processes) to degrade, rendering the material biopersistent. In a very elegant study, Zenobi-Wong and co-workers developed a bioink based on a combination of clinically compliant biomaterials (all FDA approved for clinical use) alginate, gellan gum, and cartilage ECM particles that could be *in situ* cross-linked by coextrusion with a cation-loaded polymer and a support bath containing mono- and divalent cations.[354] Bioprinting of the bioink together with cells proved successful, yielding constructs with tensile mechanical properties of 116 kPa and high cell viability. The developed bioink was used to create tissue-engineered ears, noses, menisci, and intervertebral discs (Figure 10b). Although these constructs show promise, different cartilaginous tissues account for different biochemical and mechanical properties, which was not taken into consideration in this first study.

Tissue engineering of load-bearing cartilage, i.e., articular cartilage of the synovial joints, presents a more difficult challenge due to the outstanding mechanical properties of its multizonal structure. Thus, regeneration of these tissues requires significant attention to the structure and mechanical properties of the implanted materials. Traditionally, FDM techniques have used polymer thermoplastics, such as PCL and PLA, which are stiff and show poor resilience upon compression, unlike the mechanical properties of native articular cartilage.[355−360] Moreover, cell culture on these types of materials generally results in cell morphologies that are not representative of chondrocytes (spread vs rounded), promoting dedifferentiation of the cells.[361−363] In comparison, fabrication of hydrogel-based scaffolds, where chondrogenic differentiation is more likely to occur, results in mechanical properties that are rather low compared to the native tissue. Thus, efforts have been focused on the development of novel materials, or combinations thereof, which result in scaffolds with adequate mechanical properties while maintaining and promoting a chondrogenic phenotype (Table 4). Kun-Che et al. developed water-born elastic and biodegradable polyurethane nanoparticles based on PCL-diol and polyethylene butylene adipate diol as soft segments and isophorone diisocyanate as the hard segment, both used to fabricate scaffolds via FDM.[364,365] The resulting scaffolds displayed a dynamic Young's modulus of 0.4 MPa with a shape recovery that ranged from 88 to 57% for 1−10% strain, respectively. These materials induced aggregation of MSCs and promoted chondrogenesis both *in vitro* and *in vivo*. However, even if elastic in nature, articular cartilage is subjected to strains of approximately 30% on a daily and cyclic basis and is capable of recovering 100% of its initial shape after a long period of rest.[366] In order to match the mechanical properties of articular cartilage, traditional hydrogels such as GelMa, alginate, or the thermoresponsive poly(PNIPAm) have been slowly substituted by more complex polymer networks that aim at generating scaffolds with a higher compressive modulus. In the last years, Malda and co-workers have created an important library of bioprintable hydrogel systems and combinations of bioprinted hydrogels covalently attached to FDM thermoplasts to tackle this issue.[367−372] These include cell-laden microcarriers based on PCL and encapsulated with GelMa-gellan gum bioinks and two component hydrogels based on a thermoresponsive triblock copolymer of PEG-NIPAm-HPMACys (*N*-(hydroxypropyl methacrylamide) partially cross-linked to a PEG- or HA-modified macromolecule and grafted to a thermoplastic network, between others, with mechanical properties that are on the order of hundreds of kPa. In this regard and similar to the work described previously, Atala and co-workers developed an integrated tissue-organ printer (ITOP) that allowed the simultaneous deposition and modeling of several materials within the same printer.[373] By these means, they fabricated hydrogel-based, thermoplast-supported scaffolds for the regeneration of various tissues such as cartilage, bone, and skeletal muscle.

Another important approach to regenerate articular cartilage is based on microfracture techniques that aim at the recruitment of MSCs from the bone marrow, forming a clot on the damaged area that should later be remodeled, prompted by the scaffold's material, into functional tissue. Thus, the designed scaffolds need to fulfill the requirements of two different phases, mimicking and promoting the formation of articular cartilage in one phase or layer and the dramatically different underlying subchondral bone.[374,375] Gao et al. provided a good example of this biphasic system and the required development of materials with specific mechanical properties that can be printed onto scaffolds mimicking the osteochondral interface.[376] They synthesized a high-strength supramolecular hydrogel based on the copolymerization of two hydrogen-bonding materials: *N*-acryloyl glycinamide and *N*-[tris(hydroxymethyl)methyl] acrylamide. The resulting copolymer is thermoresponsive and could be deposited following sol−gel processes, reaching a compressive strength of 8.4 MPa but a Young's modulus of only 137 kPa for the less porous hydrogels. Loading of the material with transforming growth factor-β (TGF-β) on the cartilage-mimicking phase and β-tricalcium phosphate on the deep bone-mimicking phase resulted in materials with compressive Young's moduli of 16 and 23 kPa, respectively. The combination of these onto a biphasic scaffold showed potential to regenerate osteochondral defects on an *in vivo* rat model.

6.2. Bone

Bone is a hierarchically structured bioceramic composite connective tissue forming the skeleton that confers structure,

https://dx.doi.org/10.1021/acs.chemrev.9b00789
Chem. Rev. 2020, 120, 11032−11092

support, and organ protection while allowing for movement. Bone is composed of 65% (wt) inorganic material, 25% (wt) organic material, and 10% (wt) water. The inorganic component of bone (bone apatite) is mainly HAp that appears as small platelets of approximately 5 nm in thickness, 50 nm in width, and 100 nm in length, surrounding and infiltrating the collagen fibrils.[379−381] Apatite appears in a plethora of variations from its stoichiometric ratio with ions from the physiological fluids exchanging for any of its main components, PO_4^{3-}, Ca^{2+}, or OH^-.[382,383] The organic phase of bone is primarily composed of collagen I (>90 wt %) and minor amounts of glycoproteins, such as alkaline phosphatase, fibronectin, osteopontin, osteoadherin, and proteoglycans such as versican.[384] It also contains minor amounts of γ-glutamic-acid-containing proteins such as osteocalcin and matrix gla protein. The inorganic and organic components arrange into a very well-defined radial and hierarchical structure. Collagen fibers, mineralized by nanosized HAp, form fibril arrays that localize surrounding the blood vessels on the Haversian channels, all together forming the osteon. Osteons form the compact bone that appears to cylindrically surround the trabecular or spongy bone (Figure 11a). Although compact bone and spongy bone are comprised of the same components, they differ largely in their structure, porosity (10% vs 50−90%, respectively), and mechanical properties (the former ten times higher than the latter).[382,385]

Bones come in many shapes and sizes, and most of them (few exceptions) arise from the endochondral ossification process. Flat bones, such as the ones of the skull, are formed by direct differentiation of clustered stem cells into osteoblasts, depositing a collagen I-rich ECM via a process known as intramembranous bone formation. Long bones, however, are formed after the cartilage from the bone anlage. Hypertrophic chondrocytes of the deep zone of cartilage are primarily responsible for bone formation. They enlarge, direct mineralization, attract surrounding chondroclasts, and promote the differentiation of perochondrial cells into osteoblasts that form the bone collar and promote vascularization, forming the primary spongiosa. After completing these essential functions, hypertrophic chondrocytes undergo apoptosis, leaving a cartilaginous scaffold behind that serves as a template for bone formation, the so-called growth plate. Osteoblasts from the primary spongiosa will form trabecular bone, and the bone collar will eventually become cortical bone. This ossification process occurs in two distinct centers (primary and secondary), giving rise to the long bones (Figure 10).[353,386]

Bone is capable of self-healing upon fracture or when small defects are to be bridged (generally considered as less than two times the diameter of the affected bone).[389,390] Upon fracture and after an initial inflammation stage, bone healing occurs similarly to the endochondral formation. Stem cells are recruited from the skeletal and vascular tissue, forming an initial cartilaginous callus that is later vascularized. The increase in vascularization is reflected as an increased blood flow into the damaged area. On the periphery of the callus, the periosteum swells, initiating the primary bone formation. Chondrocytes within the newly formed callus proliferate and differentiate, reaching hypertrophy. Hypertrophic chondrocytes mineralize the existing matrix template and undergo apoptosis. After this initial phase, resorption and remodeling occur simultaneously, and secondary bone formation begins.[387] Osteoclasts resorb the formed matrix template that, after being cleared by macrophages, is remodeled by differentiated osteoblasts, which will form the osteoid. This coupled process continues until a balance between the resorbed and remodeled matrix is reached (Figure 11b).[391]

However, bone is unable to successfully heal large defects (critical size defects), which are currently treated using autologous bone grafts, generally successful but complicated by the limited availability and extra surgery steps. Thus, bone regeneration or TERM appears as an attractive alternative to this problem.[392] Three main problems arise when TERM bone replacements are conceived: (i) the scaffold material should have high mechanical properties while being biodegradable and porous (allowing for cell infiltration and new matrix deposition); (ii) the scaffold material should have a sophisticated hierarchical structure to mimic that of the native tissue; and (iii) the need for vascularization in such large tissue substitutes.[393−396]

In contrast to articular cartilage, bone regeneration strategies have profited from traditional stiff materials such as cements, ceramics, and metal alloys.[397−401] The FDM of ceramic and/or metal-reinforced polymers has proven successful in mimicking the overall mechanical properties of the native tissue and, in some examples, the structure.[402−405] However, as explained above, this technique has a limitation with the amount of cells that can be successfully loaded within the manufactured scaffold. Bioprinting of robust scaffolds that can reach the high mechanical properties of bone and allow for vascularization remains elusive due to the lack of adequate materials (Table 5). Initial approaches to overcome this issue have focused on the reinforcement of cell-laden hydrogels such as gellan gum with more robust thermoplastic materials such as PCL using a multicompartment approach.[406] The work by De Giglio et al. used porous interconnected PCL FDM scaffolds that were later infiltrated with a gellan gum matrix loaded with either human umbilical vein endothelial (HUVEC) or stem cells. Exploiting their osteogenic properties, strontium ions were used as a cross-linking agent and finally assembled within compartments of different sizes. This multicompartment and cell coculture system showed a high Young's modulus of 135 MPa and a higher osteogenic potential (alkaline phosphatase activity, osteopontin, and osteocalcin expression) compared to the individual materials and composite materials cross-linked with Ca^{2+} ions. Following the approach of reinforcing hydrogel materials, Keriquel et al. reported *in situ* laser-assisted bioprinting of MSCs *in vivo*.[407] The technique is based on a near-infrared pulsed laser beam coupled to a scanning mirror and a focusing system. A ribbon is used to spread the cell-laden bioink in which the beam is focused. The energy generated creates a cavitation bubble that will then propel a microdroplet containing the cell-loaded hydrogel to the substrate of interest.[408] In this particular case, the authors used a bioink consisting of collagen I and nano HAp bearing the MSCs that were *in situ* bioprinted onto a calvaria-defect model in mice. This method provided spatial control over the cell structure and localization, thus potentially mimicking the native structure of bone and an improvement in the bone formation after two months compared to non-cellularized scaffolds.[409,410] However, the produced materials were still too thin to represent a mechanically robust system to be further exploited.

In a more sophisticated model that mimics the hierarchical structure of bone, Byambaa et al. reported the fabrication of bioprinted scaffolds with osteogenic and vasculogenic patterns (Figure 11b).[388] The microstructured scaffolds consisted of a cylindrical core of 5% (wt/vol) VEGF-GelMa loaded with HUVECs and MSCs and three successive concentric layers of 10% (wt/vol) GelMa loaded with silicate nanoparticles and

https://dx.doi.org/10.1021/acs.chemrev.9b00789
Chem. Rev. 2020, 120, 11032−11092

Table 5. Selected Bone Bioprinting References

tissue	cells	composition	structure	mechanical properties	method	sequence	comments	ref
flat bone (calvaria)	hMSCs	collagen I and nano-HAp	disk and ring, droplet based	n/a	laser-assisted bioprinting	direct deposition on bone deffects	*in vivo* rat calvaria model showing bone formation	407, 409, 410
flat bone (mandible and calvarial)	human amniotic PSCs	gelatin, fibrinogen, HA, gycerol	90 deg pattern grid	n/a	ITOP, pressure-based, thermally assisted multimaterial printing	simultaneous printing of cell-laden hydrogels and support material	*in vitro* mandible and *in vivo* in a rat calvarial model	377
long bone	HUVECs and hMSCs	VEGF-loaded GelMa and VEGF-loaded GelMa with silicate nanoparticles	radially stuck cylinders; gradient composition	n/a	extrusion-based bioprinting	printing of already photo-cross-linked hydrogels	*in vitro* sacrificial inner core to promote vascularization	388
endochondral bone	hMSCs aggregates	silk and gelatin	90 deg pattern grid	n/a	pressure-based bioprinting	n/a	*in vitro* developmental approach	411

MSCs to induce osteogenesis. These last layers also contained increasing concentrations of VEGF, aimed at promoting the formation of a capillary network (Figure 11c). The soft core allowed for a rapid (12 day) degradation, followed by cell adhesion onto the formed inner cylinder that supported the formation of a perfusable vessel-like lumen. The cells cocultured on this lumen differentiated into smooth muscle cells, while the MSCs encapsulated within the outer layer showed characteristic markers of bone niches with markedly upregulation of collagen I, osteocalcin, and osteopontin, among others.

A more realistic method to regenerate bone via bioprinting techniques, with the current state of materials, is the developmental approach. Such an approach consists in the fabrication of scaffold materials capable of generating an initial cartilage callus that can be later resorbed and remodeled into bone tissue. In this regard, Chawla et al. fabricated MSC-laden, silk-gelatin-based bioprinted scaffolds that were exposed to a 3 week chondrogenic differentiation step followed by a 2 week differentiation in osteogenic conditions.[411] Following this approach, cell gene expression patterns that closely resembled those found during *in vivo* endochondral bone formation were observed, with initial expression of early markers of chondrocyte hyperthrophy, such as RunX2 and collagen I, followed by osteogenic markers such as alkaline phosphatase, osteopontin, and osteocalcin and finally expression of osteocytic genes such as podoplanin, dentin matrix acidic phosphoprotein-1, and sclerostin. Although further studies would need to be developed, with special attention paid to matrix deposition, mineralization, remodeling, and final mechanical properties, this work represents a very interesting approach to bone regeneration via bioprinting techniques.

6.3. Blood Vessels

Blood vessels are fundamental in keeping tissues and organs alive, by transporting nutrients and collecting waste metabolites. Two distinctive processes can generate blood vessels: vasculogenesis and angiogenesis. Vasculogenesis occurs during embryological development in the presence of no other blood vessels, when progenitor endothelial cells (ECs) self-organize in response to local biological cues (e.g., provided by growth factors and ECM proteins) to form new blood vessels. Angiogenesis occurs when blood vessels already exist: in this case, new blood vessels stem out from the existing ones through cell sprouting and the formation of new tubular structures, again in response to local biological signals.[412]

Blood vessels are also organized in a vascular tree network, decreasing in dimension from the heart to the periphery of the body. Arteries bring blood from the heart to the periphery, whereas veins collect blood from the periphery back to the heart. Independent from their caliber, all vessels have an internal layer of ECs, the endothelium, deposited on top of an ECM called the basal membrane, which is typically comprised of collagen type IV, laminins, and integrins. The smallest blood vessels in our body, named capillaries, are characterized only by the endothelium and the basal membrane. Large and mature blood vessels have a more hierarchical structure comprised of three additional ECM layers on top of the basal membrane, called tunica intima (most internal layer), media, and adventitia (most external layer). These layers are organized with collagen fibers taking specific orientation (e.g., helical found in small resistance arteries or herringbone found in large elastic arteries), which contributes to the mechanical properties of blood vessels.[413] The ECM includes collagen type I fibers, which are

https://dx.doi.org/10.1021/acs.chemrev.9b00789
Chem. Rev. 2020, 120, 11032−11092

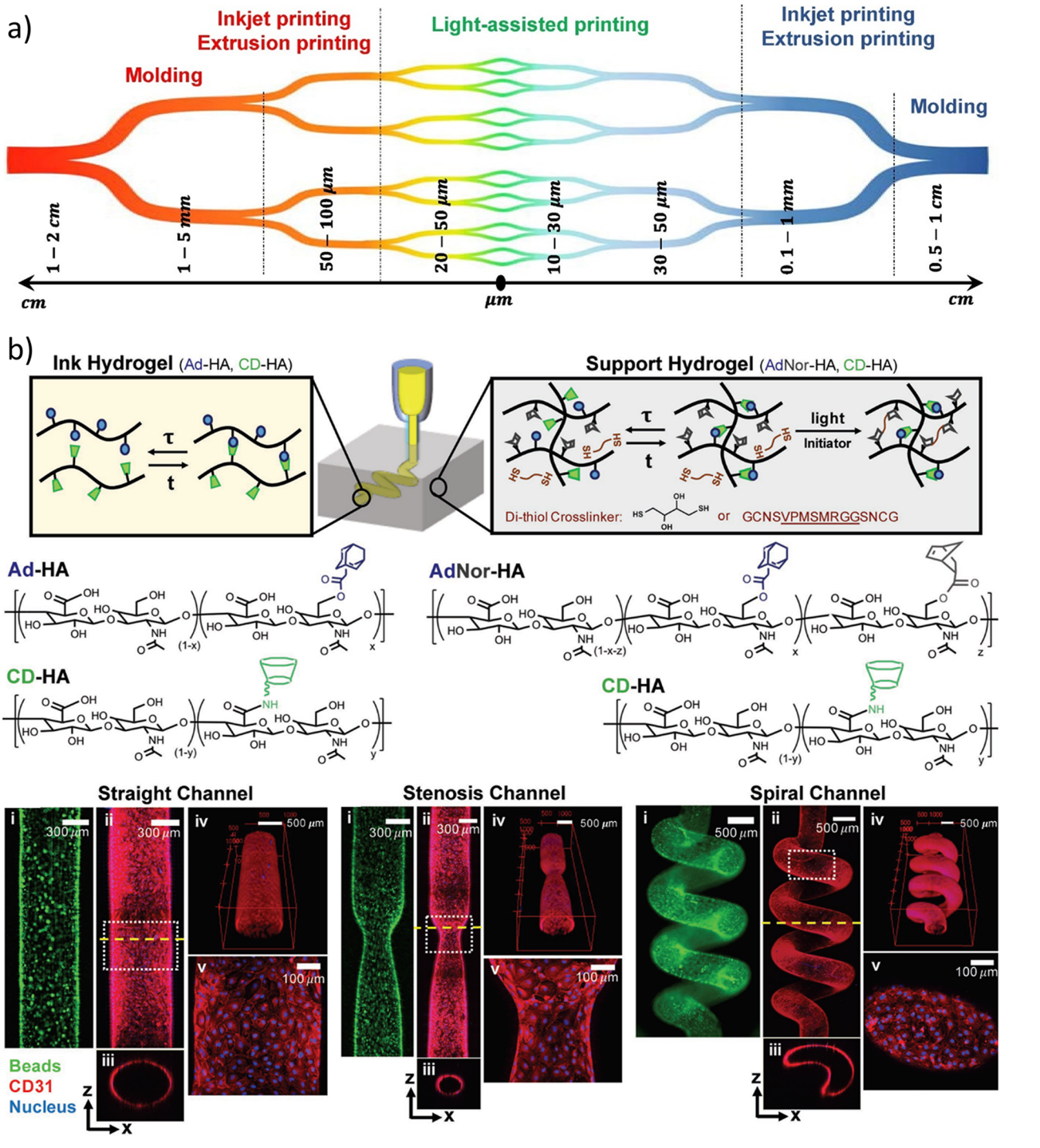

Figure 12. (a) Currently available fabrication technologies to create a branching vascular network. (b) An example of how hydrogels can be designed to provide gel-in-gel bioprinting capabilities through host−guest interactions. Different endothelialized channels of variable complex architecture are showcased. Adapted with permission from refs 415 and 418. Copyrights 2018 Elsevier Ltd. and 2018 WILEY-VCH Verlag GmbH & Co. KGaA.

present through the vessel ECM but mostly abundant in the external tunica adventitia layer. Collagen is mostly responsible for the tensile stiffness of blood vessels. Elastin is also a crucial ECM component and is still a challenging protein to be synthesized during regeneration. Elastin is mostly present in the tunica intima and media and can take various organizations (e.g., lamellae or fibers) depending on the vessel location and mechanical function in the body. Elastin confers compliance and combined with collagen prevents plastic deformation of the vessels during pulsatile flow and regulates proliferation, phenotypic modulation, and organization of vascular smooth muscle cells. Other ECM proteins include collagen type III, proteoglycans (e.g., GAGs), and glycoproteins (e.g., lectins). Proteoglycans contribute to the compressibility of blood vessels.[414]

Blood vessels vary in diameter from 1 to 2 cm to a few microns for capillaries. When approaching the fabrication of vessel constructs, different biofabrication technologies[415] could be

https://dx.doi.org/10.1021/acs.chemrev.9b00789
Chem. Rev. 2020, 120, 11032−11092

Table 6. Examples of Bioprinted Studies Where Blood Vessels Were Developed

tissue	cells	composition	structure	mechanical properties	method	sequence	comments	ref
vessels	human umbilical vein smooth muscle cells	cell spheroids; agarose as a mold	branched vessels	n/a	pressure-driven extrusion	vascular spheroids deposited onto an agarose supporting template, thus facilitating spheroid fusion	*in vitro*	302
vessels	HUVECs and human aortic smooth muscle cells	cell spheroids; alginate as a mold	vessel segments	n/a	pressure-driven extrusion	vascular spheroids deposited onto an alginate supporting template	*in vitro*	416
vessels	mouse embryonic fibroblasts	cell spheroids; agarose as a mold	vessel anatomical segments	n/a	pressure-driven extrusion	vascular spheroids deposited onto an agarose supporting template	*in vitro*	417
vessels	HUVECs	matrigel, fibrin, collagen, gelatin, agarose, pluronic, alginate, and alginate/gelatin	no structure; cell−material interactions	n/a	inkjet	different cell-laden hydrogels (i.e., bioinks) screened to assess best formulations to maintain cell viability and promote tubular formation	*in vitro*	419
vessels	HUVECs ad human dermal fibroblasts	agaorse; collagen type I; fibrin	capillaries	from ∼150 Pa to ∼1.5 KPa	pressure-driven microvalve inkjet	bioinks screened for enhanced tubular formation	*in vitro*	420
vessels	HUVECs, human umbilical aortic smooth muscle cells, human dermal fibroblasts	fibrin and collagen type I	small vessels and capillaries	from 0.6 to 6 kPa	electromagnetic microvalve inkjet	sequential bioprinting followed by fibroblast casting to replicate the tunica intima, media, and adventitia organization of mature large blood vessels	*in vitro*	421
vessels	mouse fibroblasts	tetra(PEG) tetra-acrylate derivatives with thiolated HA and gelatin	vesssel segment	from ∼100 Pa to ∼800 Pa	presure-driven extrusion	bioprinting of cell-laden filaments onto an alginate supporting template	*in vitro*	422
capillaries	human dermal fibroblasts	α,ω-poly(tetrahydrofuran-ether diacrylate)	bifurcating small vessels	from 8 MPa to 27.5 MPa	photopolymerization	fabrication of small-sized vessels seeded with cells	*in vitro*	423
vascularized heart patch	HUVECs and hiPSCs-derived CMs	alginate and PEG-fibrinogen	small vessels to vascularize a heart tissue engineered construct	n/a	microfluidic bioprinting	alternating bioprinting of CMs and HUVECs to study the most optimal configuration for vascularization of a cardiac-like tissue construct	*in vitro* and *in vivo*	167
vascularized bone	HUVECs and hMSCs	GelMA; silica nanoplates	capillary network and central vessel to vascularize a bone tissue engineered construct	∼6 kPa	pressure-driven extrusion	HUVECs and hMSCs were encapsulated in gelMA for bioprinting; different degree of methacryloyl substitution of gelMA with different degradation rate induced HUVECs to remodel the gel and form a central vessel into the surrounding bone-like constructs	*in vitro*	388
vessels	mouse fibroblasts, human ECs, hepatocytes	collagen and alginate	vessel segments of complex shapes	from ∼0.1 kPa to ∼1 kPa	pressure-driven extrusion	customization of bioprinting cartridges; cell-laden hydrogels were inserted in different compartments of the cartridges for complex construct bioprinting	*in vitro*	424
vascular network	HUVECs, rat hepatocytes	agarose, alginate, PEGDA, fibrin, matrigel, PDMS	vascular network to vascularize tissue-engineered constructs	n/a	pressure-driven extrusion (through template leaching)	carbohydrate filaments are first deposited; a cell-laden hydrogel is casted on top of them. Filaments are leached, allowing the formation of hollow tubes, which are seeded with HUVECs	*in vitro* and *in vivo*	425, 426
vascular network	HUVECs, human neonatal and mouse embryonic fibroblasts, hMSCs	GelMA, fibrin, pluronic F-127	vascular network to vascularize tissue-engineered constructs	∼10 kPa	pressure-driven extrusion	instead of carbohydrate filaments, pluronic filaments were used for template leaching	*in vitro*	317, 427
vascular network	HUVEC, human neonatal fibroblasts, human aortic smooth muscle cells, breast cancer cells	dECM, pluronic F-127	vascular network to vascularize tissue-engineered constructs	from ∼250 kPa to ∼850 kPa	pressure-driven extrusion	instead of carbohydrate filaments, pluronic filaments were used for template leaching	*in vitro*	428
vascular network	HUVECs, mouse osteoblasts	agarose, GelMA, star poly (ethylene glycol-*co*-lactide) acrylate, PEGDMA, PEGDA	vascular network to vascularize tissue engineered constructs	from ∼10 kPa to ∼200 kPa	pressure-driven extrusion	instead of carbohydrate filaments or pluronic, agarose was used	*in vitro*	318
vascular network	human hepatocytes	PVA, PLA, gelatin	vascular network to vascularize tissue-	from 2 to 6.5 kPa	pressure-driven extrusion	instead of carbohydrate filaments, PVA was used	*in vitro*	429

https://dx.doi.org/10.1021/acs.chemrev.9b00789
Chem. Rev. 2020, 120, 11032−11092

Table 6. continued

tissue	cells	composition	structure	mechanical properties	method	sequence	comments	ref
			engineered constructs					
vascular network	HUVECs	hyaluronic acid	vascular network to vascularize tissue-engineered constructs	n/a	pressure-driven extrusion	host−guest chemistry used to create cell-laden hydrogels that can be bioprinted gel-in-a-gel.	*in vitro*	
vascular network	human dermal microvascular ECs	alginate, chitosan, gellan cum, gelatin, collagen	vascular network to vascularize tissue-engineered constructs	from ∼1 MPa to ∼3.5 MPa	pressure-driven extrusion	coaxial bioprinting used to directly deliver ECs and create a lumen	*in vitro*	430
vascular network	HUVECs, hMSCs, human urothelial cells, bladder smooth muscle cells	GelMA, alginate, PEGTA	vascular network to vascularize tissue-engineered constructs	from ∼4 kPa to ∼50 kPa	pressure-driven microfluidic extrusion	coaxial bioprinting used to create more intricate geometries, possible thanks to microfluidic bioprinting	*in vitro*	431, 432
vascular network	HUVECs, mouse embryonic fibroblasts	GelMA, HA	vascular network to vascularize tissue-engineered constructs	from ∼3 kPa to ∼6 kPa	photopolymerization	branched networks created by photoprinting, after which cells were seeded	*in vitro* and *in vivo*	433
vascular constructs	human red blood cells; HEK293T; hMSCs; human lung epithelial cells and fibroblasts; HUVECs; rat primary hepatocytes	PEGDA, GelMA	vascular networks to vascularized tissue-engineered constructs	from ∼100 Pa to ∼10 kPa	photopolymerization	complex vascular networks created through photoprinting and then seeded with cells or perfused with red blood cells	*in vitro and in vivo*	55

https://dx.doi.org/10.1021/acs.chemrev.9b00789
Chem. Rev. 2020, 120, 11032−11092

most optimally used for different dimension ranges (Figure 12a, Table 6). One of the first bioprinting strategies to fabricate a vessel was reported by Norotte et al., who used spheroids of vascular and supporting cells of 300−500 μm that were deposited next to each other onto an agarose-printed mold. Due to the nonadhesive properties of agarose, the spheroids fused, thus creating single or branched blood vessels.[302] This approach was followed by Tan et al.[416] who used alginate instead of agarose as a spheroid-fusing biomaterial bed and more recently by Kucukgul et al.[417] who returned to agarose and developed an algorithm to bioprint large vessels with anatomical fidelity to patient medical data sets. The use of low cell-adhesive biomaterials such as alginate and agarose allows us to create supporting beds that are ideal for spheroid fusion and further tissue maturation during culture. However, these approaches require a large amount of cells and long culturing times for tissue maturation, thus resulting often in mechanically weak constructs.

An alternative approach to spheroid bioprinting is to directly embed cells into a hydrogel, thus processing such bioinks into vascular-like structures. In order to choose the right hydrogel, the capacity of cells to form tubular structures once embedded in these biomaterials needs to be assessed. Benning et al.[419] screened different commercially available hydrogels that are also often used for bioprinting, namely, Matrigel, fibrin, collagen, gelatin, agarose, Pluronic F-127, alginate, and alginate/gelatin mixtures. Whereas gelatin was able to support the proliferation of ECs, collagen and fibrin supported tubular formation. Bioprinted EC spheroids in fibrin and collagen mixtures showed also good viability and the capacity to sprout. Similarly, Kreimendhal et al.[420] showed that blends of agarose and collagen type I could be promising bioinks for EC and fibroblast mixture bioprinting, resulting in tubule formation and increased storage modulus compared to collagen alone or blends of agarose and fibrin. In a follow-up study, the same group fabricated functional blood vessels replicating the tunica intima, media, and adventitia organization by bioprinting ECs in gelatin, smooth muscle cells in fibrin, and fibroblasts cast on top of the bioprinted multilayer construct.[421] These vessels showed cellular reorganization and positive staining for VE-cadherin, collagen type IV, and smooth muscle actin, as well as limited permeability, thus confirming their biological functionality.

A hybrid approach between spheroid bioprinting and cell-laden hydrogel bioprinting has been proposed by Skardal et al.[422] who co-cross-linked tetra(PEG) tetra-acrylate derivatives with thiolated HA and gelatin and used this as a bioink to encapsulate fibroblasts. Cell-laden filaments were then deposited onto an agarose bed to form a vascular-like graft, which showed cell viability for 4 weeks. Despite solving the limitation of needing large cell quantities, this approach has not yet been demonstrated with ECs, which limits its applicability. The above-mentioned approaches show promising results in the biofabrication of relatively large single vessels or vessels with simple branching. Scaffolds with as small dimensions as vessels bifurcating into capillaries have been successfully fabricated by 2PP using α,ω-poly(tetrahydrofuran-ether diacrylate), which displayed fast fabrication kinetics and good mechanical properties for small vessel grafts.[423] Yet, true bioprinting strategies incorporating ECs in such small vessels have yet to be reported.

In the broader perspective of composite tissues, it would be ideal to devise biofabrication strategies where a vascular network can be directly incorporated into a second targeted tissue. This would hold promise to create larger biological constructs if the integrated vascular network can be perfused and can connect to the host vasculature after implantation. In this direction, Maiullari et al.[167] used microfluidic bioprinting to create different constructs to study the vascularization of cardiac constructs. CMs were either alternated with ECs every 2 or 4 layers or deposited adjacent to each other in "Janus"-like fibers. Cells were encapsulated in a mixture of alginate and PEG monoacrylate fibrinogen, which was cross-linked by calcium ions and UV exposure. Alginate was used only to provide shape stability during bioprinting and later removed by chelating the calcium ions. All constructs showed enhanced cardiac differentiation *in vitro* and connected to the host vasculature after implantation in mice, with Janus fibers outperforming the other architecture in terms of vascular network organization. Similarly, Byambaa et al.[388] developed bioprinted vascularized bone constructs, where GelMA with different degrees of methacryloyl substitutions was used (Figure 11b). In particular, GelMA with ∼34% substitution was used to covalently bind vascular endothelial growth factor (VEGF) and ECs, whereas GelMA with 94% substitution was combined with silica nanoplates and used to bioprint bone-marrow-derived MSCs that were induced to differentiate into osteoblasts by the nanoplates. The different degree of methacryloyl substitution resulted in a different degradation rate, which induced the ECs to remodel the gel and form a central vessel of 0.5 mm into the surrounding bone-like constructs. To further explore the role of geometrical confinement of cell-laden bioprinted hydrogels, Kang et al.[424] developed a prefabricated cartridge that could be filled with different cell−material formulations and used it in a proof-of-concept study to demonstrate its versatility by combining ECs with hepatic cells, which were encapsulated in either alginate or collagen. Despite the authors showing several different complex prefabricated shapes of the cartridges to be used for bioprinting, this approach still has to reveal its full potential in creating vascularized functional tissues.

An alternative, easy, and straightforward method to create such vascular networks is to print a leachable biomaterial that can be removed after embedding the printed network in a desired cell-laden hydrogel. Miller et al. pioneered this approach and showed that by using carbohydrate−glass it was possible to create a relative simple network comprised of two primary vessels of 1 mm in diameter connected by four secondary vessels of 300 μm in diameter. Such a network was embedded in various hydrogels including agarose, alginate, PEG, fibrin, and Matrigel and showed to support EC adhesion and proliferation, thus enabling endothelialization of the channels resulting from the network dissolution. This resulted in enhanced survival and functionality of hepatic cells embedded in the surrounding hydrogel.[425] When implanted, these constructs supported physiological blood flow typical of the femoral artery and showed connection with the host femoral artery in a rat animal model.[426] A similar approach was developed by Kolesky et al., who used bioprinting to create both the fugitive inks as well as the bioinks to develop cell-laden constructs.[317] As a fugitive material, pluronic F-127 was used, whereas the bioprinted construct was developed by blending gelatin and fibrin. A vascular network as small as 200 μm could be created. This resulted in the sustained culture of biological constructs larger than 1 cm^3 for more than 6 weeks and successful differentiation of adult stem cells into bone cells (osteoblasts).[427] Xu et al.[428] also used Pluronic F-127 as a fugitive material, with decellularized ECM (dECM) as a gel to encapsulate ECs,

https://dx.doi.org/10.1021/acs.chemrev.9b00789
Chem. Rev. 2020, 120, 11032−11092

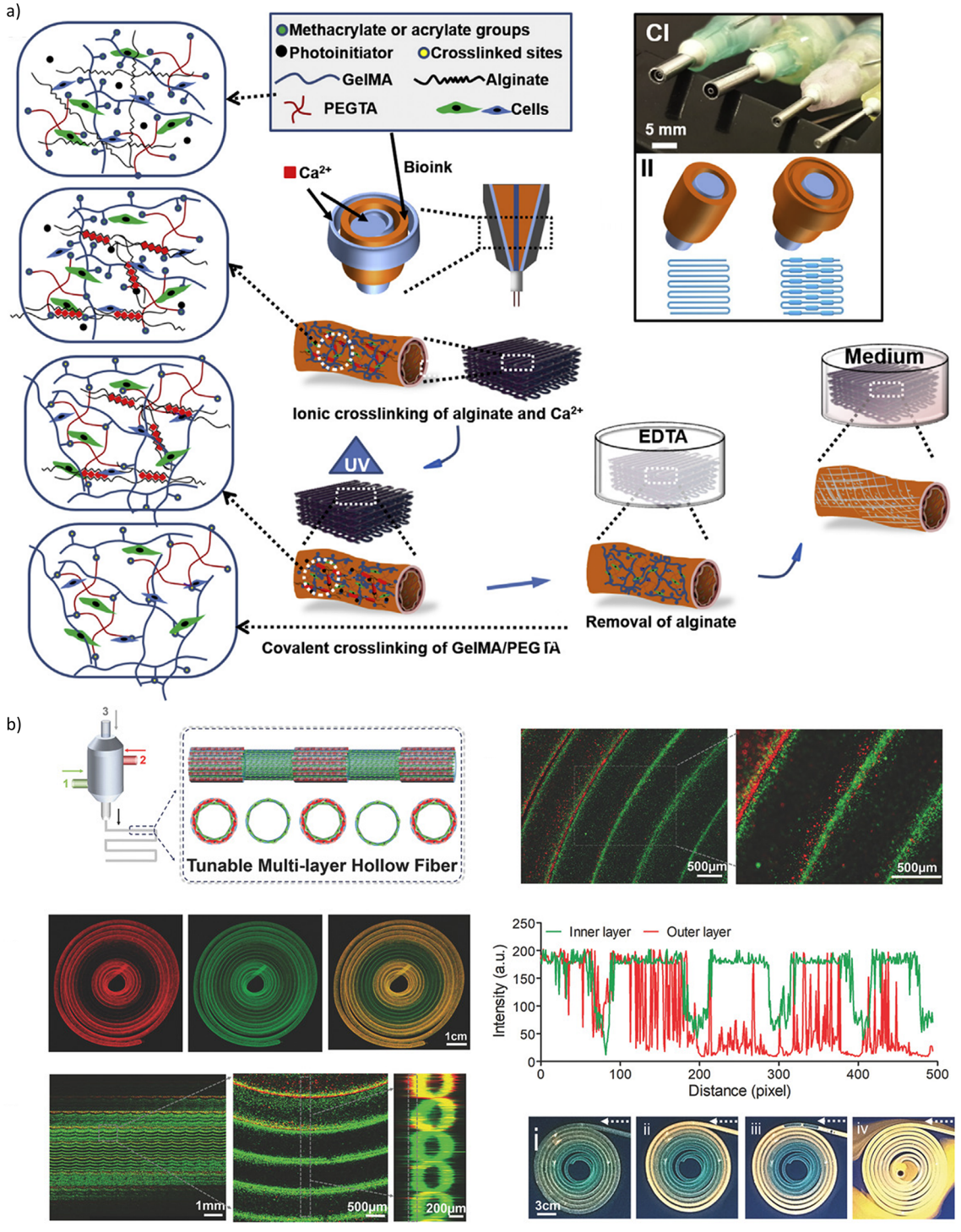

Figure 13. Examples of coaxial fibers produced with core−shell nozzles: (a) vessels created with bioink composition with dual cross-linking (ionically cross-linked alginate and UV covalently cross-linked acrylate 4-arm PEG with GelMA) and (b) perfusable hollow fibers created with a coaxial extrusion system combining GelMA, alginate, and 8-arm acrylate PEG. Adapted with permission from refs 431 and 432. Copyrights 2016 Elsevier Ltd. and 2018 WILEY-VCH Verlag GmbH & Co. KGaA.

SMCs, and fibroblasts alone or in combination, thus creating single vessels of diameters varying between 1.4 mm and 0.5 mm with a tunica intima, media, and adventitia, respectively. Alternatively, Bertassoni et al.[318] elaborated a similar strategy using agarose instead of Pluronic F-127 and demonstrated the fabrication of vascular networks of more complex architecture inside different hydrogels like GelMA, star poly(ethylene glycol-*co*-lactide) acrylate (SPELA), PEG dimethacrylate (PEGDMA), and PEG diacrylate (PEGDA). Pimentel et al.[429] were able to fabricate a branched vascular network with branching in both horizontal and vertical planes with dimensions varying from 1.3 mm to 0.5 mm. The templating agent used was PVA coated with PLA. The vascular tree was then incorporated in gelatin cross-linked by transglutaminase in which hepatocytes were

https://dx.doi.org/10.1021/acs.chemrev.9b00789
Chem. Rev. 2020, 120, 11032−11092

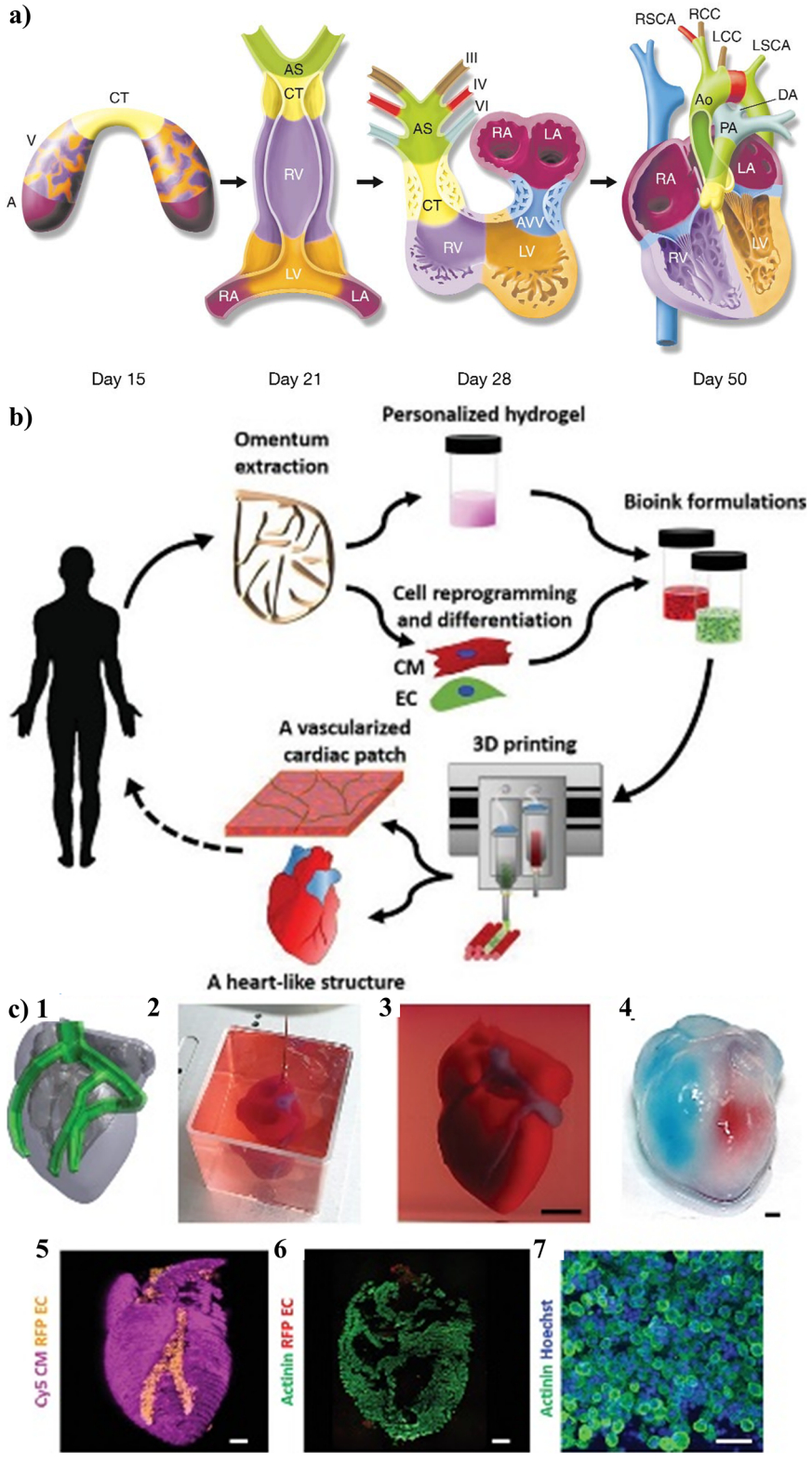

Figure 14. (a) Schematic of the heart development showing the formation of the different compartments until the complete formation at day 50 and (b) schematic of one of the approached investigated to produce cardiac patches and heart-like constructs. (c) 1 - 3D model of the heart construct; 2 - bioprinting in a supporting bath of alginate microparticles; 3, 4 - printed constructs before and after bath removal (red and blue colored to show hollow compartments divided by a septum area); 5 - confocal showing CMs and ECs; and 6, 7 - immunostaining sections of the bioprinted constructs. Adapted with permission from refs 434 and 435. Copyrights 2000 Springer Nature and 2019 Noor et al. (published by WILEY-VCH Verlag GmbH & Co. KGaA).

embedded at high density. The improved nutrient perfusion resulted in supporting cell spheroid assembly with enhanced oxygen diffusion. As in the work of Miller, the presence of a PLA coating on the templating material could be beneficial for EC

https://dx.doi.org/10.1021/acs.chemrev.9b00789
Chem. Rev. 2020, 120, 11032−11092

Table 7. Bioprinting Studies Aiming at the Manufacturing of Heart Tissue

tissue	cells	composition	structure	mechanical properties	method	sequence	comments	ref
myocardium patch	human cardiac progenitor cells, hMSCs and human dermal microvascular ECs	heart-derived ECM or collagen printed on top of a PCL scaffold	stacked layers composed of alternated bioinks	n/a	pressure- or piston-driven extrusion	two support layers of PCL were printed followed by multiple layers	implants of 8 mm diameter and 0.5 mm thickness were implanted subcutaneously in mice and in rat myocardial infarct model	446
myocardium patch	HUVEC and hMSCs	polyester urethane urea porous film, matrigel	stacked layers with PEUU substrate and 2 layers of bioinks	PEUU with 0.78 MPa (tensile strength)	laser-induced forward transfer	PEUU prepared with TIPS placed on collector slide; HUVEC-deposited 0/90 grid and hMSCs in squares inside grid (2 layers)	implants were tested in rats with induced MI by ligation of the left anterior descending coronary artery	449
cardiac *in vitro* model	human fetal CMs progenitors	alginate and alginate−RGD mixture (1:1)	square blocks with 20 × 20 mm and composed of 6 perpendicular layers; thickness 463−513 μm	n/a	piston-driven extrusion	30 million cells/mL of gel were printed and cross-linked with $CaCl_2$	*in vitro* culture during 7 days	447
myocardium patch	human cardiac-derived progenitor cells	gelatin and HA	20 × 20 mm and composed of 6 perpendicular layers.	n/a	piston-driven extrusion	thiol-modified HA was mixed with thiol reactive cross-linker and 30 million cells/mL	*in vivo* evaluation on MI mice model after ligation of the left anterior descending coronary; implant during 28 days	448
myocardium patch	hiPSC-CMs, HUVEC, human adult ventricular cardiac fibroblasts	biomaterial-free approach	cell spheroids (33000 cells) were dispensed on a needle array to produce one layer construct	n/a	regenova, vacuum pick-and-place	after spheroid fusion (72 h), construct is removed from a needle array and further matured before implantation	patch was glued or sutured in nude rats and kept *in vivo* for 1 week	161
myocardium patch	hiPSC-CMs, smooth muscle cells and ECs	GelMA	patch size of 2 × 2 mm with 100 μm thickness	n/a	multiphoton	patches were seeded and cultured for 1 day prior to implantation	patches were implanted and sutured in nude mice after ligation of the left anterior descending coronary and kept *in vivo* during 4 weeks	451
myocardium patch	human cardiac-derived progenitor cells	GelMa and GelMA/ECM	patches with 10 mm diameter and 0.6 mm thickness or 10 × 10 × 0.6 mm (3 layers 0/90°)	3 kPa GelMa, 5 kPa GelMA/ECM	pressure-driven system	3 million cells/mL; white-light cross-linking postprinting at 4 °C during 5 min	patches were implanted in rats under pericardium or sutured to the ventricle; non MI model; explants performed on days 7 and 14	450
myocardium	HUVEC, neonatal rat CMs, hiPSCs- CMs	alginate and GelMA	scaffolds with 5.5 × 3.5 × 0.75 mm^3; fiber resolution 120 μm postprinting and 150 μm postswelling	5.2−22.6 kPa depending on fiber spacing	pump-driven with coaxial nozzle	initial cross-linking of alginate ECs bioink with $CaCl_2$; post-cross-linking of GelMa with UV; postseeding of the construct with CMs	*In vitro* evaluation with and without perfusion	162
aortic heart valve	porcine aortic valve interstitial cells and human aortic root smooth muscle cells	alginate and gelatin mixture	CT-based porcine heart valve geometry or grids	ultimate tensile strength 840−400 kPa; elastic modulus 1.44−0.98 MPa	piston-driven extrusion	2 million cells/mL mixed with alginate and gelatin, bioprinted, and post-cross-linked with $CaCl_2$	*in vitro* culture during 7 days	453
aortic heart valve	human aortic valvular interstitial cells	methacrylated HA and GelMa	cuboids with 5 × 5 × 1.5 mm or CAD design model of valve with 26 mm diameter and 8 mm height	13−4.2 kPa	piston-driven extrusion	5 million cells/mL encapsulated in biomaterial mixture and post-cross-linked with UV for 5 min	*in vitro* culture during 7 days	452

https://dx.doi.org/10.1021/acs.chemrev.9b00789
Chem. Rev. 2020, 120, 11032−11092

adhesion and proliferation, although the thickness of such coating should be carefully controlled to still allow nutrient diffusion through the engineered construct. All the above-mentioned templating approaches rely on different materials for the cell-encapsulating and the templating compartments.

In a very elegant approach, Song et al.[418] designed a dual hydrogel strategy where HA was either modified with host−guest chemistry (adamantine and cyclodextrin) alone or with host−guest chemistry and norbornene-thiolene for further UV cross-linking (Figure 12b). This dual system was then used to create a 3D culture device where the host−guest-modified HA could be used to pattern geometrically specific channels within the dual cross-linked HA network by controlling degradation (Figure 12b). This approach was then used to study endothelialization and ECs sprouting in response to defined vascular morphogenetic signals (e.g., VEGF).

Although these templating approaches have yielded promising results in terms of enhanced tissue nutrient perfusion, maintenance of cell viability and functionality, and connection to host vasculature, and thus should be definitely considered for follow-up preclinical studies, the fabrication of branch-tree networks with variable vessel diameter during processing proves still difficult. A possible solution to the fabrication of such more physiological vascular trees could be offered by coaxial bioprinting, where branching could be promoted either by incorporating and releasing angiogenetic factors or by changing the diameter of the coaxial fibers during bioprinting by using core−shell printing nozzles. Promising results in this direction have been obtained by Akkineni et al.,[430] who fabricated implants made of hollow fibers with diameters ranging between 600 and 800 μm, with highly concentrated alginate as shell material and alginate, chitosan, gellan gum, gelatin, and collagen hydrogels as core materials. These hollow fibers were then successfully covered by ECs, which adhered and proliferated in the internal lumen. Fibers of different structural morphology have been also created, by controlling the flow rate of core and shell compartments, spanning from straight to wavy and helical morphology.[376] Jia et al.[431] and Pi et al.[432] moved this strategy significantly forward with the fabrication of more intricate networks of similar dimensions made of GelMA, alginate, and 4-arm PEG-tetra-acrylate (PEGTA) or GelMA, alginate, and 8-arm PEG acrylate with a tripentaerythritol core (Figure 13a,b). The fabrication of these more versatile vascular networks was enabled by combining microfluidic principles in the design of the bioprinting cartridges and will certainly hold promise to provide more control over the design of the vascular network that can be created. However, the incorporation of these networks with other tissues remains to be demonstrated.

Another possibility to fabricate a vascular network of different dimensions (between 50 and 250 μm) has been shown by Zhu et al.,[433] who used DLP to create a vascular network of ECs embedded in GelMA into a GelMA/HA blend containing fibroblasts. ECs contained in such constructs were able to reorganize the hydrogel network and form tubular networks, which were shown to be functional *in vitro* and *in vivo*. A more recent approach by the Miller group radically opened new avenues to the fabrication of intricate and branched vascular networks through DLP, using food dye additives as photo-absorbers to pattern the vasculature within a hydrogel carrier and showing functional oxygenation and vascularization in a lung *in vitro* model and in a murine hepatic animal model.[55] The fabrication of such intricate and branched complex vascular networks certainly opens new doors to the biofabrication of more physiological large-scale engineered tissues, although vessel size reduction while branching and connection to capillaries remain open challenges.

6.4. Heart

The heart is a highly compartmentalized organ that is responsible for the continuous circulation of the blood throughout the body. The generation of the heart and associated circulation systems is the earliest events occurring during development to support and promote the rapid growth of the embryo. Both the heart and the great vessel system have to be continuously remodeled at a very fast pace to support all the necessary demands during and after gestation. The formation of precardiac cells occurs from mesodermal cell precursors after the migration of cells through the streak: cells that pass from the primitive node, midstreak, and posterior streak form the outflow tract, ventricles, and atria, respectively. These cells form the cardiac crescent, which is stimulated with factors of the BMP and FGF family by the endoderm inducing the heart formation, and this process starts in the third week of gestation. After a complex orchestration of the different cells, different heart tissues are gradually formed, passing through different stages over approximately 50 days until the aorta, left and right ventricle, atrium, and arteries are formed (Figure 14a).[434]

A matured human heart is composed of an estimate of 9 billion cells between CMs, ECs, smooth muscle cells, fibroblasts, and other connective tissue cells, immune cells, and other specialized cells, with a variable turnover from birth to adulthood.[436,437] The ECM of the heart is highly dynamic, and during the initial stages of heart development hyaluronans are the main component of the cardiac jelly (acellular component that separates the endocardium and myocardium).[438] Other ECM components that are formed during heart development are fibronectin, fibrillin, proteoglycans, and collagens type I, III, and IV, and these change after birth.[438] Unbalances in ECM composition during development have been associated with cardiac malformation (e.g., congenital heart disease), highlighting the importance of the spatiotemporal expression of its constituents tightly bound to cell migration, reorganization, and ultimately differentiation.

6.4.1. Myocardium. In the case of myocardium, the tissue in healthy conditions has as main ECM components glycoproteins, proteoglycans, and GAGs and is populated by CMs, myofibroblasts, ECs, pericytes, and immune cells.[439,440] Upon myocardium infarct induced by occlusion of coronary arteries, tissue necrosis occurs, and significant reduction of contraction is observed due to cell death. Upon cell death, a cascade of signals triggers fibroblasts and other cells in the surrounding tissue to repair the affected tissue, although only in mild cases this regeneration occurs. Furthermore, significant changes on the ECM level are observed upon invasion of the affected area by macrophages and fibroblasts.[440] Several TERM strategies are currently under investigation to improve tissue repair or to replace the affected tissue upon severe myocardium infarct events.[441−444] Acellular patches, cellular therapies, endogenous repair, and combined strategies are the main groups of strategies. Bioprinting has been used to develop myocardium patches aimed for implantation on top of the affected tissue (Table 7).[161,162,445−449] A cardiac patch to treat heart infarct ischemic tissue was recently developed.[446] The patches were manufactured with pepsin-digested heart dECM.[445,446] The ECM was combined with human cardiac progenitor cells or hMSCs.[446] The patches were produced by alternating bioinks in each layer,

https://dx.doi.org/10.1021/acs.chemrev.9b00789
Chem. Rev. 2020, 120, 11032−11092

and the final constructs were composed of a PCL scaffold support and up to 10 layers of bioink. The developed patches were implanted in the epicardium of a myocardium-infarct mouse model, and echocardiographic results showed that only hMSC bioink patches that were supplemented with VEGF were able to decrease dilation and increase contractile area.

LIFT was also used to produce myocardium patches for potential infarcted patients.[449] In this technique, gold-coated slides were used as support for HUVECs and hMSCs that upon irradiation with laser pulses were selectively transferred to the target slide containing a porous polyester urethane urea film coated with Matrigel. HUVECs were patterned in an orthogonal grid, and squares of hMSCs were printed inside the grid. Patches were implanted in an induced myocardial infarction rat model, and results after 8 weeks showed improved cardiac function, wall thickness, reduced fibrosis, and higher capillary density when compared with control groups (untreated patch or patch with randomly cultured cells).

Cardiac patches were also manufactured from cell spheroids, composed of hiPSC-CMs, HUVECs, and human adult ventricular cardiac fibroblasts, with an alternative pick and place bioprinting system.[161] In this approach, cell spheroids are selectively placed in a needle array until fusion of the spheroids is achieved. After removal from the needle array, the bioprinted constructs were further matured and implanted in the heart of rats. The implants integrated well *in vivo*, but further analyses are required to understand the mechanical integrity of the printed tissue and the application of nonmatured iPSC-derived CMs.

For bioprinting of other cardiac tissue, human fetal CM progenitor cells were used in piston-driven bioprinting.[447,448] Alginate with different concentrations and with or without RGD was tested with progenitor cells.[447] Similar constructs, including progenitor cells, were further improved by being bioprinted with a mixture of gelatin and HA bioink.[448] Upon implantation in a mouse myocardium infarct model, the cardiac parameters, namely, end-diastolic and systolic volumes, were improved when compared with the controls, and histological analysis showed a thicker infarct wall and lower fibrotic tissue. Beijleri et al.[450] investigated the combination of a cardiac progenitor isolated from the right atrial tissue of pediatric patients and combined the cells with gelMA or gelMA with decellularized and digested porcine ventricular tissue ECM to form bioinks. Scaffolds were bioprinted with a pressure-driven system and cultured *in vitro* where the scaffolds containing the ECM-derived gel showed improved gene expression of cardiac markers when compared with gelMA-bioprinted scaffolds. An *in vivo* test performed by implantation of the gelMA with ECM on the heart of rats showed that the patch maintained the shape, and new blood vessels invaded the patches, which were recovered after 14 days. Further evaluation of the patches containing cells and relevant disease models will be required to determine the suitability of these patches for the treatment of affected myocardium tissue.

A multiphoton bioprinting laser-based system was recently used to manufacture acellular myocardium scaffold patches mimicking the native ECM by patterning GelMA with a submicron resolution.[451] These constructs were seeded with hiPSC-CMs, smooth muscle cells, and ECs and implanted on the myocardial infarction mouse model. Results showed improved cardiac function on scaffolds seeded with cells when compared to acellular scaffolds, but further understanding of the integration of this implant requires additional testing.

For the development of a bioprinted full thickness myocardium tissue, vascularization is essential for the viability of the tissue upon implantation. Recently, a new strategy to bioprint perfusable vascularized channels was developed by manufacturing a mixture of alginate, GelMA, and acrylate PEG printed through the shell channel of a coaxial nozzle and calcium ions through the core to initiate alginate cross-linking. The constructs were then further cross-linked by UV light exposure after fabrication.[431] Endothelialized myocardium tissue was manufactured following a similar bioprinting strategy, by manufacturing fibers containing ECs, bioprinted in a mixture of GelMA and alginate, which migrated after bioprinting to the periphery of the fibers,[162] and by seeding CMs after maturation of the vascular network. HUVECs formed a vascular lumen after keeping the bioprinted tissue 15 days in culture. CMs seeded on top of the constructs started beating after 48 h. Constructs were further matured under perfusion *in vitro* in a custom microfluidic bioreactor, and cell viability improved when compared with controls with no perfusion.

6.4.2. Heart Valves. Bioprinting heart valves is another focus of cardiac tissue being investigated (Table 7).[452,453] The heart comprises four different valves, namely, the aortic (located between the aorta and left ventricle), pulmonary (between the right ventricle and pulmonary trunk), right or tricuspid, and left or mitral atrioventricular valves (between the atria and ventricles). These different heart valves have as their main function the maintenance of unidirectional blood flow by opening and closing in coordination with the heartbeat. The valves are composed of a root section, a cartilage-like ring (annulus fibrosa) connected to the heart muscle, and the leaflets (right and left atrioventricular valves) or cusps (aortic and pulmonary valves).[454] While the annulus is mainly composed of fibrous collagen, the leaflets and cusps are formed with a triple layer arrangement termed fibrosa, spongiosa, and atrialis (atrioventricular valves) or ventricularis (aortic and pulmonary valves).[454,455] The fibrosa layer is mainly composed of fibrillar collagen type I and III; the spongiosa is composed of proteoglycans with dispersed collagen fibers; and the atrialis and ventricularis layers are mainly composed of elastin with radial orientation. The valves are mainly composed of adult valve interstitial cells located throughout the three ECM layers and valvular ECs that form the superficial layer of the valves.[455]

Diseases such as aortic and mitral valve stenosis (closure or deformation of the valve opening) and mitral regurgitation (incomplete closure) are some of the most common valve diseases with an increased prevalence in the elderly.[456] In children, congenital heart diseases and more specifically valve diseases also have a high incidence. Synthetic or mechanical heart valves surgically implanted are the only currently available treatment for patients with affected valves, but failure of these valves can occur due to infection, thrombosis, or even valve failure (e.g., by calcification of leaflets).[457] Furthermore, in children a constant revision or replacement might be required due to the growth of the valve size.[458]

Tissue-engineered approaches have been developed to manufacture heart valves spanning from decellularized scaffolds from allogenic or xenogenic source valves, scaffolds manufactured by electrospinning or molding techniques, and bioprinting.[459] Duan et al. used bioprinting to manufacture heart valves by combining alginate and gelatin with porcine aortic valve interstitial cells or human aortic root smooth muscle cells.[453] A 3D model of porcine aortic valves was created with a micro-CT image data set, and this model was used to manufacture the constructs. Smooth muscle cells combined with the hydrogel mixture were used to print the valve root, and interstitial cells

https://dx.doi.org/10.1021/acs.chemrev.9b00789
Chem. Rev. 2020, 120, 11032−11092

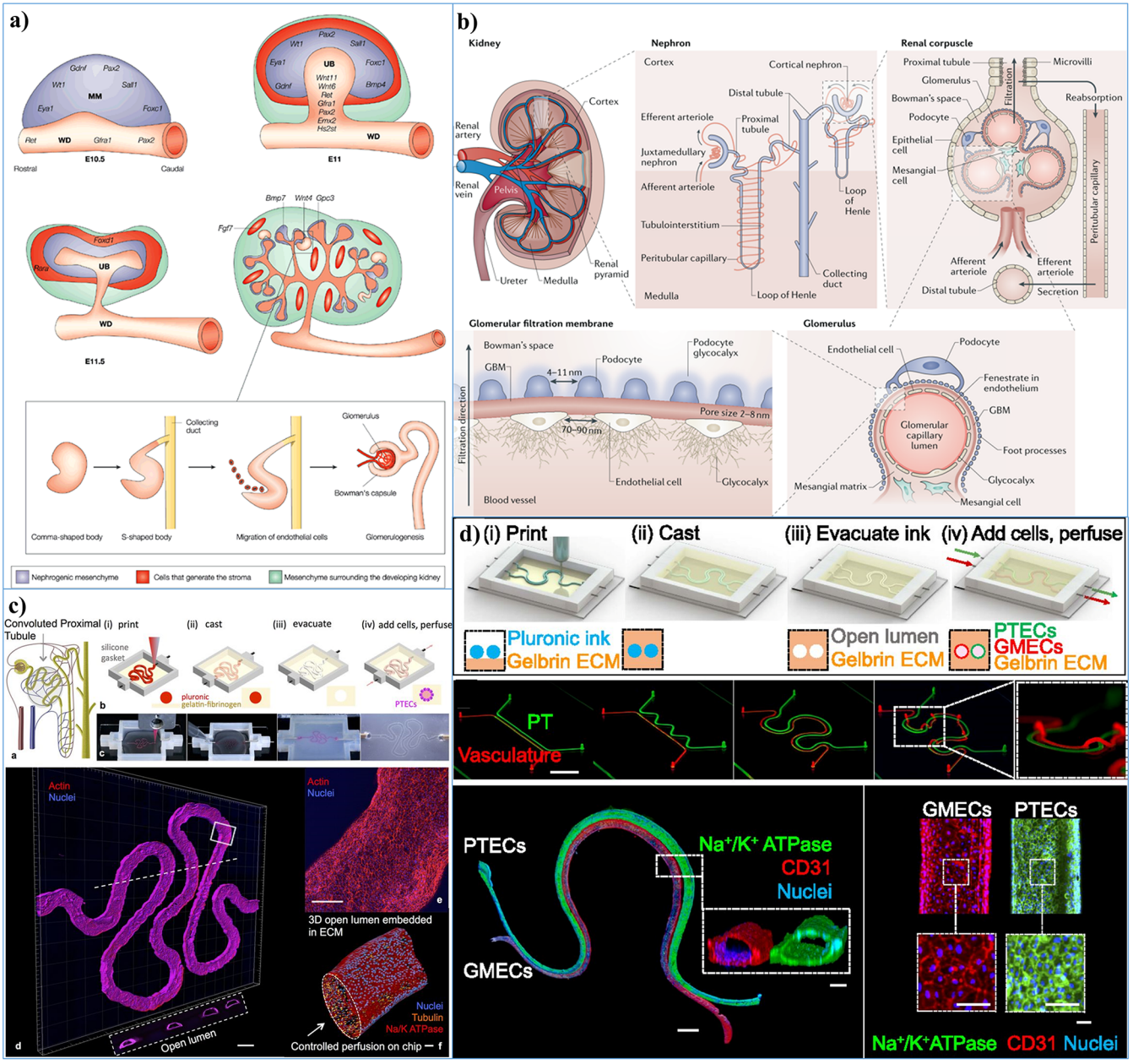

Figure 15. (a) Renal development starts from two populations of progenitors. After several events, the branching starts to occur with the formation of the nephron filtration units. (b) Kidney physiology: one million nephron units, and each nephron is compartmentalized where filtration occurs while urine is produced. (c) and (d) Examples of bioprinting studies where convoluted channels have been produced with sacrificial 3D printing and postseeded with renal epithelial and ECs. Adapted with permission for refs 469, 470, 474, and 475. Copyrights 2002 Springer Nature, 2018, Springer Nature, 2019 Lin et al. (published by National Academy of Sciences), and 2016 Homan et al. (published by Springer Nature).

were used to print the valve leaflets. Live/dead assays showed that the bioprinted valves had a high cell viability (81−83%) for both populations of cells. In a follow-up study, the same group used methacrylate HA and GelMa with human aortic valvular interstitial cells.[452] The constructs were cross-linked under UV and placed in culture for 7 days. Results showed new collagen and GAG deposition. Despite this initial result, no functionality test on the bioprinted valves was performed, and longer cell culture experiments with more extensive characterization were required before having a valve ready for *in vivo* testing.

6.4.3. Future Outlook for Bioprinting Cardiac Tissue. These achievements have been focused on the development of cardiac patches for infarcted myocardium as a deliverable mechanism of cells and an ECM-like supporting matrix for the regeneration of the affected tissue. These bioprinted cardiac tissues are rather simplified when compared to the native counterparts, and only some of the bioprinted tissues were tested *in vivo*. Some preliminary *in vivo* validation in small animal models of the different bioprinted constructs showed promising results, although these are probably insufficient if evaluated on large-size animals. The regeneration of the thin myocardium of small animal models might be easier due to the low thickness of the tissue and to the low demands of vascularization. So far, only morphological embryonic heart-like scaffolds have been bioprinted.[51] A chicken embryonic heart was fixed and stained, and a stack of fluorescent images allowed the generation of a 3D

https://dx.doi.org/10.1021/acs.chemrev.9b00789
Chem. Rev. 2020, 120, 11032−11092

Table 8. Bioprinting Studies Where Urinary Systems Such as Kidney and Urethra Have Been Investigated

tissue	cells	composition	structure	mechanical properties	method	sequence	comments	ref
proximal tubule (tubular *in vitro* model)	human-immortalized PTECs	gelatin−fibrin	convoluted tubule on a PDMS printed chamber	n/a	pressure-driven	printing of PDMS chamber; cast one-layer hydrogel; print pluronic fiber; cast second layer of hydrogels; leach pluronic to form tube; culture cells inside tube	*in vitro* model cultured with perfusion during 65 days; drug tests were performed with cyclosporine A (know nephrotoxin)	469
proximal tubule (tubular *in vitro* model)	human immortalized PTECs	gelatin−fibrin	adjacent convoluted tubules on a PDMS printed chamber	n/a	pressure-driven	printing of PDMS chamber, printing (pluronic) or two parallel channels, cast gelatin and fibrin gel, removal of sacrificial material, perfusion of PTECs, and glomerular microvascular ECs	sacrificial 3D printing, Reabsorption of albumin	470
renal organoids (perfusable chamber)	vascular bed with HUVECs and human neonatal dermal fibroblasts; ESC-derived renal organoids	gelatin−fibrin	PDMS-printed perfusable chamber	n/a	pressure-driven	printing of PDMS chamber, formation of prevascular bed in fibrin, manual seeding of organoids, perfusion	maturation and vascularization were observed when perfusion was applied	471
proximal tubule (layered *in vitro* model)	HUVEC, primary human RPTEC, and renal fibroblasts	thermoresponsive NovoGel	layered construct (one layer of interstitium with a second layer to create a border)	n/a	piston-driven	fibroblasts and HUVEC (50:50) were combined with hydrogel and printed in transwell and matured for 3 days; RPTEC were added on top of bioprinted construct	*in vitro* culture up to 30 days; toxicity studies performed with cisplastin	472, 478
urethra	rabbit urothelial cells (UCs) and smooth muscle cells (SMCs)	PCL, PLCL fibrinogen, gelatin, and HA	concentric tubular construct; outer layers with urothelial cells bioink; middle later of PCL or PLCL with inner layers with smooth muscle cells bioink	Tensile stress ∼0.1−1 MPa; Young modulus ∼0.8−1.25 MPa	pressure-driven	SMCs: 10−20 M/mL; UCs: 5−10 M/mL; first thermoplastic was printed (4 layers in *Z*); the inner layers with UCs were printed; 3 layers of SMCs were printed on the outside	*in vitro* culture up to 7 days post printing	476

https://dx.doi.org/10.1021/acs.chemrev.9b00789
Chem. Rev. 2020, 120, 11032−11092

model containing the outer and inner morphology. In order to be printed, the model was scaled up to match printing resolution, and no cells were included. In a recent study, Noor et al. also demonstrated in a proof-of-concept study that a heart-like structure could be produced with two cell (CMs and ECs) populations on omentum dECM bioinks that were selectively dispensed on a supporting bath containing alginate microparticles with medium supplemented with xanthan gum (Figure 14b,c).[435] Similarly, Lee et al. also demonstrated the manufacturing of a heart valve and heart-like constructs where a supporting bath was essential to maintain the geometrical shape of 20 μm collagen-based filaments.[54] These examples of heart-like models provide essential insights that much more is needed both at the cellular but also at the biomaterial-ink composition levels to make a full-size functional organ. Furthermore, the levels of function and maturity are yet to be demonstrated.

When envisioning human myocardium regeneration, a simple scale up of the bioprinted constructs might not be enough, and the inclusion of vasculature might be essential. Another point of consideration is the choice of cells that can be expanded in sufficient numbers to create large size tissue constructs. PSCs might be a promising alternative, but maturity and function should be ensured.[460] Several protocols have already been established to generate cardiovascular progenitors.[461,462] Perfusion and vascularization are also essential to keep tissue viable *in vitro*, while maturation occurs and upon implantation and during regeneration. Another point normally not discussed is that the designed tissue implants of the modulation require integration and regeneration while avoiding immune reaction. Similarly, these and many more unknowns should be considered for the bioprinting of a full heart, and there is still a long road until achieving a full functional health for replacement therapy.

6.5. Kidneys

The kidneys are complex organs that continuously filter the blood while maintaining homeostasis and waste excretion functions. These functions involve the regulation of osmolality, volume, acid−base status, and ionic composition of the body fluids, as well as removal of metabolic byproducts out of blood circulation.[463] Moreover, kidneys produce hormones such as calcitriol, erythropoietin, and renin, which have an effect on calcium metabolism, erythropoiesis, and systemic blood pressure, respectively.[464]

The kidney development derives from the formation of the intermediate mesoderm from the mesoderm layer. Three types of kidneys are initially developed, namely, the pronephros, mesonephros, and metanephros. The two initial structures are temporary and with limited or no known function, and the kidneys are only formed from the metanephros.[465] The formation of the kidney starts by the two distinct cell populations derived from the intermediate mesoderm, the metanephric mesenchyme (MM), and ureteric bud (UB) cells (outgrown from the Wolffian duct) (Figure 15a). Upon the cross contact of these two progenitor cells, a process termed branch morphogenesis (formation of the ureteric tree) occurs followed by differentiation of the MM cells that condense and segregate to cap mesenchyme and renal stromal cells, and these start to form structures such as renal vesicles (initial epithelial structure) that initiate the development of the nephron structure.[465] The process of development continues with the glomerulus structure where ECs, mesangial cells, podocytes, and epithelial cells form a complex filtration unit where the formation of filtrate from blood flow starts.[466] Each nephron consists of a renal corpuscle and a sequence of specialized tubules, including the proximal tubule, loop of Henle, distal tubule, and collecting duct (Figure 15b).[463] This highly compartmentalized filtration unit has more than 20 different cell types distributed in successive sections with distinct functions. Blood is brought to the renal corpuscle by a network of capillaries that form the glomerulus surrounded by the Bowman's capsule. Solutes below the molecular size of albumin (68 kDa) pass the glomerular filter and constitute the primary urine, which travels through the nephron tubule sections where essential components present in the filtrate are reabsorbed until the final urine is then excreted through the collecting duct. The development of nephrons in humans terminates after birth, and the number of these units varies in a human organ from 200 thousand to 2 million.[465]

Kidney ECM and renal basement membrane compositions change during development, during maturity, and in pathological conditions.[467] The main ECM components found in the kidney basement membrane are collagen type IV, laminins, sulfated proteoglycans, and entacin/nidogen.[467] The different sections of the nephron have variable compositions of the basement membrane, revealing the complexity of the extracellular composition. Recently, Nagao et al. characterized and quantified human kidney cortex tissue with chromatography and mass spectroscopy.[468] The obtained results showed that the cortex tissue is composed of collagen type IV (37%), collagen type I (20%), laminin (8.6%), heparan sulfate proteoglycans (3%), fibrilin-1 (2.8%), and many others.

Chronic kidney disease (CKD) is an increasing health and societal problem, resulting in loss of kidney function in patients, ultimately requiring organ transplant. It is estimated that 10% of the world population is affected by CKD. Critical organ shortage makes extended duration of dialysis inevitable, thus leading to morbidity. Hence, there is an urgent need for novel therapies. Upcoming regenerative approaches develop into two directions: first, the endogenous repair and alleviation of renal disease progression, and second, the provision of transplantable organs or functional organ units. For both approaches, fundamental challenges must be addressed, and *in vitro* 3D models capable of simulating kidney functions will allow better understanding of the different regeneration strategies. Bioprinting can be an essential asset to create such 3D models to investigate renal development, disease, and regeneration *in vitro* while allowing new knowledge that can be essential for full organ manufacturing.

6.5.1. Renal Bioprinting. Due to the complexity of the kidney and the nephron, only simplifications of the nephron focusing on specific sections have been designed and manufactured by bioprinting (Table 8). These bioprinted models have been mainly developed for drug toxicity screening, but these could also be envisioned to study for instance regeneration post injury. A proximal tubule-like segment of the nephron was bioprinted in a hybrid approach combined with a perfusable chip (Figure 15c,d).[469−471] Perfusable channels were prepared by depositing a sacrificial ink (pluronic), connecting the inlet and outlet ports of a PDMS-printed chip. After removal of the sacrificial material previously encapsulated inside a casted hydrogel composed of gelatin and fibrin, the chips were seeded by perfusion of immortalized human proximal tubular epithelial cells (PTECs). With this approach, the direct bioprinting of cells was avoided. The PTECs cultured on the chips were left to mature for up to two months, and nephrotoxicity with a known

https://dx.doi.org/10.1021/acs.chemrev.9b00789
Chem. Rev. 2020, 120, 11032−11092

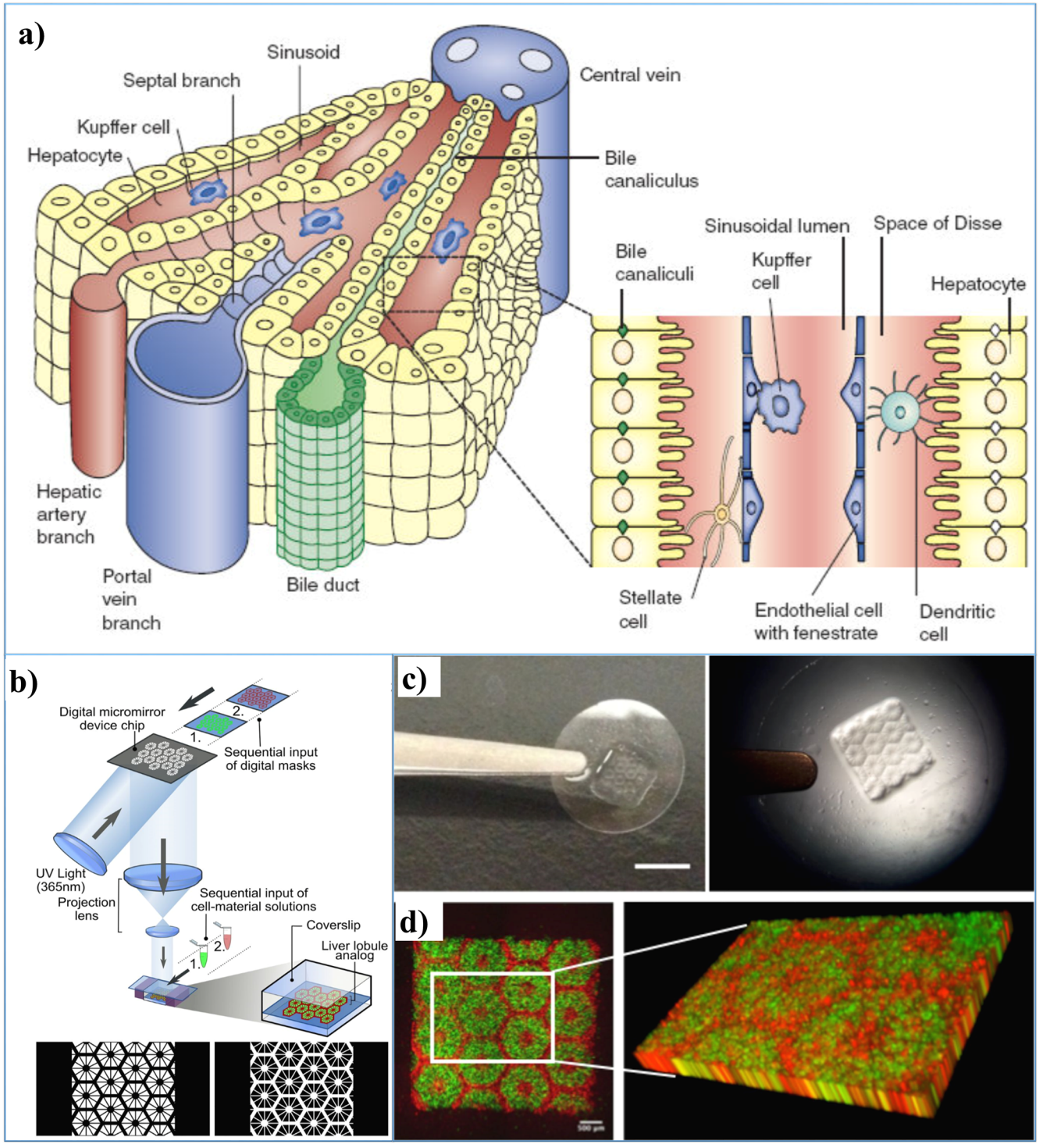

Figure 16. Liver: (a) schematic representation of the liver lobule sections showing a complex cellular organization radiating from the central vein and surrounded by hepatic artery, portal vein, and bile duct. (b) Schematic representation of a DLP-based bioprinting approach to manufacture liver lobule models. (c) Bioprinted construct on a round coverslip. (d) Confocal microscopy image and 3D reconstruction of the bioprinted tissue with hepatic cells stained in green and HUVECs and ADSCs used as support cells stained in red (scale bar 500 μm). Adapted with permission from refs 34 and 485. Copyright 2016 Ma et al. (published by National Academy of Sciences) and 2006 Springer Nature.

compound was tested. Results showed that the epithelial layer was gradually disrupted in correlation with the dose of nephrotoxin used. A follow-up study by Lin et al.[470] used the same approach to produce two parallel channels where one channel was seeded with glomerular microvascular ECs and the adjacent channel with PTECs (Figure 15d). Transport reabsorption function between the adjacent tubules was tested with fluorescently labeled human albumin and inulin. Results showed that inulin was retained in the epithelial compartment, while the albumin was reabsorbed.

Organovo developed recently a similar proximal tubule-like tissue bioprinted in a transwell membrane.[472] In this case and in

https://dx.doi.org/10.1021/acs.chemrev.9b00789
Chem. Rev. 2020, 120, 11032−11092

contrast with the approach designed by Homan et al., fibroblasts and HUVECs were mixed with a proprietary thermoresponsive hydrogel and bioprinted in a layered structure. After 3 days in culture, renal PTECs were seeded on top of the bioprinted layers. After maturation, the tissue showed microvascular networks, tight junction, and polarization of the renal cells. Nephrotoxicity was also tested on the mature tissue with cisplatin, a known nephrotoxic drug. Results of clinically relevant concentrations and dosage of cisplatin showed a detrimental effect on cell metabolism and cell viability with increased drug concentrations.

The bioprinting approaches developed have mainly focused on the development of *in vitro* tissue models that could be used to screen drugs. These specific bioprinted nephron sections are a small portion of the full nephron structure and function, and further models are necessary to understand what is needed to manufacture a better mimicking nephron functional unit. Recent achievements such as the ones that allow the generation of nephron organoids[149,151] might be difficult to achieve in the near term with bioprinting due to the resolution limitations, lack of suitable cells, and suitable bioinks that allow a further maturation and rearrangement of tissue. For this reason, more research should be oriented at understanding which bioprintable hydrogel facilitates organogenesis and tubulogenesis *in vitro*. PEG-based hydrogels were used to evaluate tubulogenesis formation of renal cell lines or primary human renal proximal tubule epithelial cells.[473] In this work, heparin and matrix metalloproteinase (MMP) cleavable chains were added to the hydrogel preparation, and tubulogenesis was more evident when compared with nondegradable (MMP-free) or heparin-free hydrogels. Nephrotoxicity of the tubular structure was tested by incubating the 3D cultures with different concentrations of cisplastin for 48 h. Furthermore, the transepithelial transport functionality of the tubular structure showed cells with functional anion transporter due to the presence of luciferase yellow inside the tubules even after long washing periods. In a recent example, organoids have also been coupled with printing techniques to investigate the vascularization of previously formed renal organoids.[471] Despite that this study only made use of 3D printing to build a perfusion chamber to encase the prevascularized bed and the manually dispensed organoids, a similar approach could be envisioned with bioprinting for both the vasculature bed and the organoids. In this study, it was shown that a preformed vascular bed and controlled flow are important for further maturation and vascularization of previously formed organoids.

In addition to the kidney, another tissue from the urinary system that has been manufactured by bioprinting is the urethra.[476] Scaffolds were prepared in a pressure-based bioprinter equipped with three dispensing heads: one for the deposition of a support tubular construct manufactured with PCL or/and combinations of PCL and poly(lactide-*co*-caprolactone) (PLCL) and two other cartridges to dispense the bioinks. Two bioinks were prepared by combining fibrinogen, gelatin, and HA with rabbit autologous cells (urothelial cells and smooth muscle cells). The thermoplastic polymer was deposited first in a tubular form. Next, two tubular layers of urothelial cells and three tubular layers with smooth muscle cells were deposited concentrically on the inside and outside of the polymer, respectively. Cell viability was above 93% after 1 day and 75% after 7 days in culture. Further *in vivo* validation will be required to evaluate this bioprinted urethra construct.

6.5.2. Outlook Kidney Bioprinting. The ambition of bioprinting a full kidney might still be decades away from being possible. Several challenges need to be addressed before the complexity of the structures that can be bioprinted can mimic with some extent the multitude of functions of the kidney filtration unit. The challenges persist on all aspects spanning from the cells that should be used for the bioprinting to the biomaterials used for the bioink formulations. Regarding cell source, the new development of kidney organoids might allow the production of a multitude of predifferentiated cells that could allow researchers to produce constructs with relevant cells that can be found in the human organs.[150,152] These organoids are self-assembled constructs, and the same organogenesis identified in these 3D models might not be possible to achieve with current bioprinting techniques, as further control on single-cell bioprinting would be required. Furthermore, one could argue if it is necessary to place accurately the cells in known positions or if cellular rearrangement is possible postbioprinting. Dispensing the multitude of different cells would also require a multiprint head system capable of individually dispensing each cell type. Another important topic that will require extensive research is the development of suitable bioinks. In a recent study performed by Sebinger et al., multiple ECM molecules and growth factors were screened with kidney rudiments, and results showed remarkable changes on the development on kidney organoid rudiments *in vitro*.[477] This shows that an accurate selection and control of the deposition of the ECM molecules of choice could dictate the success of the bioprinted organ. Other points such as maturation conditions *in vitro* with the use of custom developed bioreactors should also be taken into consideration and will certainly be a point of future research.

7. ENDODERM

The endoderm germ layer gives rise to tissues such as thyroid, liver, pancreas, lung, thymus, and the gastrointestinal tract. Initial development on the bioprinting of liver functional units and pancreatic tissue implants is covered in the following sections.

7.1. Liver

Liver is the largest organ in the human body, weighing an average of 1.4 kg. It consists of a large right lobe and a small left lobe separated by a band of connective tissue, which anchors the liver to the abdominal cavity. The tissue is made up of hexagonal units, called lobules, mainly constituted of hepatocytes (Figure 16a). Many blood vessels and bile ducts run between the liver cells. The portal vein brings the blood from the digestive organs, carrying nutrients and also toxic substances. Once they reach the liver, these substances are processed, stored, altered, detoxified, and passed back into the blood or released in the bowel to be eliminated, such as alcohol and byproducts of medication. The liver is also involved in the metabolism of fats, carbohydrates, and proteins. Fat metabolism takes place by β-oxidation and is converted to energy by hepatocytes. By carbohydrate metabolism, the liver maintains the sugar balance in the blood. Excess sugar in the blood is converted into glycogen in the liver. In the case of low blood sugar, the glycogen stored in the liver cells is broken down and released into the blood. For protein metabolism, liver cells metabolize the amino acids from proteins to synthesize carbohydrates and fat. The toxic byproduct in the form of ammonia is converted into urea and released into the blood, which is filtered in the kidney and excreted through the urine.

https://dx.doi.org/10.1021/acs.chemrev.9b00789
Chem. Rev. 2020, 120, 11032−11092

Table 9. Examples of Bioprinted Liver Tissues with Cells and Biomaterials Used

tissue	cells	composition	structure	mechanical properties	method	sequence	comments	ref
liver (*in vitro* model)	human hepatic stellate cells (HSCs), HUVECs, and human hepatocytes	NovoGel	square construct	n/a	piston-driven	150 million cells/mL; compartmentalized parenchymal and nonparenchymal bioinks	*in vitro* maturation for 3 days post printing; toxicity screening during 28 days	480
liver (on-a-chip model)	HepG2	GelMA	7 × 7 droplet array with an 800 μm droplet diameter	5 kPa	piston-driven	spheroids were formed by fusion in PDMS mold during 5 days, mixed with GelMA, 7 × 7; droplet array was formed by bioprinting and post cross-linked with UV (850 mW, 15 s)	*in vitro* culture up to 6 days	481
liver (patch)	HepG2	alginate	scaffolds with 25 × 25 mm; 0/90° layer deposition	n/a	pressure-driven	$CaCl_2$ post cross-linking	*in vitro*	482
liver (*in vitro* model)	hiPSCs and hESCs	alginate	ring structures with 40 layers	n/a	electromagnetic DOD printing	10 million cells/mL at day 6 differentiation; $CaCl_2$ cross-linking and $BaCl_2$ post cross-linking	*in vitro* culture during 21 days with differentiation protocol	484
liver (organ-on-a-chip)	HepG2 and HUVEC	PCL collagen (for HepG2) and gelatin (HUVEC)	different layered arrangements were bioprinted with bioinks inside a PCL casing	n/a	pressure-driven printing	50k cells/mL (HUVEC); 20 M cells/mL (HepG2)	*in vitro* culture during 6 days with or without perfusion	483
liver (*in vitro* model)	hiPSCs-derived Hepatic progenitor cells, HUVEC and ADSCs	GelMA and glycidal methacrylated HA	200 μm thickness	~5 kPa stiffness	sterelithography	40 M cells/mL (iPSCs-derived); 40 M cells/ml (HUVEC) and 0.8 M cells/ml (ADSCs). Two step:a) cross-linking with mask iPSCs-derived bioink. Replacement of non cross-linked areas with bioink cointaining HUVEC and ADSCs and cross-link with UV (88 mW/cm2)	*in vitro* culture 10 days post printing	34
liver (*In vitro* model)	primary human hepatocytes, stellate, and Kupffer cells	decellularized liver ECM, HA, and gelatin	7 × 7 mm meander layer	100 Pa before cross-linking and 100 Pa–20 kPa after UV cross-linking	pressure-driven	cell spheroids were formed during 3 days in hanging drops, mixed with hydrogels to allow thiol–acrylate bond precross-linking before printing, secondary cross-linking with UV (18 W/cm^2, 2–4 s)	*in vitro* culture during 14 days	486

https://dx.doi.org/10.1021/acs.chemrev.9b00789
Chem. Rev. 2020, 120, 11032−11092

The liver has a central portal vein with radially distributed bile ducts, portal venules, and arterioles, all connected by a network of channels called sinusoids. The sinusoids are formed by ECs and Kupffer cells and are surrounded by hepatocytes and stellate cells. Kupffer cells are macrophages responsible for the removal of toxic substances and pathogens, while the hepatocytes are responsible for detoxification, lipid and carbohydrate metabolism, and protein synthesis. Liver stellate cells, whose complete function is not fully known, are quiescent cells triggered by liver damage and responsible for scar tissue formation.

The liver has remarkable regeneration capacity when hepatic resection is performed.[479] However, this regenerating capacity is impaired when continuous damage is induced and/or acquired or there are congenital diseases. The reasons for this diminished capacity are not yet fully understood; however, in most cases, the presence of highly fibrotic and scarred tissue leads ultimately to liver failure, and a transplant is required.

7.1.1. Liver Bioprinting. The possibility of creating bioprinted liver tissue patches is being pursued by several research groups, which aim at mimicking native healthy or pathological tissues *in vitro* and ultimately implantable tissues for regenerative medicine applications (Table 9). *In vitro* models are also envisioned as a suitable platform for drug screening and development.[480,481] Most attempts to create liver-like tissue have used cell lines[46,482,483] as the main cellular constituent. Only recently, PSCs[34,484] have been used in bioprinted liver constructs. Faulkner-Jones et al. reported bioprinted hiPSCs and hESCs that were differentiated toward hepatocyte-like cells.[484] Droplet-on-demand, electromechanical valve-bioprinting heads were used to selectively dispense hydrogel droplets and ionic cross-linking solution. Layers created by the dispensed droplets of alginate were subsequently cross-linked by dispensing droplets of calcium ions, and constructs with 20 and 40 layers were manufactured. Albumin secretion was used as a readout to understand the differentiation and function of the bioprinted hepatocyte-like cells encapsulated in alginate constructs. Results showed reduced albumin secretion from bioprinted cells when compared with the 2D controls.

The need for vascularization in liver is an important aspect that should be strongly considered. Initial approaches have combined ECs with primary hepatic cells to develop a bioprinted liver model.[480] In this approach, multicellular constructs composed of primary hepatocytes, hepatic stellates, and HUVECs were bioprinted with NovoGel. The 3D models manufactured did not mimic exactly the liver morphology, but the presence of a vascular network shows that the combination of essential cells such as ECs could improve the produced models. The produced liver models were tested with a hepatotoxic drug, and results matched those reported clinically. The level of complexity of this bioprinted liver model showed to be a step closer to native tissue with comparable lipid and glycogen storage and vimentin patterning expression. However, since the construct was envisioned as an *in vitro* model, it requires further validation if the aim is to be used for tissue regeneration.

Perfusion is an essential aspect that needs to be taken into consideration to mimic the culture conditions *in vitro* as close as possible to the native organ. For this, a recent approach was developed by combining a PDMS microfluidic chip or microbioreactor with an array of bioprinted GelMA droplets encapsulating HepG2 aggregates.[481] Hepatic biomarkers were measured in the medium supernatant. A dose−response study of a hepatotoxic compound was also tested on static culture conditions. Albumin, alpha-1 antitrypsin, transferrin, and ceruloplasmin secretion showed that the constructs remained functional up to 30 days in culture. Similarly, a liver organ-on-a-chip manufactured with bioprinting, where the chamber and the cell bioprinting (HepG2 and HUVECs) were performed in a single step, was recently investigated.[483] Different configurations of cells and hydrogels have been deposited inside a PCL chamber. The liver model was composed of a bottom layer of HepG2 cells encapsulated in collagen and a top layer of ECs encapsulated in gelatin. After incubation, the gelatin dissolved, leaving a cavity that allowed medium perfusion. Urea and albumin secretions were quantified during the 6 days of cell culture period. Results showed an improvement of the secretion on static coculture conditions and an additional improvement with the addition of perfusion when compared to nonperfused hepatocyte conditions.

Ma et al. recently used a stereolithograhy bioprinting approach to manufacture scaffolds mimicking the hepatic lobule microarchitecture (Figure 16b−d).[34] Hepatic progenitors cells (HPCs) derived from hiPSCs were bioprinted either alone or in combination with HUVECs and adipose-derived stem cells. An increase in cell cluster size, gene expression, cytochrome P450 induction, and metabolite secretion was observed on the triculture models when compared to HPCs alone.

DECM has also been used as a suitable bioink for liver bioprinting, due to the presence of essential growth factors and proteins such as collagen, elastin, and GAGs. Skardal et al.[486] investigated the combination of HA and gelatin-based hydrogels with liver dECM and bioprinted with previously prepared spheroids composed of primary human hepatocytes, stellate cells, and Kupffer cells. The spheroids bioprinted with hydrogel containing dECM were more viable when compared with bioprinted gelatin constructs. Urea and albumin were secreted from the bioprinted constructs throughout the 14 days of culture.

7.1.2. Outlook on Liver Bioprinting. Similarly to the previously covered organs, the manufacturing of a full liver might still require decades of research. Despite the innate regenerative capacity of the liver, in some pathological cases a full bioprinted organ might be a suitable alternative to donor organs. As with other organs, multiple cell lines have been initially used in proof-of-concept studies, but gradually the inclusion of more relevant PSCs has also started to be reported. Furthermore, PSC differentiation protocols have also been established.[487] Minimal functions have already been demonstrated in some of the bioprinted models (e.g., albumin secretion), but other functions performed by the liver might only be possible as the models become gradually more complex and more representative. The availability of liver *in vitro* models is highly interesting for pharmaceutical companies to perform preclinical toxicity and metabolite screenings as alternatives to currently performed *in vivo* or 2D cultures.[488] This gradual adoption of these alternatives might provide a further development of such bioprinted models that will facilitate further knowledge essential to build a fully functional liver.

7.2. Pancreas

The pancreas has two main functions in the human body, the production and release of digestive enzymes (exocrine function) and the production of hormones such as insulin and glucagon to regulate blood sugar levels (endocrine function). The pancreas develops from the embryonic posterior foregut, emerging as a bud from the dorsal and ventral sides of the gut tube, formed

https://dx.doi.org/10.1021/acs.chemrev.9b00789
Chem. Rev. 2020, 120, 11032−11092

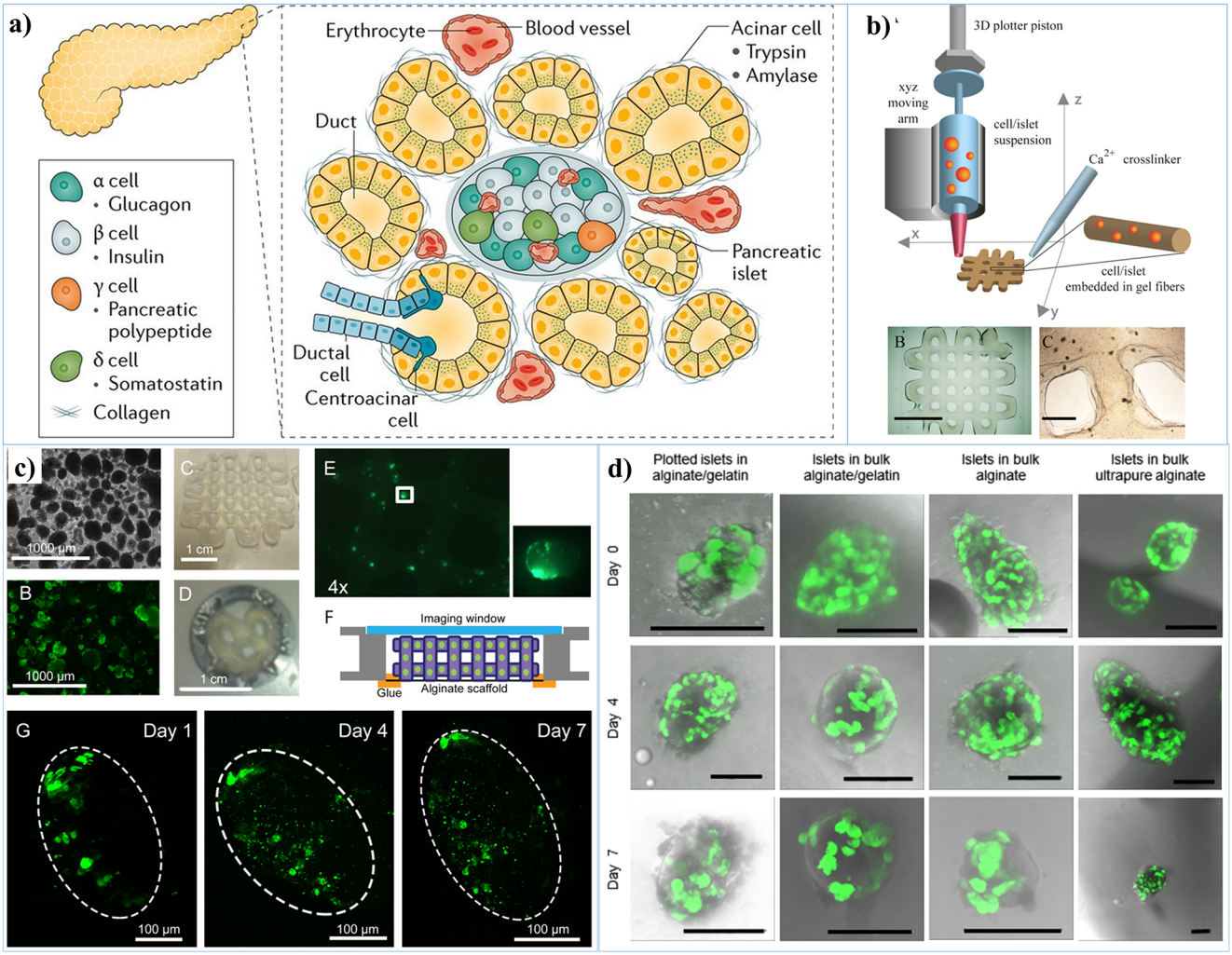

Figure 17. Pancreas: (a) simplified schematic representing the endocrine cellular composition (insulin-secreting β cells and glucagon-secreting α cells) and exocrine cellular composition (95% of the total tissue composed of acinar cells responsible for the production of digestive enzymes and network duct cells that facilitate transport of enzymes to the intestine) of the pancreatic tissue. (b) Schematic representation of piston-driven bioprinting approach to manufacture islet encapsulating implants. (c and d) Manufactured implants showing cell viability up to 7 days. Adapted with permission from refs 498 and 499. Copyrights 2017 Springer Nature and 2015 IOP Publishing, Ltd.

following the folding of the definitive endoderm. The early specification of the pancreatic anlage is mediated by retinoic signaling and by inhibition of hedgehog signaling.[489,490] The endocrine specification takes place in some of the pancreatic progenitor cells upon inhibition of Notch signaling, activating transcription factors for endocrine cell differentiation.[491,492] Following the migration of endocrine progenitors in the surrounding mesenchyme, they rearrange into islands of specialized cell types called islets of Langerhans, named after the German pathologist who discovered them in 1869.[493] These islets compromise five endocrine cell types, namely α, β, δ, PP, and ε cells, which produce glucagon, insulin, somatostatin, pancreatic polypeptide, and ghrelin hormones, respectively (Figure 17a). Endodermal cell differentiation through exocrine and endocrine signaling induces insulin-secreting cells as early as 4 months of gestation, with a final mature islet cell mass achieving a diameter of approximately 150 μm.

Traditionally, two types of diabetes have been classified, although a recent suggestion proposed five distinct types.[494] These all affect a patient's ability to control blood sugar level and the ability of insulin to trigger the body to take up glucose. Type 1 diabetes (T1D) is the result of a reduction of pancreas β-cell mass caused by an autoimmune response, impairing insulin secretion and leading to hyperglycemia. In contrast, type 2 diabetes (T2D) is generally characterized by a limited autoimmune response but still exhibits β-cell loss and, in addition, the onset of insulin resistance that prevents the body from taking up glucose and, therefore, leading to hyperglycemia.

While T2D can be often mitigated through diet, exercise, and lifestyle, T1D patients rely on daily insulin injections to control blood glucose levels. Therapies such as islet transplantation have been tested as an alternative treatment, and phase 3 clinical trials showed that 87.5% of the treated patients showed glycemic control after 1 year.[495] Despite the positive results, these patients must take immunosuppression therapy, triggering potential adverse effects such as renal dysfunction, and long-term insulin independence often cannot be maintained.[496]

7.2.1. Pancreas Bioprinting. Most bioprinting efforts with respect to TERM of the pancreas have focused on creating a construct to facilitate implantation of allogenic islet cells (Table 10). While the implant of islets of Langerhans and its cellular constituents is a highly promising diabetes therapy, many

https://dx.doi.org/10.1021/acs.chemrev.9b00789
Chem. Rev. 2020, 120, 11032−11092

Table 10. Bioprinting of Pancreatic Islets Implants

tissue	cells	composition	structure	mechanical properties	method	sequence	comments	ref
islets (transplant scaffold carrier)	β-cell line and human islets	alginate, gelatin, HA, matrigel	layered 0/90 pattern	n/a	plunger-driven printing (plotting)	cells were mixed with hydrogels and post-cross-linked with different concentrations of $CaCl_2$ for 15−30 min	*in vitro* culture post bioprinting during 14 days; abdominal and subcutaneous implantated *in vivo* during 7 days	498
islets (transplant scaffold carrier)	primary islets (rat)	alginate with (MC)	square 9 × 9 mm, strand distance 3 mm, 4 layers, 0/90	n/a	pressure-assisted extrusion	islets were mixed with alginate/MC, bioprinted, and cross-linked with strontium chloride ($SrCl_2$)	an average of 20% of the apoptic cells were observed in the plotted contructs with small variations during 7 days of *in vitro* culture	500
islets (transplant scaffold carrier)	primary islets (mouse), bone marrow derived endothelial progenitor cells (EPC, mouse) or ECs (MS1, CRL-2279), blood isolated T cells (human)	GelMA and alginate blends	single-layer 0/90 pattern	n/a	plunger extrusion-based	core: islets with hydrogel blends; shell: EPC with hydrogel blend; constructs were printed and cross-linked with UV during and after printing followed by $CaCl_2$ (10 min)	bioprinted constructs cultured for up to 3 days; cell -ree disks implanted subcutaneously for 21 days	502
pancreatic tumor model	human tumor- derived cancer, stellate and ECs	alginate-based	layered	n/a	extrusion-based	stromal bioink 200 M cells/mL (75% stellate cells + 25% HUVECs); tumor bioink 150 to 300 M cells/mL (75% tumor cells + 25% HUVECs); bioprinting; cross-linking with $CaCl_2$	*in vitro* and *in vivo* subcutaneous implantation in immunodeficient mice	503

challenges remain in order for this approach to successfully return lost endocrine functionality.[497] Critical considerations targeted by the bioprinting approach include cell viability during processing, the maintenance of islet function (e.g., insulin release), and the long-term survival of the islet mass by limiting the immune response toward the implanted cells while ensuring sufficient nutrient supply.

To prevent immune cell interaction with transplanted islets, several bioprinted carriers are currently under investigation. Marchioli et al.[498] developed a bioprinted scaffold from alginate or alginate in combination with gelatin, HA, or matrigel for islet implantation (Figure 17b−d). The islet carrier scaffold showed good cellular viability both *in vitro* and *in vivo*, but the metabolic activity was reduced likely due to the small mesh size of the hydrogels used for bioprinting. Glucose and lactate concentrations quantified throughout the cell culture period were similar for all the encapsulated islet conditions. Glucose stimulation to test insulin release from the islets showed reduced function when β-cells or human islets were bioprinted, while islets retrieved from the bioprinted constructs showed a return of stimulated insulin release. This suggests that an optimization of the hydrogel composition to allow insulin release might improve the performance of the bioprinted construct.

Toward this goal, Duin et al.[500] employed a bioink comprised of alginate and methylcellulose (MC), with the latter improving printability of the alginate filaments and microporosity.[501] Significant improvements were observed for insulin diffusion through alginate/MC scaffolds compared to scaffolds made from alginate alone; however, bioprinted islets were smaller and more fragmented, had reduced viability, and were more apoptotic compared to free-floating control islets.[500] Overall, this is reflected in the analysis of islet function, with bioprinted islets cultured *in vitro* for 4 days achieving appreciable insulin release in response to glucose stimulation but then losing function by day 7.

Liu et al.[502] recently reported a customized coaxial bioprinting approach capable of printing core/shell filaments with an islet-rich core surrounded by an outer-shell layer. Using a customized cooling print head and an alginate/GelMA composite bioink, the outer shell is intended to better protect the islet and also used to deliver a surrounding layer of support cells; these include ECs to improve islet engraftment into the host tissue and T regulatory cells to reduce the immune response. While this approach resulted in viable bioprinted islets, the functional release of insulin was again diminished with the reduced diffusion of insulin cited as a probable cause.

In addition to functional units and islets carriers, bioprinting has been used to develop pancreatic disease models.[503] Tumor models were bioprinted by depositing two bioinks: one containing pancreatic stellate cells and ECs and the tumor bioink with pancreatic cancer with different combinations.

7.2.2. Outlook of Pancreas Bioprinting. Similar to other organs, the bioprinting of the full pancreas is in its infancy, and much more research is required until it becomes a realistic possibility. The preliminary work performed on bioprinting specific cell types or entire islets of Langerhans indicates so far that constructs do not achieve the same functionality as the native organ. Future work will certainly focus on the development of appropriate hydrogels to allow insulin diffusion from the constructs. Furthermore, vascularization strategies will continue to be a focus of researchers to ensure the nutrient supply for islet viability and to improve the systemic release of insulin from the

https://dx.doi.org/10.1021/acs.chemrev.9b00789
Chem. Rev. 2020, 120, 11032−11092

implanted construct. Patient-derived PSC-derived β cells might be a future asset in terms of bioprinting implants and the full pancreas as a syngeneic cell source that has been shown to secrete insulin[504] and even reverse diabetes in animal models.[505]

8. OTHER BIOPRINTED TISSUE

8.1. Glands

The very first example of bioprinting applied to a gland is for the regeneration of sweat glands, which play an important role in thermoregulation. Huang et al.[506] used a 2:1 mixture of gelatin and alginate to encapsulate epithelial progenitor cells of sweat glands for bioprinting. Constructs containing cells alone or added with epidermal growth factors (EGFs) and/or dermal ECM were fabricated. The presence of dermal ECM was shown to support cell differentiation, whereas the addition of both dermal ECM and EGF resulted in functional regeneration of sweat glands in the burned paws of mice. Interestingly, the same group found that pore size of bioprinted constructs with the same hydrogel composition had a remarkable influence on gland self-organization and morphogenesis, with 300 μm pores guiding *in vitro* organization.[507]

Salivary glands have also been looked at as a target for bioprinting to aid in facilitating cell spatial organization. Adine et al.[508] used a magnetic bioprinter to steer the self-assembly of stem cells derived from dental pulp through magnetic nanoparticles and without the use of any hydrogels for cell encapsulation. Cell spheroids were then differentiated into salivary gland epithelial cells and assessed in an *ex vivo* transplanted tissue model. Biological constructs showed the presence of a neuronal cell subpopulation, which was important for the reinnervation, a critical process in the correct function of salivary glands. Furthermore, secretion of α-amylase, an enzyme produced during salivary gland function, was also successfully monitored.

A final example of gland bioprinting was reported by Bulanova et al.[509] for the thyroid, an organ responsible for the regulation of hormone synthesis essential for growth, neurological development, and homeostasis. Spheroids of embryonic thyroid and ECs were formed and bioprinted adjacent to each other on a collagen substrate. The spheroids fused, forming a vascularized thyroid construct that restored thyroid activity in a hypothyroid mouse model. These few successful reports demonstrate that bioprinting is a promising technology to fabricate biologically functional gland constructs and could spur further applications for other gland tissues.

8.2. Cornea

The cornea is responsible for ~80% of the refractive power of the whole eye. It has a particular collagen fiber orientation, forming between 200 and 250 lamellae that are responsible for the tissue strength and spherical geometry. Collagen lamellae are aligned in the mid and posterior parts and interwoven in the anterior part of the tissue. This particular alignment is also responsible for the transmission and refraction of light subsequently focused onto the retina. Considering this particular organization, current TERM approaches have proven to be challenging. Therefore, bioprinting has been studied in view of the possibility to recreate such a microstructural ECM architecture. In a proof-of-concept study, Wu et al.[510] encapsulated human corneal epithelial cells into an alginate/gelatin/collagen hydrogel mixture, showing that cells survived the bioprinting process. As the hydrogel degraded, cells were able to remodel it during culture, enhanced their proliferation, and expressed higher content of cytokeratin 3, a specific protein of corneal ECM. The fabricated constructs had a classical squared pore grid, which is far from the native organization of corneal collagen fibers. Isaacson et al.[511] recently showed that collagen/alginate mixtures at different collagen concentrations (6 mg/mL and 8 mg/mL) and ratios (2:1 or 3:1) could be used to bioprint corneal keratinocytes into anatomically shaped corneal constructs through the interpolation of clinical data sets. The resulting construct maintained the anatomical shape during culture, where higher collagen concentrations and the 3:1 collagen/alginate ratio resulted in higher resolution. Further studies of this promising approach should aim at assessing functional markers *in vitro* and *in vivo*. The most promising bioprinted corneal construct fabricated to date was reported by Sorkio et al.,[164] who used laser-assisted bioprinting to deposit both the epithelial and the stromal compartments of the cornea. For the epithelial layer, limbal epithelial stem cells derived from ESCs were used and encapsulated in human recombinant laminin-521 for bioprinting. For the stromal layer, human adipose tissue-derived stem cells were used and encapsulated in human collagen type I for bioprinting. The two layers were separated by an acellular compartment bioprinted from a mixture of collagen, human plasma, thrombin, and HA. The resulting construct showed stratification on the epithelial side, which was also positive for cytokeratin-3 on the apical side and for progenitor markers like p40 and p63α; the stromal side showed similar cell alignment and organization compared to native cornea. The construct integrated well in a porcine corneal organ culture model, yet *in vivo* studies are needed to further validate this approach.

In addition to the cornea, bioprinting of retinal ganglion cells and glia,[28] as well as of retinal pigment epithelial cell lines,[512] has been successfully reported. In both studies, cells were bioprinted without the use of carrying hydrogels, which will be needed when more complex eye tissues, such as frontal cornea and the retina, are constructed.

8.3. Muscle

Patients that undergo muscular trauma or tumor ablation might lose large portions of tissue, and alternatives to transplantation are required. The bioprinting community has started to investigate the possibility to replicate the highly aligned ECM architecture of the muscle tissue while ensuring anisotropic properties. Garcia-Lizarribar et al.[513] screened different blends of GelMA with methacrylated alginate or carboxymethyl cellulose (CMC) or with PEGDA. Mixtures with alginate and CMC resulted in durable bioprinted constructs and maintained cell viability and myotube formation, which is a classic marker for myocyte differentiation. Similar results have been obtained by Mozetic et al.[514] using Pluronic and assessing myocyte differentiation by gene expression of a panel of myocyte differentiation markers. Costantini et al.[45] moved beyond these initial studies by using coaxial microfluidic bioprinting where alginate was used as a sacrificial bioink to build softer regions within a PEG-fibrinogen hydrogel containing myoblasts. The aligned constructs resulted in myoblast differentiation assessed both at a genetic and at a protein level with a parallel organization. In addition, these constructs were successfully engrafted *in vivo*, maintaining myocyte phenotype. A further improvement in muscle bioprinting has been demonstrated by Choi et al.,[71] who used dECM from porcine skeletal muscle to create a gel-like formulation where myocytes were embedded and bioprinted in between the fibers of a PCL scaffold acting as a

https://dx.doi.org/10.1021/acs.chemrev.9b00789
Chem. Rev. 2020, 120, 11032−11092

mechanical stabilizer. The resulting biological constructs were not only positive for muscle markers as assessed at a genetic and protein level but also supported significantly longer myocyte alignment and increased mechanical properties compared to collagen. To further replicate the hierarchical structure of muscle, Yeo et al.[515] developed a construct by combining AM, electrospinning, and bioprinting that once wrapped could form a cylindrical scaffold. PCL was used for AM and electrospinning to create a scaffold with macro- and nanofibers, where the macrofibers had a more mechanically supportive role and the nanofibers further guided myocyte alignment after bioprinting in an alginate/PEG bioink. These constructs again were shown to support myocyte adhesion, proliferation, and differentiation.

Despite all these approaches demonstrating successful myocyte differentiation, they used already differentiated myocytes, typically from an animal cell line, which are less relevant for clinical translation. In an attempt to get close to clinically relevant biological constructs, Kim et al.[516] used human muscle progenitor cells encapsulated in a mixture of gelatin, HA, and fibrinogen in glycerol. The cell-laden bioink was bioprinted between PCL AM fibers acting as a mechanical support, as previously described in other studies. High density constructs supported cell alignment and differentiation and showed vascular and neural integration *in vivo* and a recovery of up to 82% of the muscular force of contraction of the native muscle. The same group previously demonstrated that these kinds of biological bioprinted constructs could be produced with human scaled dimensions, although further preclinical studies in larger animal models are needed before starting translation into clinics.[377]

Bioprinting of the muscle−tendon interface tissue also has been attempted. Merceron et al.[75] used again a mixture of gelatin, HA, and fibrinogen to encapsulate myocytes and fibroblasts for muscle and tendon tissues, respectively. The bioink was coprinted in between polyurethane fibers for the muscle side and PCL fibers for the tendon side. Instead of contiguous variation from the muscle to tendon, Laternser et al.[517] preferred to bioprint myocytes and tenocytes in alternating layers. GelMA alone or in combination with PEGDMA was used as the hydrogel, without the use of other mechanically supporting thermoplastic polymers. In both studies, *in vitro* evaluation showed the support of muscle−tendon tissue regeneration, thus suggesting that bioprinting could be a promising tool for the regeneration of this composite interface tissue.

8.4. Reproductive System

Bioprinting of constructs for the reproductive system has been limited to a few studies. Laronda et al.[518] showed that ovarian follicle viability and functionality were significantly influenced by gelatin scaffold pore geometry, with 30° and 60° providing a better nesting environment. This resulted in the exciting recovery of fertility in a sterilized mouse model and the subsequent healthy survival of newborn pups. While only this one study shows the promise of biofabrication approaches for the reproductive system, we think that this should be a field of application where more and more research should be conducted because organs of the reproductive system are particularly susceptible to environmental variations, such as radiation, and could benefit from bioprinting approaches.

9. CONCLUSIONS AND FUTURE OUTLOOK

Since the first experiments of cell bioprinting were successfully demonstrated in 2003,[26] many advances have been made. While many tissues or organ units have been envisioned and manufactured, the level of complexity needed to make relevant tissue and organ replacements is still not understood.

Several questions remain open when approaching complex regeneration strategies as in the case of organs. These biological systems are comprised of multiple tissues intimately connected to each other, and multiple cell types direct tissue development and homeostasis. We do not know what level of biomimicry of the native tissue or organ is needed: do we need to copy the whole organ structure, or can we achieve functional recovery with a tissue patch that is implanted in the damaged organ? In addition to the level of biomimicry, we also do not know if we need to use all the cellular subpopulations of if we could achieve differentiation into the needed phenotypes from a single-cell population such as PSCs. Can bioprinting make use of organoid technology to achieve more complex organ regeneration? Bioprinting technology would have to be sufficiently equipped to answer these questions, where multimaterial depositing systems can recreate the intrinsic heterogeneity of more complex structures.[86,519] Furthermore, comparative studies will be important to assess whether the biomimicry level that bioprinting can achieve is sufficient compared to other strategies, such as upscaling organoid production for further cell-therapy-based implantation,[520−522] where biomimicry is limited and left to cellular self-assembly, or decellularized organs from human donors or other species,[523−525] where the most exquisite degree of biomimicry would be achieved.

In the context of biomimetic and complex tissues, bioprinting could offer an exciting technology platform to incorporate lympathic, vascular, and neural networks, thus capturing the complexity of multiple tissue and organ systems. In this respect, biomaterials able to modulate the innate immune response[526,527] may also be good candidates for bioprinting.[526,527]

The ultimate exploitation of the true potential of the different bioprinting technologies will be gradually proven as new biomaterials and suitable cells are selected to efficiently be used as regenerative medicine therapies for tissues and eventually as a suitable replacement for organs. Despite these ambitious aims, the complexity is enormous, and much more studies are necessary to achieve these goals. In the short run, the tissue and organ models are slowly being adopted as alternative 3D screening models for the cosmetic and pharmaceutical industries. In parallel, as an astounding amount of data is being generated in the pursuit of optimal cell−biomaterial interactions for the regeneration of targeted tissues and from the use of such 3D screening models for cosmetic and pharmaceutical applications, we advocate for the use of advanced bioinformatics tools like artificial intelligence. This will allow us to navigate through the big data generated by bioprinting in a more rational manner, which will enable us to better streamline the manufacturing processes to get step-by-step closer to multitissue regeneration. Ultimately, we also advocate for the integration of multiple technologies in an automated fashion, to cover the biofabrication line from production and maturation to quality assessment of the bioprinted constructs. To achieve this, the assembly of a bioprinting station for production, followed by bioreactor technology for biological maturation and advanced imaging for quality assessment, could be envisioned. Such an automated integrated bioprocessing line would ensure a faster

https://dx.doi.org/10.1021/acs.chemrev.9b00789
Chem. Rev. 2020, 120, 11032−11092

translation from the academia to the industry through the implementation of several standard operating procedures that are direly needed to pass through the approval of regulatory bodies.

AUTHOR INFORMATION

Corresponding Authors

Lorenzo Moroni − *Department of Complex Tissue Regeneration, MERLN Institute for Technology-Inspired Regenerative Medicine, Maastricht University, 6211 LK Maastricht, The Netherlands;* orcid.org/0000-0003-1298-6025; Email: l.moroni@maastrichtuniversity.nl

Carlos Mota − *Department of Complex Tissue Regeneration, MERLN Institute for Technology-Inspired Regenerative Medicine, Maastricht University, 6211 LK Maastricht, The Netherlands;* orcid.org/0000-0001-5935-6245; Email: c.mota@maastrichtuniversity.nl

Authors

Sandra Camarero-Espinosa − *Department of Complex Tissue Regeneration, MERLN Institute for Technology-Inspired Regenerative Medicine, Maastricht University, 6211 LK Maastricht, The Netherlands;* orcid.org/0000-0003-0414-7141

Matthew B. Baker − *Department of Complex Tissue Regeneration, MERLN Institute for Technology-Inspired Regenerative Medicine, Maastricht University, 6211 LK Maastricht, The Netherlands;* orcid.org/0000-0003-1731-3858

Paul Wieringa − *Department of Complex Tissue Regeneration, MERLN Institute for Technology-Inspired Regenerative Medicine, Maastricht University, 6211 LK Maastricht, The Netherlands;* orcid.org/0000-0002-3290-5125

Complete contact information is available at: https://pubs.acs.org/10.1021/acs.chemrev.9b00789

Notes

The authors declare no competing financial interest.

Biographies

Dr. Carlos Mota is an Assistant Professor in the Department of Complex Tissue Regeneration, MERLN Institute for Technology-inspired Regenerative Medicine, Maastricht University, The Netherlands. Dr. Mota received his PhD in Biomaterials from the BIOS research doctorate school in Biomolecular Sciences at the University of Pisa, Italy, in March 2012. Currently, his main research interests focus on biofabrication, bioprinting, and additive manufacturing techniques for the development of tissue-engineered constructs.

Dr. Sandra Camarero-Espinosa developed her doctoral studies at the Adolphe Merkle Institute (Switzerland) and obtained her PhD degree in Polymer Chemistry and Bioengineering in 2015. After gaining a fellowship from the Swiss National Science Foundation, she moved to Brisbane (Australia) to work at the Australian Institute for Bioengineering and Nanotechnology. Sandra is now a postdoctoral researcher at the MERLN Institute where she works on the development of instructive biomaterial scaffolds for the regeneration of complex tissues.

Dr. Matthew Baker received his B.S. in chemistry at Clemson University (2006) and his PhD in Physical Organic Chemistry at the University of Florida (2012). After his PhD, he pursued a postdoctoral study at the Eindhoven University of Technology to design and characterize water-soluble supramolecular polymers. In 2015, he joined the MERLN Institute at Maastricht University to develop polymeric and supramolecular materials for tissue engineering and started the BioMatt group as an Assistant Professor in 2017. His research interests include the synthesis and characterization of novel and dynamic materials to mimic the cellular environment and to influence cellular behavior.

Dr. Paul Wieringa completed a dual PhD in 2014 from the University of Twente (NL) and Scuola Superiore Sant'Anna (IT) on 3D electrospun scaffolds for nerve regeneration. After his postdoctoral fellow at the MERLN Institute from 2014 to 2017, he became an Assistant Professor in 2018 at MERLN and is currently leading a research group on creating 3D *in vitro* models of tissue innervation to explore neurogenic tissue repair strategies.

Prof. Lorenzo Moroni received his PhD cum laude in 2006 from Twente University on 3D scaffolds for osteochondral regeneration. Since 2014, he has worked at Maastricht University, as a founding member of the MERLN Institute for Technology-Inspired Regenerative Medicine. In 2016, he became Full Professor in biofabrication for regenerative medicine. Since 2019, he has been chair of the Complex Tissue Regeneration department and Vice Director of MERLN. His research group aims at developing biofabrication technologies to control cell fate, with applications spanning from skeletal to vascular, neural, and organ regeneration. From his research efforts, three products have already reached the market.

ACKNOWLEDGMENTS

We are grateful to the Dutch Kidney Foundation (Nierstichting Nederland, grant 18OI17 − Innovation Call 2018) and to the European Research Council starting grant "Cell Hybridge" (Grant #637308) and H2020-NMP-PILOTS-2015 "FAST" (Grant #685825), under the Horizon 2020 framework program for financial support. We also acknowledge support from the Dutch Province of Limburg and from the research programme Innovation Fund Chemistry, which is partly financed by The Netherlands Organisation for Scientific Research (NWO). The authors would like to thank Rogier Trompert for the illustrations.

REFERENCES

(1) Harrison, R. H.; St-Pierre, J. P.; Stevens, M. M. Tissue Engineering and Regenerative Medicine: A Year in Review. *Tissue Eng., Part B* **2014**, *20*, 1.

(2) Gomes, M. E.; Rodrigues, M. T.; Domingues, R. M. A.; Reis, R. L. Tissue Engineering and Regenerative Medicine: New Trends and Directions-a Year in Review. *Tissue Eng., Part B* **2017**, *23*, 211.

(3) Langer, R.; Vacanti, J. P. Tissue Engineering. *Science* **1993**, *260*, 920.

(4) Place, E. S.; Evans, N. D.; Stevens, M. M. Complexity in Biomaterials for Tissue Engineering. *Nat. Mater.* **2009**, *8*, 457.

(5) Lutolf, M. P.; Hubbell, J. A. Synthetic Biomaterials as Instructive Extracellular Microenvironments for Morphogenesis in Tissue Engineering. *Nat. Biotechnol.* **2005**, *23*, 47.

(6) Mano, J. F.; Silva, G. A.; Azevedo, H. S.; Malafaya, P. B.; Sousa, R. A.; Silva, S. S.; Boesel, L. F.; Oliveira, J. M.; Santos, T. C.; Marques, A. P.; et al. Natural Origin Biodegradable Systems in Tissue Engineering and Regenerative Medicine: Present Status and Some Moving Trends. *J. R. Soc., Interface* **2007**, *4*, 999.

(7) Slaughter, B. V.; Khurshid, S. S.; Fisher, O. Z.; Khademhosseini, A.; Peppas, N. A. Hydrogels in Regenerative Medicine. *Adv. Mater.* **2009**, *21*, 3307.

(8) Caplan, A. I. Adult Mesenchymal Stem Cells for Tissue Engineering Versus Regenerative Medicine. *J. Cell. Physiol.* **2007**, *213*, 341.

(9) Gimble, J. M.; Katz, A. J.; Bunnell, B. A. Adipose-Derived Stem Cells for Regenerative Medicine. *Circ. Res.* **2007**, *100*, 1249.
(10) Robinton, D. A.; Daley, G. Q. The Promise of Induced Pluripotent Stem Cells in Research and Therapy. *Nature* **2012**, *481*, 295.
(11) Groll, J.; Boland, T.; Blunk, T.; Burdick, J. A.; Cho, D. W.; Dalton, P. D.; Derby, B.; Forgacs, G.; Li, Q.; Mironov, V. A.; et al. Biofabrication: Reappraising the Definition of an Evolving Field. *Biofabrication* **2016**, *8*, 013001.
(12) Mota, C.; Puppi, D.; Chiellini, F.; Chiellini, E. Additive Manufacturing Techniques for the Production of Tissue Engineering Constructs. *J. Tissue Eng. Regener. Med.* **2015**, *9*, 174.
(13) Ligon, S. C.; Liska, R.; Stampfl, J.; Gurr, M.; Mulhaupt, R. Polymers for 3d Printing and Customized Additive Manufacturing. *Chem. Rev.* **2017**, *117*, 10212.
(14) Murphy, S. V.; Atala, A. 3d Bioprinting of Tissues and Organs. *Nat. Biotechnol.* **2014**, *32*, 773.
(15) Ozbolat, I. T.; Hospodiuk, M. Current Advances and Future Perspectives in Extrusion-Based Bioprinting. *Biomaterials* **2016**, *76*, 321.
(16) Mandrycky, C.; Wang, Z.; Kim, K.; Kim, D. H. 3d Bioprinting for Engineering Complex Tissues. *Biotechnol. Adv.* **2016**, *34*, 422.
(17) Holzl, K.; Lin, S.; Tytgat, L.; Van Vlierberghe, S.; Gu, L.; Ovsianikov, A. Bioink Properties before, During and after 3d Bioprinting. *Biofabrication* **2016**, *8*, 032002.
(18) Gudapati, H.; Dey, M.; Ozbolat, I. A Comprehensive Review on Droplet-Based Bioprinting: Past, Present and Future. *Biomaterials* **2016**, *102*, 20.
(19) Zhang, Y. S.; Yue, K.; Aleman, J.; Mollazadeh-Moghaddam, K.; Bakht, S. M.; Yang, J.; Jia, W.; Dell'Erba, V.; Assawes, P.; Shin, S. R.; Dokmeci, M. R.; Oklu, R.; Khademhosseini, A.; et al. 3d Bioprinting for Tissue and Organ Fabrication. *Ann. Biomed. Eng.* **2017**, *45*, 148.
(20) Gao, B.; Yang, Q.; Zhao, X.; Jin, G.; Ma, Y.; Xu, F. 4d Bioprinting for Biomedical Applications. *Trends Biotechnol.* **2016**, *34*, 746.
(21) Tomasina, C.; Bodet, T.; Mota, C.; Moroni, L.; Camarero-Espinosa, S. Bioprinting Vasculature: Materials, Cells and Emergent Techniques. *Materials* **2019**, *12*, 2701.
(22) Pereira, F. D. A. S.; Parfenov, V.; Khesuani, Y. D.; Ovsianikov, A.; Mironov, V. In *3d Printing and Biofabrication*; Ovsianikov, A., Yoo, J., Mironov, V., Eds.; Springer International Publishing: Cham, 2018.
(23) Choudhury, D.; Anand, S.; Naing, M. W. The Arrival of Commercial Bioprinters - Towards 3d Bioprinting Revolution! *Int. J. Bioprinting* **2018**, DOI: 10.18063/ijb.v4i2.139.
(24) Mota, C.; Moroni, L. *High Throughput Screening With biofabrication Platforms*; Academic Press: Boston, 2015.
(25) Cui, X.; Boland, T. Human Microvasculature Fabrication Using Thermal Inkjet Printing Technology. *Biomaterials* **2009**, *30*, 6221.
(26) Wilson, W. C., Jr.; Boland, T. Cell and Organ Printing 1: Protein and Cell Printers. *Anat. Rec.* **2003**, *272*, 491.
(27) Saunders, R. E.; Gough, J. E.; Derby, B. Delivery of Human Fibroblast Cells by Piezoelectric Drop-on-Demand Inkjet Printing. *Biomaterials* **2008**, *29*, 193.
(28) Lorber, B.; Hsiao, W. K.; Hutchings, I. M.; Martin, K. R. Adult Rat Retinal Ganglion Cells and Glia Can Be Printed by Piezoelectric Inkjet Printing. *Biofabrication* **2014**, *6*, 015001.
(29) Demirci, U.; Montesano, G. Single Cell Epitaxy by Acoustic Picolitre Droplets. *Lab Chip* **2007**, *7*, 1139.
(30) Guo, F.; Mao, Z.; Chen, Y.; Xie, Z.; Lata, J. P.; Li, P.; Ren, L.; Liu, J.; Yang, J.; Dao, M.; et al. Three-Dimensional Manipulation of Single Cells Using Surface Acoustic Waves. *Proc. Natl. Acad. Sci. U. S. A.* **2016**, *113*, 1522.
(31) Parfenov, V. A.; Koudan, E. V.; Bulanova, E. A.; Karalkin, P. A.; Das Pereira, F.; Norkin, N. E.; Knyazeva, A. D.; Gryadunova, A. A.; Petrov, O. F.; Vasiliev, M. M.; et al. Scaffold-Free, Label-Free and Nozzle-Free Biofabrication Technology Using Magnetic Levitational Assembly. *Biofabrication* **2018**, *10*, 034104.
(32) Durmus, N. G.; Tekin, H. C.; Guven, S.; Sridhar, K.; Arslan Yildiz, A.; Calibasi, G.; Ghiran, I.; Davis, R. W.; Steinmetz, L. M.; Demirci, U. Magnetic Levitation of Single Cells. *Proc. Natl. Acad. Sci. U. S. A.* **2015**, *112*, No. E3661.
(33) Marycz, K.; Kornicka, K.; Rocken, M. Static Magnetic Field (Smf) as a Regulator of Stem Cell Fate - New Perspectives in Regenerative Medicine Arising from an Underestimated Tool. *Stem Cell Rev. Rep.* **2018**, *14*, 785.
(34) Ma, X.; Qu, X.; Zhu, W.; Li, Y. S.; Yuan, S.; Zhang, H.; Liu, J.; Wang, P.; Lai, C. S.; Zanella, F.; et al. Deterministically Patterned Biomimetic Human Ipsc-Derived Hepatic Model Via Rapid 3d Bioprinting. *Proc. Natl. Acad. Sci. U. S. A.* **2016**, *113*, 2206.
(35) Ooi, H. W.; Mota, C.; Ten Cate, A. T.; Calore, A.; Moroni, L.; Baker, M. B. Thiol-Ene Alginate Hydrogels as Versatile Bioinks for Bioprinting. *Biomacromolecules* **2018**, *19*, 3390.
(36) Michael, S.; Sorg, H.; Peck, C. T.; Koch, L.; Deiwick, A.; Chichkov, B.; Vogt, P. M.; Reimers, K. Tissue Engineered Skin Substitutes Created by Laser-Assisted Bioprinting Form Skin-Like Structures in the Dorsal Skin Fold Chamber in Mice. *PLoS One* **2013**, *8*, No. e57741.
(37) Xing, J. F.; Zheng, M. L.; Duan, X. M. Two-Photon Polymerization Microfabrication of Hydrogels: An Advanced 3d Printing Technology for Tissue Engineering and Drug Delivery. *Chem. Soc. Rev.* **2015**, *44*, 5031.
(38) Dobos, A.; Van Hoorick, J.; Steiger, W.; Gruber, P.; Markovic, M.; Andriotis, O. G.; Rohatschek, A.; Dubruel, P.; Thurner, P. J.; Van Vlierberghe, S.; Baudis, S.; Ovsianikov, A.; et al. Thiol-Gelatin-Norbornene Bioink for Laser-Based High-Definition Bioprinting. *Adv. Healthcare Mater.* **2019**, 1900752.
(39) Bernal, P. N.; Delrot, P.; Loterie, D.; Li, Y.; Malda, J.; Moser, C.; Levato, R. Volumetric Bioprinting of Complex Living-Tissue Constructs within Seconds. *Adv. Mater.* **2019**, *31*, No. e1904209.
(40) Kelly, B. E.; Bhattacharya, I.; Heidari, H.; Shusteff, M.; Spadaccini, C. M.; Taylor, H. K. Volumetric Additive Manufacturing Via Tomographic Reconstruction. *Science* **2019**, *363*, 1075.
(41) Mark, D.; Haeberle, S.; Roth, G.; von Stetten, F.; Zengerle, R. Microfluidic Lab-on-a-Chip Platforms: Requirements, Characteristics and Applications. *Chem. Soc. Rev.* **2010**, *39*, 1153.
(42) Whitesides, G. M. The Origins and the Future of Microfluidics. *Nature* **2006**, *442*, 368.
(43) Barata, D.; van Blitterswijk, C.; Habibovic, P. High-Throughput Screening Approaches and Combinatorial Development of Biomaterials Using Microfluidics. *Acta Biomater.* **2016**, *34*, 1.
(44) Colosi, C.; Shin, S. R.; Manoharan, V.; Massa, S.; Costantini, M.; Barbetta, A.; Dokmeci, M. R.; Dentini, M.; Khademhosseini, A. Microfluidic Bioprinting of Heterogeneous 3d Tissue Constructs Using Low-Viscosity Bioink. *Adv. Mater.* **2016**, *28*, 677.
(45) Costantini, M.; Testa, S.; Mozetic, P.; Barbetta, A.; Fuoco, C.; Fornetti, E.; Tamiro, F.; Bernardini, S.; Jaroszewicz, J.; Swieszkowski, W.; et al. Microfluidic-Enhanced 3d Bioprinting of Aligned Myoblast-Laden Hydrogels Leads to Functionally Organized Myofibers in Vitro and in Vivo. *Biomaterials* **2017**, *131*, 98.
(46) Snyder, J.; Son, A. R.; Hamid, Q.; Wu, H.; Sun, W. Hetero-Cellular Prototyping by Synchronized Multi-Material Bioprinting for Rotary Cell Culture System. *Biofabrication* **2016**, *8*, 015002.
(47) Zhao, H.; Chen, Y.; Shao, L.; Xie, M.; Nie, J.; Qiu, J.; Zhao, P.; Ramezani, H.; Fu, J.; Ouyang, H.; et al. Airflow-Assisted 3d Bioprinting of Human Heterogeneous Microspheroidal Organoids with Microfluidic Nozzle. *Small* **2018**, *14*, No. e1802630.
(48) Abelseth, E.; Abelseth, L.; De la Vega, L.; Beyer, S. T.; Wadsworth, S. J.; Willerth, S. M. 3d Printing of Neural Tissues Derived from Human Induced Pluripotent Stem Cells Using a Fibrin-Based Bioink. *ACS Biomater. Sci. Eng.* **2019**, *5*, 234.
(49) De la Vega, L.; Rosas Gómez, D.; Abelseth, E.; Abelseth, L.; Allisson da Silva, V.; Willerth, S. M. 3d Bioprinting Human Induced Pluripotent Stem Cell-Derived Neural Tissues Using a Novel Lab-on-a-Printer Technology. *Appl. Sci.* **2018**, *8*, 2414.
(50) Groll, J.; Burdick, J. A.; Cho, D. W.; Derby, B.; Gelinsky, M.; Heilshorn, S. C.; Jungst, T.; Malda, J.; Mironov, V. A.; Nakayama, K.; et al. A Definition of Bioinks and Their Distinction from Biomaterial Inks. *Biofabrication* **2019**, *11*, 013001.

https://dx.doi.org/10.1021/acs.chemrev.9b00789
Chem. Rev. 2020, 120, 11032−11092

(51) Hinton, T. J.; Jallerat, Q.; Palchesko, R. N.; Park, J. H.; Grodzicki, M. S.; Shue, H. J.; Ramadan, M. H.; Hudson, A. R.; Feinberg, A. W. Three-Dimensional Printing of Complex Biological Structures by Freeform Reversible Embedding of Suspended Hydrogels. *Sci. Adv.* **2015**, *1*, No. e1500758.
(52) Highley, C. B.; Song, K. H.; Daly, A. C.; Burdick, J. A. Jammed Microgel Inks for 3d Printing Applications. *Adv. Sci. (Weinh.)* **2019**, *6*, 1801076.
(53) Bertlein, S.; Brown, G.; Lim, K. S.; Jungst, T.; Boeck, T.; Blunk, T.; Tessmar, J.; Hooper, G. J.; Woodfield, T. B. F.; Groll, J. Thiol-Ene Clickable Gelatin: A Platform Bioink for Multiple 3d Biofabrication Technologies. *Adv. Mater.* **2017**, *29*, 1703404.
(54) Lee, A.; Hudson, A. R.; Shiwarski, D. J.; Tashman, J. W.; Hinton, T. J.; Yerneni, S.; Bliley, J. M.; Campbell, P. G.; Feinberg, A. W. 3d Bioprinting of Collagen to Rebuild Components of the Human Heart. *Science* **2019**, *365*, 482.
(55) Grigoryan, B.; Paulsen, S. J.; Corbett, D. C.; Sazer, D. W.; Fortin, C. L.; Zaita, A. J.; Greenfield, P. T.; Calafat, N. J.; Gounley, J. P.; Ta, A. H.; et al. Multivascular Networks and Functional Intravascular Topologies within Biocompatible Hydrogels. *Science* **2019**, *364*, 458.
(56) Hospodiuk, M.; Dey, M.; Sosnoski, D.; Ozbolat, I. T. The Bioink: A Comprehensive Review on Bioprintable Materials. *Biotechnol. Adv.* **2017**, *35*, 217.
(57) Gungor-Ozkerim, P. S.; Inci, I.; Zhang, Y. S.; Khademhosseini, A.; Dokmeci, M. R. Bioinks for 3d Bioprinting: An Overview. *Biomater. Sci.* **2018**, *6*, 915.
(58) Gopinathan, J.; Noh, I. Recent Trends in Bioinks for 3d Printing. *Biomater. Res.* **2018**, *22*, 11.
(59) Tarassoli, S. P.; Jessop, Z. M.; Kyle, S.; Whitaker, I. S. In *3d Bioprinting for Reconstructive Surgery*; Thomas, D. J., Jessop, Z. M., Whitaker, I. S., Eds.; Woodhead Publishing, 2018.
(60) Hofmann, M. 3d Printing Gets a Boost and Opportunities with Polymer Materials. *ACS Macro Lett.* **2014**, *3*, 382.
(61) Jungst, T.; Smolan, W.; Schacht, K.; Scheibel, T.; Groll, J. Strategies and Molecular Design Criteria for 3d Printable Hydrogels. *Chem. Rev.* **2016**, *116*, 1496.
(62) Malda, J.; Visser, J.; Melchels, F. P.; Jüngst, T.; Hennink, W. E.; Dhert, W. J. A.; Groll, J.; Hutmacher, D. W. 25th Anniversary Article: Engineering Hydrogels for Biofabrication. *Adv. Mater.* **2013**, *25*, 5011.
(63) Lee, J. M.; Yeong, W. Y. Design and Printing Strategies in 3d Bioprinting of Cell-Hydrogels: A Review. *Adv. Healthcare Mater.* **2016**, *5*, 2856.
(64) Wang, X.; Jiang, M.; Zhou, Z.; Gou, J.; Hui, D. 3d Printing of Polymer Matrix Composites: A Review and Prospective. *Composites, Part B* **2017**, *110*, 442.
(65) Mondschein, R. J.; Kanitkar, A.; Williams, C. B.; Verbridge, S. S.; Long, T. E. Polymer Structure-Property Requirements for Stereolithographic 3d Printing of Soft Tissue Engineering Scaffolds. *Biomaterials* **2017**, *140*, 170.
(66) Zhang, Z.; Jin, Y.; Yin, J.; Xu, C. X.; Xiong, R. T.; Christensen, K.; Ringeisen, B. R.; Chrisey, D. B.; Huang, Y. Evaluation of Bioink Printability for Bioprinting Applications. *Appl. Phys. Rev.* **2018**, *5*, 041304.
(67) Shirazi, S. F.; Gharehkhani, S.; Mehrali, M.; Yarmand, H.; Metselaar, H. S.; Adib Kadri, N.; Osman, N. A. A Review on Powder-Based Additive Manufacturing for Tissue Engineering: Selective Laser Sintering and Inkjet 3d Printing. *Sci. Technol. Adv. Mater.* **2015**, *16*, 033502.
(68) Torgersen, J.; Qin, X. H.; Li, Z. Q.; Ovsianikov, A.; Liska, R.; Stampfl, J. Hydrogels for Two-Photon Polymerization: A Toolbox for Mimicking the Extracellular Matrix. *Adv. Funct. Mater.* **2013**, *23*, 4542.
(69) Hutmacher, D. W.; Schantz, T.; Zein, I.; Ng, K. W.; Teoh, S. H.; Tan, K. C. Mechanical Properties and Cell Cultural Response of Polycaprolactone Scaffolds Designed and Fabricated Via Fused Deposition Modeling. *J. Biomed. Mater. Res.* **2001**, *55*, 203.
(70) Lee, J.-S.; Hong, J. M.; Jung, J. W.; Shim, J.-H.; Oh, J.-H.; Cho, D.-W. 3d Printing of Composite Tissue with Complex Shape Applied to Ear Regeneration. *Biofabrication* **2014**, *6*, 024103.
(71) Choi, Y. J.; Kim, T. G.; Jeong, J.; Yi, H. G.; Park, J. W.; Hwang, W.; Cho, D. W. 3d Cell Printing of Functional Skeletal Muscle Constructs Using Skeletal Muscle-Derived Bioink. *Adv. Healthcare Mater.* **2016**, *5*, 2636.
(72) Appuhamillage, G. A.; Reagan, J. C.; Khorsandi, S.; Davidson, J. R.; Voit, W.; Smaldone, R. A. 3d Printed Remendable Polylactic Acid Blends with Uniform Mechanical Strength Enabled by a Dynamic Diels-Alder Reaction. *Polym. Chem.* **2017**, *8*, 2087.
(73) Ge, Z.; Tian, X.; Heng, B. C.; Fan, V.; Yeo, J. F.; Cao, T. Histological Evaluation of Osteogenesis of 3d-Printed Poly-Lactic-Co-Glycolic Acid (Plga) Scaffolds in a Rabbit Model. *Biomed. Mater.* **2009**, *4*, 021001.
(74) Moroni, L.; de Wijn, J. R.; van Blitterswijk, C. A. 3d Fiber-Deposited Scaffolds for Tissue Engineering: Influence of Pores Geometry and Architecture on Dynamic Mechanical Properties. *Biomaterials* **2006**, *27*, 974.
(75) Merceron, T. K.; Burt, M.; Seol, Y. J.; Kang, H. W.; Lee, S. J.; Yoo, J. J.; Atala, A. A 3d Bioprinted Complex Structure for Engineering the Muscle-Tendon Unit. *Biofabrication* **2015**, *7*, 035003.
(76) Muller, M.; Becher, J.; Schnabelrauch, M.; Zenobi-Wong, M. Nanostructured Pluronic Hydrogels as Bioinks for 3d Bioprinting. *Biofabrication* **2015**, *7*, 035006.
(77) England, S.; Rajaram, A.; Schreyer, D. J.; Chen, X. Bioprinted Fibrin-Factor Xiii-Hyaluronate Hydrogel Scaffolds with Encapsulated Schwann Cells and Their in Vitro Characterization for Use in Nerve Regeneration. *Bioprinting* **2017**, *5*, 1.
(78) Rajaram, A.; Schreyer, D.; Chen, D. Bioplotting Alginate/Hyaluronic Acid Hydrogel Scaffolds with Structural Integrity and Preserved Schwann Cell Viability. *3d Print Addit Manuf* **2014**, *1*, 194.
(79) Harper, M. M.; Connolly, M. L.; Goldie, L.; Irvine, E. J.; Shaw, J. E.; Jayawarna, V.; Richardson, S. M.; Dalby, M. J.; Lightbody, D.; Ulijn, R. V. Biogelx: Cell Culture on Self-Assembling Peptide Gels. *Methods Mol. Biol.* **2018**, *1777*, 283.
(80) Alakpa, E. V.; Jayawarna, V.; Lampel, A.; Burgess, K. V.; West, C. C.; Bakker, S. C.J.; Roy, S.; Javid, N.; Fleming, S.; Lamprou, D. A.; Yang, J.; Miller, A.; Urquhart, A. J.; Frederix, P. W.J.M.; Hunt, N. T.; Peault, B.; Ulijn, R. V.; Dalby, M. J.; et al. Tunable Supramolecular Hydrogels for Selection of Lineage-Guiding Metabolites in Stem Cell Cultures. *Chem.* **2016**, *1*, 298.
(81) Kesti, M.; Müller, M.; Becher, J.; Schnabelrauch, M.; D'Este, M.; Eglin, D.; Zenobi-Wong, M. A Versatile Bioink for Three-Dimensional Printing of Cellular Scaffolds Based on Thermally and Photo-Triggered Tandem Gelation. *Acta Biomater.* **2015**, *11*, 162.
(82) Jia, J.; Richards, D. J.; Pollard, S.; Tan, Y.; Rodriguez, J.; Visconti, R. P.; Trusk, T. C.; Yost, M. J.; Yao, H.; Markwald, R. R.; et al. Engineering Alginate as Bioink for Bioprinting. *Acta Biomater.* **2014**, *10*, 4323.
(83) Ouyang, L.; Highley, C. B.; Rodell, C. B.; Sun, W.; Burdick, J. A. 3d Printing of Shear-Thinning Hyaluronic Acid Hydrogels with Secondary Cross-Linking. *ACS Biomater. Sci. Eng.* **2016**, *2*, 1743.
(84) Pati, F.; Jang, J.; Ha, D. H.; Won Kim, S.; Rhie, J. W.; Shim, J. H.; Kim, D. H.; Cho, D. W. Printing Three-Dimensional Tissue Analogues with Decellularized Extracellular Matrix Bioink. *Nat. Commun.* **2014**, *5*, 3935.
(85) Shi, W.; Sun, M.; Hu, X.; Ren, B.; Cheng, J.; Li, C.; Duan, X.; Fu, X.; Zhang, J.; Chen, H.; Ao, Y. Structurally and Functionally Optimized Silk-Fibroin-Gelatin Scaffold Using 3d Printing to Repair Cartilage Injury in Vitro and in Vivo. *Adv. Mater.* **2017**, *29*, 1701089.
(86) Nadernezhad, A.; Khani, N.; Skvortsov, G. A.; Toprakhisar, B.; Bakirci, E.; Menceloglu, Y.; Unal, S.; Koc, B. Multifunctional 3d Printing of Heterogeneous Hydrogel Structures. *Sci. Rep.* **2016**, *6*, 33178.
(87) Kopf, M.; Campos, D. F.; Blaeser, A.; Sen, K. S.; Fischer, H. A Tailored Three-Dimensionally Printable Agarose-Collagen Blend Allows Encapsulation, Spreading, and Attachment of Human Umbilical Artery Smooth Muscle Cells. *Biofabrication* **2016**, *8*, 025011.
(88) Hausmann, M. K.; Ruhs, P. A.; Siqueira, G.; Lauger, J.; Libanori, R.; Zimmermann, T.; Studart, A. R. Dynamics of Cellulose Nanocrystal Alignment During 3d Printing. *ACS Nano* **2018**, *12*, 6926.

https://dx.doi.org/10.1021/acs.chemrev.9b00789
Chem. Rev. 2020, 120, 11032−11092

(89) Voet, V. S. D.; Strating, T.; Schnelting, G. H. M.; Dijkstra, P.; Tietema, M.; Xu, J.; Woortman, A. J. J.; Loos, K.; Jager, J.; Folkersma, R. Biobased Acrylate Photocurable Resin Formulation for Stereolithography 3d Printing. *ACS Omega* **2018**, *3*, 1403.
(90) Billiet, T.; Gevaert, E.; De Schryver, T.; Cornelissen, M.; Dubruel, P. The 3d Printing of Gelatin Methacrylamide Cell-Laden Tissue-Engineered Constructs with High Cell Viability. *Biomaterials* **2014**, *35*, 49.
(91) Aduba, D. C.; Margaretta, E. D.; Marnot, A. E. C.; Heifferon, K. V.; Surbey, W. R.; Chartrain, N. A.; Whittington, A. R.; Long, T. E.; Williams, C. B. Vat Photopolymerization 3d Printing of Acid-Cleavable Peg-Methacrylate Networks for Biomaterial Applications. *Mater. Today Commun.* **2019**, *19*, 204.
(92) Schuller-Ravoo, S.; Teixeira, S. M.; Feijen, J.; Grijpma, D. W.; Poot, A. A. Flexible and Elastic Scaffolds for Cartilage Tissue Engineering Prepared by Stereolithography Using Poly(Trimethylene Carbonate)-Based Resins. *Macromol. Biosci.* **2013**, *13*, 1711.
(93) Markstedt, K.; Mantas, A.; Tournier, I.; Martínez Ávila, H.; Hägg, D.; Gatenholm, P. 3d Bioprinting Human Chondrocytes with Nanocellulose−Alginate Bioink for Cartilage Tissue Engineering Applications. *Biomacromolecules* **2015**, *16*, 1489.
(94) Bergmann, C.; Lindner, M.; Zhang, W.; Koczur, K.; Kirsten, A.; Telle, R.; Fischer, H. 3d Printing of Bone Substitute Implants Using Calcium Phosphate and Bioactive Glasses. *J. Eur. Ceram. Soc.* **2010**, *30*, 2563.
(95) Senatov, F. S.; Niaza, K. V.; Zadorozhnyy, M. Y.; Maksimkin, A. V.; Kaloshkin, S. D.; Estrin, Y. Z. Mechanical Properties and Shape Memory Effect of 3d-Printed Pla-Based Porous Scaffolds. *J. Mech. Behav. Biomed. Mater.* **2016**, *57*, 139.
(96) Zhou, X.; Nowicki, M.; Cui, H.; Zhu, W.; Fang, X.; Miao, S.; Lee, S.-J.; Keidar, M.; Zhang, L. G. 3d Bioprinted Graphene Oxide-Incorporated Matrix for Promoting Chondrogenic Differentiation of Human Bone Marrow Mesenchymal Stem Cells. *Carbon* **2017**, *116*, 615.
(97) Ho, C. M.; Mishra, A.; Lin, P. T.; Ng, S. H.; Yeong, W. Y.; Kim, Y. J.; Yoon, Y. J. 3d Printed Polycaprolactone Carbon Nanotube Composite Scaffolds for Cardiac Tissue Engineering. *Macromol. Biosci.* **2017**, *17*, 1600250.
(98) Liu, F. Y.; Vyas, C.; Poologasundarampillai, G.; Pape, I.; Hinduja, S.; Mirihanage, W.; Bartolo, P. Structural Evolution of Pcl During Melt Extrusion 3d Printing. *Macromol. Mater. Eng.* **2018**, *303*, 1700494.
(99) Gloria, A.; Frydman, B.; Lamas, M. L.; Serra, A. C.; Martorelli, M.; Coelho, J. F. J.; Fonseca, A. C.; Domingos, M. The Influence of Poly(Ester Amide) on the Structural and Functional Features of 3d Additive Manufactured Poly(Epsilon-Caprolactone) Scaffolds. *Mater. Sci. Eng., C* **2019**, *98*, 994.
(100) Mironov, V.; Boland, T.; Trusk, T.; Forgacs, G.; Markwald, R. R. Organ Printing: Computer-Aided Jet-Based 3d Tissue Engineering. *Trends Biotechnol.* **2003**, *21*, 157.
(101) Jakab, K.; Neagu, A.; Mironov, V.; Markwald, R. R.; Forgacs, G. Engineering Biological Structures of Prescribed Shape Using Self-Assembling Multicellular Systems. *Proc. Natl. Acad. Sci. U. S. A.* **2004**, *101*, 2864.
(102) Dhariwala, B.; Hunt, E.; Boland, T. Rapid Prototyping of Tissue-Engineering Constructs, Using Photopolymerizable Hydrogels and Stereolithography. *Tissue Eng.* **2004**, *10*, 1316.
(103) Hafeez, S.; Ooi, H. W.; Morgan, F. L. C.; Mota, C.; Dettin, M.; Van Blitterswijk, C.; Moroni, L.; Baker, M. B. Viscoelastic Oxidized Alginates with Reversible Imine Type Crosslinks: Self-Healing, Injectable, and Bioprintable Hydrogels. *Gels* **2018**, *4*, 85.
(104) Wu, Q. H.; Therriault, D.; Heuzey, M. C. Processing and Properties of Chitosan Inks for 3d Printing of Hydrogel Microstructures. *ACS Biomater. Sci. Eng.* **2018**, *4*, 2643.
(105) Highley, C. B.; Rodell, C. B.; Burdick, J. A. Direct 3d Printing of Shear-Thinning Hydrogels into Self-Healing Hydrogels. *Adv. Mater.* **2015**, *27*, 5075.
(106) Burdick, J. A.; Prestwich, G. D. Hyaluronic Acid Hydrogels for Biomedical Applications. *Adv. Mater.* **2011**, *23*, 41.
(107) Klotz, B. J.; Gawlitta, D.; Rosenberg, A.; Malda, J.; Melchels, F. P. W. Gelatin-Methacryloyl Hydrogels: Towards Biofabrication-Based Tissue Repair. *Trends Biotechnol.* **2016**, *34*, 394.
(108) Stichler, S.; Jungst, T.; Schamel, M.; Zilkowski, I.; Kuhlmann, M.; Bock, T.; Blunk, T.; Tessmar, J.; Groll, J. Thiol-Ene Clickable Poly(Glycidol) Hydrogels for Biofabrication. *Ann. Biomed. Eng.* **2017**, *45*, 273.
(109) Zhu, J. Bioactive Modification of Poly(Ethylene Glycol) Hydrogels for Tissue Engineering. *Biomaterials* **2010**, *31*, 4639.
(110) Li, C.; Faulkner-Jones, A.; Dun, A. R.; Jin, J.; Chen, P.; Xing, Y.; Yang, Z.; Li, Z.; Shu, W.; Liu, D.; et al. Rapid Formation of a Supramolecular Polypeptide-DNA Hydrogel for in Situ Three-Dimensional Multilayer Bioprinting. *Angew. Chem., Int. Ed.* **2015**, *54*, 3957.
(111) Wang, L. L.; Highley, C. B.; Yeh, Y. C.; Galarraga, J. H.; Uman, S.; Burdick, J. A. Three-Dimensional Extrusion Bioprinting of Single- and Double-Network Hydrogels Containing Dynamic Covalent Crosslinks. *J. Biomed. Mater. Res., Part A* **2018**, *106*, 865.
(112) Pekkanen, A. M.; Mondschein, R. J.; Williams, C. B.; Long, T. E. 3d Printing Polymers with Supramolecular Functionality for Biological Applications. *Biomacromolecules* **2017**, *18*, 2669.
(113) Roppolo, I.; Chiappone, A.; Angelini, A.; Stassi, S.; Frascella, F.; Pirri, C. F.; Ricciardi, C.; Descrovi, E. 3d Printable Light-Responsive Polymers. *Mater. Horiz.* **2017**, *4*, 396.
(114) Kuhnt, T.; Marroquin Garcia, R.; Camarero-Espinosa, S.; Dias, A.; Ten Cate, A. T.; van Blitterswijk, C. A.; Moroni, L.; Baker, M. B. Poly(Caprolactone-Co-Trimethylenecarbonate) Urethane Acrylate Resins for Digital Light Processing of Bioresorbable Tissue Engineering Implants. *Biomater. Sci.* **2019**, *7*, 4984.
(115) Petersen, S. R.; Wilson, J. A.; Becker, M. L. Versatile Ring-Opening Copolymerization and Postprinting Functionalization of Lactone and Poly(Propylene Fumarate) Block Copolymers: Resorbable Building Blocks for Additive Manufacturing. *Macromolecules* **2018**, *51*, 6202.
(116) Luo, Y.; Dolder, C. K.; Walker, J. M.; Mishra, R.; Dean, D.; Becker, M. L. Synthesis and Biological Evaluation of Well-Defined Poly(Propylene Fumarate) Oligomers and Their Use in 3d Printed Scaffolds. *Biomacromolecules* **2016**, *17*, 690.
(117) Wang, Z.; Abdulla, R.; Parker, B.; Samanipour, R.; Ghosh, S.; Kim, K. A Simple and High-Resolution Stereolithography-Based 3d Bioprinting System Using Visible Light Crosslinkable Bioinks. *Biofabrication* **2015**, *7*, 045009.
(118) Lim, K. S.; Schon, B. S.; Mekhileri, N. V.; Brown, G. C. J.; Chia, C. M.; Prabakar, S.; Hooper, G. J.; Woodfield, T. B. F. New Visible-Light Photoinitiating System for Improved Print Fidelity in Gelatin-Based Bioinks. *ACS Biomater. Sci. Eng.* **2016**, *2*, 1752.
(119) Ruskowitz, E. R.; DeForest, C. A. Proteome-Wide Analysis of Cellular Response to Ultraviolet Light for Biomaterial Synthesis and Modification. *ACS Biomater. Sci. Eng.* **2019**, *5*, 2111.
(120) Hart, L. R.; Li, S.; Sturgess, C.; Wildman, R.; Jones, J. R.; Hayes, W. 3d Printing of Biocompatible Supramolecular Polymers and Their Composites. *ACS Appl. Mater. Interfaces* **2016**, *8*, 3115.
(121) Trombetta, R.; Inzana, J. A.; Schwarz, E. M.; Kates, S. L.; Awad, H. A. 3d Printing of Calcium Phosphate Ceramics for Bone Tissue Engineering and Drug Delivery. *Ann. Biomed. Eng.* **2017**, *45*, 23.
(122) Sultan, S.; Siqueira, G.; Zimmermann, T.; Mathew, A. P. 3d Printing of Nano-Cellulosic Biomaterials for Medical Applications. *Curr. Opin. Biomed. Eng.* **2017**, *2*, 29.
(123) Jackson, R. J.; Patrick, P. S.; Page, K.; Powell, M. J.; Lythgoe, M. F.; Miodownik, M. A.; Parkin, I. P.; Carmalt, C. J.; Kalber, T. L.; Bear, J. C. Chemically Treated 3d Printed Polymer Scaffolds for Biomineral Formation. *ACS Omega* **2018**, *3*, 4342.
(124) Martin, J. J.; Fiore, B. E.; Erb, R. M. Designing Bioinspired Composite Reinforcement Architectures Via 3d Magnetic Printing. *Nat. Commun.* **2015**, *6*, 8641.
(125) Mannoor, M. S.; Jiang, Z.; James, T.; Kong, Y. L.; Malatesta, K. A.; Soboyejo, W. O.; Verma, N.; Gracias, D. H.; McAlpine, M. C. 3d Printed Bionic Ears. *Nano Lett.* **2013**, *13*, 2634.

https://dx.doi.org/10.1021/acs.chemrev.9b00789
Chem. Rev. 2020, 120, 11032−11092

(126) Gopinathan, J.; Noh, I. Click Chemistry-Based Injectable Hydrogels and Bioprinting Inks for Tissue Engineering Applications. *Tissue Eng. Regener. Med.* **2018**, *15*, 531.
(127) Lou, J.; Liu, F.; Lindsay, C. D.; Chaudhuri, O.; Heilshorn, S. C.; Xia, Y. Dynamic Hyaluronan Hydrogels with Temporally Modulated High Injectability and Stability Using a Biocompatible Catalyst. *Adv. Mater.* **2018**, *30*, No. 1705215.
(128) Li, Y. C.; Zhang, Y. S.; Akpek, A.; Shin, S. R.; Khademhosseini, A. 4d Bioprinting: The Next-Generation Technology for Biofabrication Enabled by Stimuli-Responsive Materials. *Biofabrication* **2017**, *9*, 012001.
(129) Kirillova, A.; Maxson, R.; Stoychev, G.; Gomillion, C. T.; Ionov, L. 4d Biofabrication Using Shape-Morphing Hydrogels. *Adv. Mater.* **2017**, *29*, 1703443.
(130) Lin, Q. M.; Li, L. Y.; Tang, M.; Hou, X. S.; Ke, C. F. Rapid Macroscale Shape Morphing of 3d-Printed Polyrotaxane Monoliths Amplified from Ph-Controlled Nanoscale Ring Motions. *J. Mater. Chem. C* **2018**, *6*, 11956.
(131) Kokkinis, D.; Schaffner, M.; Studart, A. R. Multimaterial Magnetically Assisted 3d Printing of Composite Materials. *Nat. Commun.* **2015**, *6*, 8643.
(132) Ooi, H. W.; Hafeez, S.; van Blitterswijk, C. A.; Moroni, L.; Baker, M. B. Hydrogels That Listen to Cells: A Review of Cell-Responsive Strategies in Biomaterial Design for Tissue Regeneration. *Mater. Horiz.* **2017**, *4*, 1020.
(133) Badeau, B. A.; Comerford, M. P.; Arakawa, C. K.; Shadish, J. A.; DeForest, C. A. Engineered Modular Biomaterial Logic Gates for Environmentally Triggered Therapeutic Delivery. *Nat. Chem.* **2018**, *10*, 251.
(134) van Esch, J. H.; Klajn, R.; Otto, S. Chemical Systems out of Equilibrium. *Chem. Soc. Rev.* **2017**, *46*, 5474.
(135) Burdick, J. A.; Murphy, W. L. Moving from Static to Dynamic Complexity in Hydrogel Design. *Nat. Commun.* **2012**, *3*, 1269.
(136) Rosales, A. M.; Anseth, K. S. The Design of Reversible Hydrogels to Capture Extracellular Matrix Dynamics. *Nat. Rev. Mater.* **2016**, *1*, 15012.
(137) Shi, Q.; Yu, K.; Kuang, X.; Mu, X. M.; Dunn, C. K.; Dunn, M. L.; Wang, T. J.; Qi, H. J. Recyclable 3d Printing of Vitrimer Epoxy. *Mater. Horiz.* **2017**, *4*, 598.
(138) Goor, O.; Hendrikse, S. I. S.; Dankers, P. Y. W.; Meijer, E. W. From Supramolecular Polymers to Multi-Component Biomaterials. *Chem. Soc. Rev.* **2017**, *46*, 6621.
(139) Liu, W.; Zhang, Y. S.; Heinrich, M. A.; De Ferrari, F.; Jang, H. L.; Bakht, S. M.; Alvarez, M. M.; Yang, J.; Li, Y. C.; Trujillo-de Santiago, G.; et al. Rapid Continuous Multimaterial Extrusion Bioprinting. *Adv. Mater.* **2017**, *29*, 1.
(140) Kuribayashi-Shigetomi, K.; Onoe, H.; Takeuchi, S. Cell Origami: Self-Folding of Three-Dimensional Cell-Laden Microstructures Driven by Cell Traction Force. *PLoS One* **2012**, *7*, No. e51085.
(141) Kim, Y.; Yuk, H.; Zhao, R.; Chester, S. A.; Zhao, X. Printing Ferromagnetic Domains for Untethered Fast-Transforming Soft Materials. *Nature* **2018**, *558*, 274.
(142) Takahashi, K.; Yamanaka, S. Induction of Pluripotent Stem Cells from Mouse Embryonic and Adult Fibroblast Cultures by Defined Factors. *Cell* **2006**, *126*, 663.
(143) Takahashi, K.; Tanabe, K.; Ohnuki, M.; Narita, M.; Ichisaka, T.; Tomoda, K.; Yamanaka, S. Induction of Pluripotent Stem Cells from Adult Human Fibroblasts by Defined Factors. *Cell* **2007**, *131*, 861.
(144) Boheler, K. R.; Czyz, J.; Tweedie, D.; Yang, H. T.; Anisimov, S. V.; Wobus, A. M. Differentiation of Pluripotent Embryonic Stem Cells into Cardiomyocytes. *Circ. Res.* **2002**, *91*, 189.
(145) Mummery, C. L.; Zhang, J. H.; Ng, E. S.; Elliott, D. A.; Elefanty, A. G.; Kamp, T. J. Differentiation of Human Embryonic Stem Cells and Induced Pluripotent Stem Cells to Cardiomyocytes a Methods Overview. *Circ. Res.* **2012**, *111*, 344.
(146) Talkhabi, M.; Aghdami, N.; Baharvand, H. Human Cardiomyocyte Generation from Pluripotent Stem Cells: A State-of-Art. *Life Sci.* **2016**, *145*, 98.
(147) Van Hoof, D.; D'Amour, K. A.; German, M. S. Derivation of Insulin-Producing Cells from Human Embryonic Stem Cells. *Stem Cell Res.* **2009**, *3*, 73.
(148) Takasato, M.; Er, P. X.; Becroft, M.; Vanslambrouck, J. M.; Stanley, E. G.; Elefanty, A. G.; Little, M. H. Directing Human Embryonic Stem Cell Differentiation Towards a Renal Lineage Generates a Self-Organizing Kidney. *Nat. Cell Biol.* **2014**, *16*, 118.
(149) Takasato, M.; Er, P. X.; Chiu, H. S.; Maier, B.; Baillie, G. J.; Ferguson, C.; Parton, R. G.; Wolvetang, E. J.; Roost, M. S.; Chuva de Sousa Lopes, S. M.; et al. Kidney Organoids from Human Ips Cells Contain Multiple Lineages and Model Human Nephrogenesis. *Nature* **2015**, *526*, 564.
(150) Takasato, M.; Er, P. X.; Chiu, H. S.; Little, M. H. Generation of Kidney Organoids from Human Pluripotent Stem Cells. *Nat. Protoc.* **2016**, *11*, 1681.
(151) Morizane, R.; Lam, A. Q.; Freedman, B. S.; Kishi, S.; Valerius, M. T.; Bonventre, J. V. Nephron Organoids Derived from Human Pluripotent Stem Cells Model Kidney Development and Injury. *Nat. Biotechnol.* **2015**, *33*, 1193.
(152) Morizane, R.; Bonventre, J. V. Generation of Nephron Progenitor Cells and Kidney Organoids from Human Pluripotent Stem Cells. *Nat. Protoc.* **2017**, *12*, 195.
(153) Lee, M. R.; Kwon, K. W.; Jung, H.; Kim, H. N.; Suh, K. Y.; Kim, K.; Kim, K. S. Direct Differentiation of Human Embryonic Stem Cells into Selective Neurons on Nanoscale Ridge/Groove Pattern Arrays. *Biomaterials* **2010**, *31*, 4360.
(154) Ren, Y. J.; Zhang, S. M.; Mi, R. F.; Liu, Q. Y.; Zeng, X. M.; Rao, M.; Hoke, A.; Mao, H. Q. Enhanced Differentiation of Human Neural Crest Stem Cells Towards the Schwann Cell Lineage by Aligned Electrospun Fiber Matrix. *Acta Biomater.* **2013**, *9*, 7727.
(155) Sluch, V. M.; Davis, C. H.; Ranganathan, V.; Kerr, J. M.; Krick, K.; Martin, R.; Berlinicke, C. A.; Marsh-Armstrong, N.; Diamond, J. S.; Mao, H. Q.; et al. Differentiation of Human Escs to Retinal Ganglion Cells Using a Crispr Engineered Reporter Cell Line. *Sci. Rep.* **2015**, *5*, 16595.
(156) Wu, H.; Uchimura, K.; Donnelly, E. L.; Kirita, Y.; Morris, S. A.; Humphreys, B. D. Comparative Analysis and Refinement of Human Psc-Derived Kidney Organoid Differentiation with Single-Cell Transcriptomics. *Cell Stem Cell* **2018**, *23*, 869.
(157) Ouyang, L. L.; Yao, R.; Mao, S. S.; Chen, X.; Na, J.; Sun, W. Three-Dimensional Bioprinting of Embryonic Stem Cells Directs Highly Uniform Embryoid Body Formation. *Biofabrication* **2015**, *7*, 044101.
(158) Gu, Q.; Tomaskovic-Crook, E.; Wallace, G. G.; Crook, J. M. 3d Bioprinting Human Induced Pluripotent Stem Cell Constructs for in Situ Cell Proliferation and Successive Multilineage Differentiation. *Adv. Healthcare Mater.* **2017**, *6*, 1700175.
(159) Koch, L.; Deiwick, A.; Franke, A.; Schwanke, K.; Haverich, A.; Zweigerdt, R.; Chichkov, B. Laser Bioprinting of Human Induced Pluripotent Stem Cells-the Effect of Printing and Biomaterials on Cell Survival, Pluripotency, and Differentiation. *Biofabrication* **2018**, *10*, 035005.
(160) Faulkner-Jones, A.; Fyfe, C.; Cornelissen, D. J.; Gardner, J.; King, J.; Courtney, A.; Shu, W. M. Bioprinting of Human Pluripotent Stem Cells and Their Directed Differentiation into Hepatocyte-Like Cells for the Generation of Mini-Livers in 3d. *Biofabrication* **2015**, *7*, 044102.
(161) Ong, C. S.; Fukunishi, T.; Zhang, H.; Huang, C. Y.; Nashed, A.; Blazeski, A.; DiSilvestre, D.; Vricella, L.; Conte, J.; Tung, L.; Tomaselli, G. F.; Hibino, N.; et al. Biomaterial-Free Three-Dimensional Bioprinting of Cardiac Tissue Using Human Induced Pluripotent Stem Cell Derived Cardiomyocytes. *Sci. Rep.* **2017**, *7*, 4566.
(162) Zhang, Y. S.; Arneri, A.; Bersini, S.; Shin, S. R.; Zhu, K.; Goli-Malekabadi, Z.; Aleman, J.; Colosi, C.; Busignani, F.; Dell'Erba, V.; et al. Bioprinting 3d Microfibrous Scaffolds for Engineering Endothelialized Myocardium and Heart-on-a-Chip. *Biomaterials* **2016**, *110*, 45.
(163) Nguyen, D.; Hagg, D. A.; Forsman, A.; Ekholm, J.; Nimkingratana, P.; Brantsing, C.; Kalogeropoulos, T.; Zaunz, S.; Concaro, S.; Brittberg, M.; et al. Cartilage Tissue Engineering by the 3d

https://dx.doi.org/10.1021/acs.chemrev.9b00789
Chem. Rev. 2020, 120, 11032−11092

Bioprinting of Ips Cells in a Nanocellulose/Alginate Bioink. *Sci. Rep.* **2017**, *7*, 658.
(164) Sorkio, A.; Koch, L.; Koivusalo, L.; Deiwick, A.; Miettinen, S.; Chichkov, B.; Skottman, H. Human Stem Cell Based Corneal Tissue Mimicking Structures Using Laser-Assisted 3d Bioprinting and Functional Bioinks. *Biomaterials* **2018**, *171*, 57.
(165) Kerscher, P.; Kaczmarek, J. A.; Head, S. E.; Ellis, M. E.; Seeto, W. J.; Kim, J.; Bhattacharya, S.; Suppiramaniam, V.; Lipke, E. A. Direct Production of Human Cardiac Tissues by Pluripotent Stem Cell Encapsulation in Gelatin Methacryloyl. *ACS Biomater. Sci. Eng.* **2017**, *3*, 1499.
(166) Joung, D.; Truong, V.; Neitzke, C. C.; Guo, S.-Z.; Walsh, P. J.; Monat, J. R.; Meng, F.; Park, S. H.; Dutton, J. R.; Parr, A. M.; et al. 3d Printed Stem-Cell Derived Neural Progenitors Generate Spinal Cord Scaffolds. *Adv. Funct. Mater.* **2018**, *28*, 1801850.
(167) Maiullari, F.; Costantini, M.; Milan, M.; Pace, V.; Chirivi, M.; Maiullari, S.; Rainer, A.; Baci, D.; Marei, H. E.; Seliktar, D.; et al. A Multi-Cellular 3d Bioprinting Approach for Vascularized Heart Tissue Engineering Based on Huvecs and Ipsc-Derived Cardiomyocytes. *Sci. Rep.* **2018**, *8*, 13532.
(168) Edgar, R.; Mazor, Y.; Rinon, A.; Blumenthal, J.; Golan, Y.; Buzhor, E.; Livnat, I.; Ben-Ari, S.; Lieder, I.; Shitrit, A.; et al. Lifemap Discovery: The Embryonic Development, Stem Cells, and Regenerative Medicine Research Portal. *PLoS One* **2013**, *8*, No. e66629.
(169) Biggs, L. C.; Mikkola, M. L. Early Inductive Events in Ectodermal Appendage Morphogenesis. *Semin. Cell Dev. Biol.* **2014**, *25*−*26*, 11.
(170) Forni, M. F.; Trombetta-Lima, M.; Sogayar, M. C. Stem Cells in Embryonic Skin Development. *Biol. Res.* **2012**, *45*, 215.
(171) Metcalfe, A. D.; Ferguson, M. W. Tissue Engineering of Replacement Skin: The Crossroads of Biomaterials, Wound Healing, Embryonic Development, Stem Cells and Regeneration. *J. R. Soc., Interface* **2007**, *4*, 413.
(172) Evans, N. D.; Oreffo, R. O.; Healy, E.; Thurner, P. J.; Man, Y. H. Epithelial Mechanobiology, Skin Wound Healing, and the Stem Cell Niche. *J. Mech. Behav. Biomed. Mater.* **2013**, *28*, 397.
(173) Van Zuijlen, P. P. M.; Ruurda, J. J. B.; Van Veen, H. A.; Van Marle, J.; Van Trier, A. J. M.; Groenevelt, F.; Kreis, R. W.; Middelkoop, E. Collagen Morphology in Human Skin and Scar Tissue: No Adaptations in Response to Mechanical Loading at Joints. *Burns* **2003**, *29*, 423.
(174) Guo, S.; Dipietro, L. A. Factors Affecting Wound Healing. *J. Dent. Res.* **2010**, *89*, 219.
(175) Breitkreutz, D.; Koxholt, I.; Thiemann, K.; Nischt, R. Skin Basement Membrane: The Foundation of Epidermal Integrity–Bm Functions and Diverse Roles of Bridging Molecules Nidogen and Perlecan. *BioMed Res. Int.* **2013**, *2013*, 179784.
(176) Liu, S.; Zhang, H.; Duan, E. Epidermal Development in Mammals: Key Regulators, Signals from beneath, and Stem Cells. *Int. J. Mol. Sci.* **2013**, *14*, 10869.
(177) Iizuka, H. Epidermal Turnover Time. *J. Dermatol. Sci.* **1994**, *8*, 215.
(178) Rognoni, E.; Watt, F. M. Skin Cell Heterogeneity in Development, Wound Healing, and Cancer. *Trends Cell Biol.* **2018**, *28*, 709.
(179) Guillot, C.; Lecuit, T. Mechanics of Epithelial Tissue Homeostasis and Morphogenesis. *Science* **2013**, *340*, 1185.
(180) Jha, P.; Wang, X.; Auwerx, J. Analysis of Mitochondrial Respiratory Chain Supercomplexes Using Blue Native Polyacrylamide Gel Electrophoresis (Bn-Page). *Curr. Protoc. Mouse Biol.* **2016**, *6*, 1.
(181) Ventre, M.; Mollica, F.; Netti, P. A. The Effect of Composition and Microstructure on the Viscoelastic Properties of Dermis. *J. Biomech.* **2009**, *42*, 430.
(182) Driskell, R. R.; Watt, F. M. Understanding Fibroblast Heterogeneity in the Skin. *Trends Cell Biol.* **2015**, *25*, 92.
(183) Sriram, G.; Bigliardi, P. L.; Bigliardi-Qi, M. Fibroblast Heterogeneity and Its Implications for Engineering Organotypic Skin Models in Vitro. *Eur. J. Cell Biol.* **2015**, *94*, 483.
(184) Danielson, K. G.; Baribault, H.; Holmes, D. F.; Graham, H.; Kadler, K. E.; Iozzo, R. V. Targeted Disruption of Decorin Leads to Abnormal Collagen Fibril Morphology and Skin Fragility. *J. Cell Biol.* **1997**, *136*, 729.
(185) Toole, B. P.; Lowther, D. A. The Effect of Chondroitin Sulphate-Protein on the Formation of Collagen Fibrils in Vitro. *Biochem. J.* **1968**, *109*, 857.
(186) Schonherr, E.; Beavan, L. A.; Hausser, H.; Kresse, H.; Culp, L. A. Differences in Decorin Expression by Papillary and Reticular Fibroblasts in Vivo and in Vitro. *Biochem. J.* **1993**, *290*, 893.
(187) Griffin, M. F.; Leung, B. C.; Premakumar, Y.; Szarko, M.; Butler, P. E. Comparison of the Mechanical Properties of Different Skin Sites for Auricular and Nasal Reconstruction. *J. Otolaryngol. Head Neck Surg.* **2017**, *46*, 33.
(188) Ni Annaidh, A.; Bruyere, K.; Destrade, M.; Gilchrist, M. D.; Ottenio, M. Characterization of the Anisotropic Mechanical Properties of Excised Human Skin. *J. Mech. Behav. Biomed. Mater.* **2012**, *5*, 139.
(189) Ni Annaidh, A.; Bruyere, K.; Destrade, M.; Gilchrist, M. D.; Maurini, C.; Ottenio, M.; Saccomandi, G. Automated Estimation of Collagen Fibre Dispersion in the Dermis and Its Contribution to the Anisotropic Behaviour of Skin. *Ann. Biomed. Eng.* **2012**, *40*, 1666.
(190) Diridollou, S.; Patat, F.; Gens, F.; Vaillant, L.; Black, D.; Lagarde, J. M.; Gall, Y.; Berson, M. In Vivo Model of the Mechanical Properties of the Human Skin under Suction. *Skin Res. Technol.* **2000**, *6*, 214.
(191) Le, H. Q.; Ghatak, S.; Yeung, C. Y.; Tellkamp, F.; Gunschmann, C.; Dieterich, C.; Yeroslaviz, A.; Habermann, B.; Pombo, A.; Niessen, C. M.; et al. Mechanical Regulation of Transcription Controls Polycomb-Mediated Gene Silencing During Lineage Commitment. *Nat. Cell Biol.* **2016**, *18*, 864.
(192) Quan, T.; Wang, F.; Shao, Y.; Rittie, L.; Xia, W.; Orringer, J. S.; Voorhees, J. J.; Fisher, G. J. Enhancing Structural Support of the Dermal Microenvironment Activates Fibroblasts, Endothelial Cells, and Keratinocytes in Aged Human Skin in Vivo. *J. Invest. Dermatol.* **2013**, *133*, 658.
(193) Zollner, A. M.; Holland, M. A.; Honda, K. S.; Gosain, A. K.; Kuhl, E. Growth on Demand: Reviewing the Mechanobiology of Stretched Skin. *J. Mech. Behav. Biomed. Mater.* **2013**, *28*, 495.
(194) Webb, K.; Hitchcock, R. W.; Smeal, R. M.; Li, W.; Gray, S. D.; Tresco, P. A. Cyclic Strain Increases Fibroblast Proliferation, Matrix Accumulation, and Elastic Modulus of Fibroblast-Seeded Polyurethane Constructs. *J. Biomech.* **2006**, *39*, 1136.
(195) Hinz, B.; Mastrangelo, D.; Iselin, C. E.; Chaponnier, C.; Gabbiani, G. Mechanical Tension Controls Granulation Tissue Contractile Activity and Myofibroblast Differentiation. *Am. J. Pathol.* **2001**, *159*, 1009.
(196) Alizadeh, N.; Pepper, M. S.; Modarressi, A.; Alfo, K.; Schlaudraff, K.; Montandon, D.; Gabbiani, G.; Bochaton-Piallat, M. L.; Pittet, B. Persistent Ischemia Impairs Myofibroblast Development in Wound Granulation Tissue: A New Model of Delayed Wound Healing. *Wound Repair Regen* **2007**, *15*, 809.
(197) Goffin, J. M.; Pittet, P.; Csucs, G.; Lussi, J. W.; Meister, J. J.; Hinz, B. Focal Adhesion Size Controls Tension-Dependent Recruitment of Alpha-Smooth Muscle Actin to Stress Fibers. *J. Cell Biol.* **2006**, *172*, 259.
(198) Anon, E.; Serra-Picamal, X.; Hersen, P.; Gauthier, N. C.; Sheetz, M. P.; Trepat, X.; Ladoux, B. Cell Crawling Mediates Collective Cell Migration to Close Undamaged Epithelial Gaps. *Proc. Natl. Acad. Sci. U. S. A.* **2012**, *109*, 10891.
(199) Ochsner, M.; Dusseiller, M. R.; Grandin, H. M.; Luna-Morris, S.; Textor, M.; Vogel, V.; Smith, M. L. Micro-Well Arrays for 3d Shape Control and High Resolution Analysis of Single Cells. *Lab Chip* **2007**, *7*, 1074.
(200) Wang, Y.; Wang, G.; Luo, X.; Qiu, J.; Tang, C. Substrate Stiffness Regulates the Proliferation, Migration, and Differentiation of Epidermal Cells. *Burns* **2012**, *38*, 414.
(201) Aarabi, S.; Bhatt, K. A.; Shi, Y.; Paterno, J.; Chang, E. I.; Loh, S. A.; Holmes, J. W.; Longaker, M. T.; Yee, H.; Gurtner, G. C. Mechanical

https://dx.doi.org/10.1021/acs.chemrev.9b00789
Chem. Rev. 2020, 120, 11032−11092

Load Initiates Hypertrophic Scar Formation through Decreased Cellular Apoptosis. *FASEB J.* **2007**, *21*, 3250.
(202) Tarassoli, S. P.; Jessop, Z. M.; Al-Sabah, A.; Gao, N.; Whitaker, S.; Doak, S.; Whitaker, I. S. Skin Tissue Engineering Using 3d Bioprinting: An Evolving Research Field. *J. Plast. Reconstr. Aesthet. Surg.* **2018**, *71*, 615.
(203) Lee, V.; Singh, G.; Trasatti, J. P.; Bjornsson, C.; Xu, X.; Tran, T. N.; Yoo, S. S.; Dai, G.; Karande, P. Design and Fabrication of Human Skin by Three-Dimensional Bioprinting. *Tissue Eng., Part C* **2014**, *20*, 473.
(204) Koch, L.; Deiwick, A.; Schlie, S.; Michael, S.; Gruene, M.; Coger, V.; Zychlinski, D.; Schambach, A.; Reimers, K.; Vogt, P. M.; et al. Skin Tissue Generation by Laser Cell Printing. *Biotechnol. Bioeng.* **2012**, *109*, 1855.
(205) Pourchet, L. J.; Thepot, A.; Albouy, M.; Courtial, E. J.; Boher, A.; Blum, L. J.; Marquette, C. A. Human Skin 3d Bioprinting Using Scaffold-Free Approach. *Adv. Healthcare Mater.* **2017**, *6*, 1601101.
(206) Cubo, N.; Garcia, M.; Del Canizo, J. F.; Velasco, D.; Jorcano, J. L. 3d Bioprinting of Functional Human Skin: Production and in Vivo Analysis. *Biofabrication* **2017**, *9*, 015006.
(207) Derr, K.; Zou, J.; Luo, K.; Song, M. J.; Sittampalam, G. S.; Zhou, C.; Michael, S.; Ferrer, M.; Derr, P. Fully Three-Dimensional Bioprinted Skin Equivalent Constructs with Validated Morphology and Barrier Function. *Tissue Eng., Part C* **2019**, *25*, 334.
(208) Skardal, A.; Mack, D.; Kapetanovic, E.; Atala, A.; Jackson, J. D.; Yoo, J.; Soker, S. Bioprinted Amniotic Fluid-Derived Stem Cells Accelerate Healing of Large Skin Wounds. *Stem Cells Transl. Med.* **2012**, *1*, 792.
(209) Skardal, A.; Murphy, S. V.; Crowell, K.; Mack, D.; Atala, A.; Soker, S. A Tunable Hydrogel System for Long-Term Release of Cell-Secreted Cytokines and Bioprinted in Situ Wound Cell Delivery. *J. Biomed. Mater. Res., Part B* **2017**, *105*, 1986.
(210) Albanna, M.; Binder, K. W.; Murphy, S. V.; Kim, J.; Qasem, S. A.; Zhao, W.; Tan, J.; El-Amin, I. B.; Dice, D. D.; Marco, J.; et al. In Situ Bioprinting of Autologous Skin Cells Accelerates Wound Healing of Extensive Excisional Full-Thickness Wounds. *Sci. Rep.* **2019**, *9*, 1856.
(211) Auxenfans, C.; Fradette, J.; Lequeux, C.; Germain, L.; Kinikoglu, B.; Bechetoille, N.; Braye, F.; Auger, F. A.; Damour, O. Evolution of Three Dimensional Skin Equivalent Models Reconstructed in Vitro by Tissue Engineering. *Eur. J. Dermatol.* **2009**, *19*, 107.
(212) Ng, W. L.; Qi, J. T. Z.; Yeong, W. Y.; Naing, M. W. Proof-of-Concept: 3d Bioprinting of Pigmented Human Skin Constructs. *Biofabrication* **2018**, *10*, 025005.
(213) Norouzi, M.; Boroujeni, S. M.; Omidvarkordshouli, N.; Soleimani, M. Advances in Skin Regeneration: Application of Electrospun Scaffolds. *Adv. Healthcare Mater.* **2015**, *4*, 1114.
(214) Candiello, J.; Balasubramani, M.; Schreiber, E. M.; Cole, G. J.; Mayer, U.; Halfter, W.; Lin, H. Biomechanical Properties of Native Basement Membranes. *FEBS J.* **2007**, *274*, 2897.
(215) Zahouani, H.; Pailler-Mattei, C.; Sohm, B.; Vargiolu, R.; Cenizo, V.; Debret, R. Characterization of the Mechanical Properties of a Dermal Equivalent Compared with Human Skin in Vivo by Indentation and Static Friction Tests. *Skin Res. Technol.* **2009**, *15*, 68.
(216) Sander, E. A.; Lynch, K. A.; Boyce, S. T. Development of the Mechanical Properties of Engineered Skin Substitutes after Grafting to Full-Thickness Wounds. *J. Biomech. Eng.* **2014**, *136*, 051008.
(217) Esteban-Vives, R.; Corcos, A.; Choi, M. S.; Young, M. T.; Over, P.; Ziembicki, J.; Gerlach, J. C. Cell-Spray Auto-Grafting Technology for Deep Partial-Thickness Burns: Problems and Solutions During Clinical Implementation. *Burns* **2018**, *44*, 549.
(218) Natesan, S.; Wrice, N. L.; Baer, D. G.; Christy, R. J. Debrided Skin as a Source of Autologous Stem Cells for Wound Repair. *Stem Cells* **2011**, *29*, 1219.
(219) Ojeh, N.; Pastar, I.; Tomic-Canic, M.; Stojadinovic, O. Stem Cells in Skin Regeneration, Wound Healing, and Their Clinical Applications. *Int. J. Mol. Sci.* **2015**, *16*, 25476.
(220) Boucher, P. N. *3d Bio-Printing for Medical and Enhancement Purposes*; 2018.
(221) Wood, F. M.; Kolybaba, M. L.; Allen, P. The Use of Cultured Epithelial Autograft in the Treatment of Major Burn Injuries: A Critical Review of the Literature. *Burns* **2006**, *32*, 395.
(222) Gravante, G.; Di Fede, M. C.; Araco, A.; Grimaldi, M.; De Angelis, B.; Arpino, A.; Cervelli, V.; Montone, A. A Randomized Trial Comparing Recell® System of Epidermal Cells Delivery Versus Classic Skin Grafts for the Treatment of Deep Partial Thickness Burns. *Burns* **2007**, *33*, 966.
(223) Ashrafi, M.; Baguneid, M.; Bayat, A. The Role of Neuromediators and Innervation in Cutaneous Wound Healing. *Acta Derm. Venereol.* **2016**, *96*, 587.
(224) Xie, J.; Yao, B.; Han, Y.; Huang, S.; Fu, X. Skin Appendage-Derived Stem Cells: Cell Biology and Potential for Wound Repair. *Burns Trauma* **2016**, *4*, 38.
(225) DiPietro, L. A. Angiogenesis and Wound Repair: When Enough Is Enough. *J. Leukocyte Biol.* **2016**, *100*, 979.
(226) Ng, W. L.; Yeong, W. Y.; Naing, M. W. Polyvinylpyrrolidone-Based Bio-Ink Improves Cell Viability and Homogeneity During Drop-on-Demand Printing. *Materials* **2017**, *10*, 190.
(227) Moeendarbary, E.; Weber, I. P.; Sheridan, G. K.; Koser, D. E.; Soleman, S.; Haenzi, B.; Bradbury, E. J.; Fawcett, J.; Franze, K. The Soft Mechanical Signature of Glial Scars in the Central Nervous System. *Nat. Commun.* **2017**, *8*, 14787.
(228) de Luca, A. C.; Lacour, S. P.; Raffoul, W.; di Summa, P. G. Extracellular Matrix Components in Peripheral Nerve Repair: How to Affect Neural Cellular Response and Nerve Regeneration? *Neural Regener. Res.* **2014**, *9*, 1943.
(229) Burda, J. E.; Sofroniew, M. V. Reactive Gliosis and the Multicellular Response to Cns Damage and Disease. *Neuron* **2014**, *81*, 229.
(230) Dixon, A. R.; Jariwala, S. H.; Bilis, Z.; Loverde, J. R.; Pasquina, P. F.; Alvarez, L. M. Bridging the Gap in Peripheral Nerve Repair with 3d Printed and Bioprinted Conduits. *Biomaterials* **2018**, *186*, 44.
(231) Bonneh-Barkay, D.; Wiley, C. A. Brain Extracellular Matrix in Neurodegeneration. *Brain Pathol.* **2009**, *19*, 573.
(232) Stiles, J.; Jernigan, T. L. The Basics of Brain Development. *Neuropsychol. Rev.* **2010**, *20*, 327.
(233) Budday, S.; Steinmann, P.; Kuhl, E. Physical Biology of Human Brain Development. *Front. Cell. Neurosci.* **2015**, *9*, 257.
(234) Azevedo, F. A.C.; Carvalho, L. R.B.; Grinberg, L. T.; Farfel, J. M.; Ferretti, R. E.L.; Leite, R. E.P.; Filho, W. J.; Lent, R.; Herculano-Houzel, S. Equal Numbers of Neuronal and Nonneuronal Cells Make the Human Brain an Isometrically Scaled-up Primate Brain. *J. Comp. Neurol.* **2009**, *513*, 532.
(235) Lee, S. J.; Esworthy, T.; Stake, S.; Miao, S.; Zuo, Y. Y.; Harris, B. T.; Zhang, L. G. Advances in 3d Bioprinting for Neural Tissue Engineering. *Advanced Biosystems* **2018**, *2*, 1700213.
(236) Gadani, S. P.; Walsh, J. T.; Lukens, J. R.; Kipnis, J. Dealing with Danger in the Cns: The Response of the Immune System to Injury. *Neuron* **2015**, *87*, 47.
(237) Celio, M. R.; Spreafico, R.; De Biasi, S.; Vitellaro-Zuccarello, L. Perineuronal Nets: Past and Present. *Trends Neurosci.* **1998**, *21*, 510.
(238) Quraishe, S.; Forbes, L. H.; Andrews, M. R. The Extracellular Environment of the Cns: Influence on Plasticity, Sprouting, and Axonal Regeneration after Spinal Cord Injury. *Neural Plast.* **2018**, *2018*, 2952386.
(239) Geissler, M.; Gottschling, C.; Aguado, A.; Rauch, U.; Wetzel, C. H.; Hatt, H.; Faissner, A. Primary Hippocampal Neurons, Which Lack Four Crucial Extracellular Matrix Molecules, Display Abnormalities of Synaptic Structure and Function and Severe Deficits in Perineuronal Net Formation. *J. Neurosci.* **2013**, *33*, 7742.
(240) Budday, S.; Nay, R.; de Rooij, R.; Steinmann, P.; Wyrobek, T.; Ovaert, T. C.; Kuhl, E. Mechanical Properties of Gray and White Matter Brain Tissue by Indentation. *J. Mech. Behav. Biomed. Mater.* **2015**, *46*, 318.
(241) Hara, M.; Kobayakawa, K.; Ohkawa, Y.; Kumamaru, H.; Yokota, K.; Saito, T.; Kijima, K.; Yoshizaki, S.; Harimaya, K.; Nakashima, Y.; et al. Interaction of Reactive Astrocytes with Type I Collagen Induces

https://dx.doi.org/10.1021/acs.chemrev.9b00789
Chem. Rev. 2020, 120, 11032−11092

Astrocytic Scar Formation through the Integrin-N-Cadherin Pathway after Spinal Cord Injury. *Nat. Med.* **2017**, *23*, 818.
(242) Schachtrup, C.; Ryu, J. K.; Helmrick, M.; Vagena, E.; Galanakis, D. K.; Degen, J. L.; Margolis, R. U.; Akassoglou, K. Fibrinogen Triggers Astrocyte Scar Formation by Promoting the Availability of Active Tgf-B after Vascular Damage. *J. Neurosci.* **2010**, *30*, 5843.
(243) Ahuja, C. S.; Nori, S.; Tetreault, L.; Wilson, J.; Kwon, B.; Harrop, J.; Choi, D.; Fehlings, M. G. Traumatic Spinal Cord Injury-Repair and Regeneration. *Neurosurgery* **2017**, *80*, S9.
(244) Faulkner, J. R.; Herrmann, J. E.; Woo, M. J.; Tansey, K. E.; Doan, N. B.; Sofroniew, M. V. Reactive Astrocytes Protect Tissue and Preserve Function after Spinal Cord Injury. *J. Neurosci.* **2004**, *24*, 2143.
(245) Bush, T. G.; Puvanachandra, N.; Horner, C. H.; Polito, A.; Ostenfeld, T.; Svendsen, C. N.; Mucke, L.; Johnson, M. H.; Sofroniew, M. V. Leukocyte Infiltration, Neuronal Degeneration, and Neurite Outgrowth after Ablation of Scar-Forming, Reactive Astrocytes in Adult Transgenic Mice Provision of Metabolic Substrates for Neurons, and Inter-Actions with Endothelia to Create and Maintain the B. *Neuron* **1999**, *23*, 297.
(246) Macaya, D.; Spector, M. Injectable Hydrogel Materials for Spinal Cord Regeneration: A Review. *Biomed. Mater.* **2012**, *7*, 012001.
(247) Hsieh, F. Y.; Lin, H. H.; Hsu, S. h. 3d Bioprinting of Neural Stem Cell-Laden Thermoresponsive Biodegradable Polyurethane Hydrogel and Potential in Central Nervous System Repair. *Biomaterials* **2015**, *71*, 48.
(248) Aurand, E. R.; Wagner, J.; Lanning, C.; Bjugstad, K. B. Building Biocompatible Hydrogels for Tissue Engineering of the Brain and Spinal Cord. *J. Funct. Biomater.* **2012**, *3*, 839.
(249) Xu, T.; Gregory, C. A.; Molnar, P.; Cui, X.; Jalota, S.; Bhaduri, S. B.; Boland, T. Viability and Electrophysiology of Neural Cell Structures Generated by the Inkjet Printing Method. *Biomaterials* **2006**, *27*, 3580.
(250) Lee, W.; Pinckney, J.; Lee, V.; Lee, J. H.; Fischer, K.; Polio, S.; Park, J. K.; Yoo, S. S. Three-Dimensional Bioprinting of Rat Embryonic Neural Cells. *NeuroReport* **2009**, *20*, 798.
(251) Lee, Y. B.; Polio, S.; Lee, W.; Dai, G.; Menon, L.; Carroll, R. S.; Yoo, S. S. Bio-Printing of Collagen and Vegf-Releasing Fibrin Gel Scaffolds for Neural Stem Cell Culture. *Exp. Neurol.* **2010**, *223*, 645.
(252) Lozano, R.; Stevens, L.; Thompson, B. C.; Gilmore, K. J.; Gorkin, R.; Stewart, E. M.; het Panhuis, M.; Romero-Ortega, M.; Wallace, G. G. 3d Printing of Layered Brain-Like Structures Using Peptide Modified Gellan Gum Substrates. *Biomaterials* **2015**, *67*, 264.
(253) Dai, X.; Ma, C.; Lan, Q.; Xu, T. 3d Bioprinted Glioma Stem Cells for Brain Tumor Model and Applications of Drug Susceptibility. *Biofabrication* **2016**, *8*, 045005.
(254) Lu, Y. B.; Iandiev, I.; Hollborn, M.; Korber, N.; Ulbricht, E.; Hirrlinger, P. G.; Pannicke, T.; Wei, E. Q.; Bringmann, A.; Wolburg, H.; et al. Reactive Glial Cells: Increased Stiffness Correlates with Increased Intermediate Filament Expression. *FASEB J.* **2011**, *25*, 624.
(255) Miller, W. J.; Leventhal, I.; Scarsella, D.; Haydon, P. G.; Janmey, P.; Meaney, D. F. Mechanically Induced Reactive Gliosis Causes Atp-Mediated Alterations in Astrocyte Stiffness. *J. Neurotrauma* **2009**, *26*, 789.
(256) Bozza, A.; Coates, E. E.; Incitti, T.; Ferlin, K. M.; Messina, A.; Menna, E.; Bozzi, Y.; Fisher, J. P.; Casarosa, S. Neural Differentiation of Pluripotent Cells in 3d Alginate-Based Cultures. *Biomaterials* **2014**, *35*, 4636.
(257) Leipzig, N. D.; Shoichet, M. S. The Effect of Substrate Stiffness on Adult Neural Stem Cell Behavior. *Biomaterials* **2009**, *30*, 6867.
(258) O'Connor, S. M.; Stenger, D. A.; Shaffer, K. M.; Ma, W. Survival and Neurite Outgrowth of Rat Cortical Neurons in Three-Dimensional Agarose and Collagen Gel Matrices. *Neurosci. Lett.* **2001**, *304*, 189.
(259) Gu, Q.; Tomaskovic-Crook, E.; Lozano, R.; Chen, Y.; Kapsa, R. M.; Zhou, Q.; Wallace, G. G.; Crook, J. M. Functional 3d Neural Mini-Tissues from Printed Gel-Based Bioink and Human Neural Stem Cells. *Adv. Healthcare Mater.* **2016**, *5*, 1429.
(260) Di Lullo, E.; Kriegstein, A. R. The Use of Brain Organoids to Investigate Neural Development and Disease. *Nat. Rev. Neurosci.* **2017**, *18*, 573.
(261) Marroquin, J. B.; Coleman, H. A.; Tonta, M. A.; Zhou, K.; Winther-Jensen, B.; Fallon, J.; Duffy, N. W.; Yan, E.; Abdulwahid, A. A.; Jasieniak, J. J.; et al. Neural Electrodes Based on 3d Organic Electroactive Microfibers. *Adv. Funct. Mater.* **2018**, *28*, 1.
(262) Shin, S. R.; Farzad, R.; Tamayol, A.; Manoharan, V.; Mostafalu, P.; Zhang, Y. S.; Akbari, M.; Jung, S. M.; Kim, D.; Comotto, M.; et al. A Bioactive Carbon Nanotube-Based Ink for Printing 2d and 3d Flexible Electronics. *Adv. Mater.* **2016**, *28*, 3280.
(263) Quirin, S.; Vladimirov, N.; Yang, C.-T.; Peterka, D. S.; Yuste, R.; Ahrens, M. Calcium Imaging of Neural Circuits with Extended Depth-of-Field Light-Sheet Microscopy. *Opt. Lett.* **2016**, *41*, 855.
(264) Taylor, M. A.; Vanwalleghem, G. C.; Favre-Bulle, I. A.; Scott, E. K. Diffuse Light-Sheet Microscopy for Stripe-Free Calcium Imaging of Neural Populations. *J. Biophotonics* **2018**, *11*, No. e201800088.
(265) Kulesa, P. M.; McLennan, R. Neural Crest Migration: Trailblazing Ahead. *F1000Prime Rep.* **2015**, *7*, 02.
(266) Takahashi, Y.; Sipp, D.; Enomoto, H. Tissue Interactions in Neural Crest Cell Development and Disease. *Science* **2013**, *341*, 860.
(267) Kasemeier-Kulesa, J. C.; Kulesa, P. M.; Lefcort, F. Imaging Neural Crest Cell Dynamics During Formation of Dorsal Root Ganglia and Sympathetic Ganglia. *Development* **2005**, *132*, 235.
(268) Newbern, J. M. Molecular Control of the Neural Crest and Peripheral Nervous System Development. *Curr. Top. Dev. Biol.* **2015**, *111*, 201.
(269) Espinosa-Medina, I.; Outin, E.; Picard, C. A.; Chettouh, Z.; Dymecki, S.; Consalez, G. G.; Coppola, E.; Brunet, J. F. Parasympathetic Ganglia Derive from Schwann Cell Precursors. *Science* **2014**, *345*, 87.
(270) Jessen, K. R.; Mirsky, R. The Origin and Development of Glial Cells in Peripheral Nerves. *Nat. Rev. Neurosci.* **2005**, *6*, 671.
(271) Catala, M.; Kubis, N. Gross Anatomy and Development of the Peripheral Nervous System. *Handb. Clin. Neurol.* **2013**, *115*, 29.
(272) Salonen, V.; Roytta, M.; Peltonen, J. The Effects of Nerve Transection on the Endoneurial Collagen Fibril Sheaths. *Acta Neuropathol.* **1987**, *74*, 13.
(273) Ushiki, T.; Ide, C. Three-Dimensional Organization of the Collagen Fibrils in the Rat Sciatic Nerve as Revealed by Transmission- and Scanning Electron Microscopy. *Cell Tissue Res.* **1990**, *260*, 175.
(274) Bozkurt, A.; Deumens, R.; Beckmann, C.; Olde Damink, L.; Schugner, F.; Heschel, I.; Sellhaus, B.; Weis, J.; Jahnen-Dechent, W.; Brook, G. A.; et al. In Vitro Cell Alignment Obtained with a Schwann Cell Enriched Microstructured Nerve Guide with Longitudinal Guidance Channels. *Biomaterials* **2009**, *30*, 169.
(275) Kaemmer, D.; Bozkurt, A.; Otto, J.; Junge, K.; Klink, C.; Weis, J.; Sellhaus, B.; O'Dey, D. M.; Pallua, N.; Jansen, M.; et al. Evaluation of Tissue Components in the Peripheral Nervous System Using Sirius Red Staining and Immunohistochemistry: A Comparative Study (Human, Pig, Rat). *J. Neurosci. Methods* **2010**, *190*, 112.
(276) Seyer, J. M.; Kang, A. H.; Whitaker, J. N. The Characterization of Type I and Type Iii Collagens from Human Peripheral Nerve. *Biochim. Biophys. Acta, Protein Struct.* **1977**, *492*, 415.
(277) Gonzalez-Perez, F.; Udina, E.; Navarro, X. Extracellular Matrix Components in Peripheral Nerve Regeneration. *Int. Rev. Neurobiol.* **2013**, *108*, 257.
(278) Tona, A.; Perides, G.; Rahemtulla, F.; Dahl, D. Extracellular Matrix in Regenerating Rat Sciatic Nerve: A Comparative Study on the Localization of Laminin, Hyaluronic Acid, and Chondroitin Sulfate Proteoglycans, Including Versican. *J. Histochem. Cytochem.* **1993**, *41*, 593.
(279) Geuna, S.; Raimondo, S.; Ronchi, G.; Di Scipio, F.; Tos, P.; Czaja, K.; Fornaro, M. Chapter 3: Histology of the Peripheral Nerve and Changes Occurring During Nerve Regeneration. *Int. Rev. Neurobiol.* **2009**, *87*, 27.
(280) Chang, C. T.; Chen, Y. H.; Lin, C. C.; Ju, M. S. Finite Element Modeling of Hyper-Viscoelasticity of Peripheral Nerve Ultrastructures. *J. Biomech.* **2015**, *48*, 1982.
(281) Ju, M.-S.; Lin, C.-C. K.; Chang, C.-T. Researches on Biomechanical Properties and Models of Peripheral Nerves - a Review. *J. Biomech. Sci. Eng.* **2017**, *12*, 16.

https://dx.doi.org/10.1021/acs.chemrev.9b00789
Chem. Rev. 2020, 120, 11032−11092

(282) Toba, T.; Nakamura, T.; Shimizu, Y.; Matsumoto, K.; Ohnishi, K.; Fukuda, S.; Yoshitani, M.; Ueda, H.; Hori, Y.; Endo, K. Regeneration of Canine Peroneal Nerve with the Use of a Polyglycolic Acid-Collagen Tube Filled with Laminin-Soaked Collagen Sponge: A Comparative Study of Collagen Sponge and Collagen Fibers as Filling Materials for Nerve Conduits. *J. Biomed. Mater. Res.* **2001**, *58*, 622.
(283) Rath, E. M.; Kelly, D.; Bouldin, T. W.; Popko, B. Impaired Peripheral Nerve Regeneration in a Mutant Strain of Mice (Enr) with a Schwann Cell Defect. *J. Neurosci.* **1995**, *15*, 7226.
(284) Pfister, B. J.; Gordon, T.; Loverde, J. R.; Kochar, A. S.; Mackinnon, S. E.; Cullen, D. K. Biomedical Engineering Strategies for Peripheral Nerve Repair: Surgical Applications, State of the Art, and Future Challenges. *Crit. Rev. Biomed. Eng.* **2011**, *39*, 81.
(285) Blitterswijk, C. v.; Thomsen, P.; Lindahl, A.; Hubbell, J.; Williams, D. F.; Cancedda, R.; Bruijn, J. D. d.; Sohier, J. *Tissue Engineering*, 1st ed.; Academic Press: Burlington, 2008.
(286) Hubert, T.; Grimal, S.; Carroll, P.; Fichard-Carroll, A. Collagens in the Developing and Diseased Nervous System. *Cell. Mol. Life Sci.* **2009**, *66*, 1223.
(287) Belkas, J. S.; Shoichet, M. S.; Midha, R. Axonal Guidance Channels in Peripheral Nerve Regeneration. *Oper. Technol. Orthop.* **2004**, *14*, 190.
(288) Seckel, B. R. Enhancement of Peripheral Nerve Regeneration. *Muscle Nerve* **1990**, *13*, 785.
(289) Shen, Y. J.; DeBellard, M. E.; Salzer, J. L.; Roder, J.; Filbin, M. T. Myelin-Associated Glycoprotein in Myelin and Expressed by Schwann Cells Inhibits Axonal Regeneration and Branching. *Mol. Cell. Neurosci.* **1998**, *12*, 79.
(290) Taylor, J. S.; Bampton, E. T. Factors Secreted by Schwann Cells Stimulate the Regeneration of Neonatal Retinal Ganglion Cells. *J. Anat.* **2004**, *204*, 25.
(291) Lundborg, G. *Nerve Regeneration*, 1st ed.; Churchill Livingstone: London, 1988.
(292) Dubey, N.; Letourneau, P. C.; Tranquillo, R. T. Guided Neurite Elongation and Schwann Cell Invasion into Magnetically Aligned Collagen in Simulated Peripheral Nerve Regeneration. *Exp. Neurol.* **1999**, *158*, 338.
(293) Morris, J. H.; Hudson, A. R.; Weddell, G. A Study of Degeneration and Regeneration in the Divided Rat Sciatic Nerve Based on Electron Microscopy. Iv. Changes in Fascicular Microtopography, Perineurium and Endoneurial Fibroblasts. *Cell Tissue Res.* **1972**, *124*, 165.
(294) Tessier-Lavigne, M.; Goodman, C. S. The Molecular Biology of Axon Guidance. *Science* **1996**, *274*, 1123.
(295) Daly, W.; Yao, L.; Zeugolis, D.; Windebank, A.; Pandit, A. A Biomaterials Approach to Peripheral Nerve Regeneration: Bridging the Peripheral Nerve Gap and Enhancing Functional Recovery. *J. R. Soc., Interface* **2012**, *9*, 202.
(296) Kehoe, S.; Zhang, X. F.; Boyd, D. Fda Approved Guidance Conduits and Wraps for Peripheral Nerve Injury: A Review of Materials and Efficacy. *Injury* **2012**, *43*, 553.
(297) Wieringa, P. A.; Goncalves de Pinho, A. R.; Micera, S.; van Wezel, R. J. A.; Moroni, L. Biomimetic Architectures for Peripheral Nerve Repair: A Review of Biofabrication Strategies. *Adv. Healthcare Mater.* **2018**, *7*, No. 1701164.
(298) Yurie, H.; Ikeguchi, R.; Aoyama, T.; Kaizawa, Y.; Tajino, J.; Ito, A.; Ohta, S.; Oda, H.; Takeuchi, H.; Akieda, S.; et al. The Efficacy of a Scaffold-Free Bio 3d Conduit Developed from Human Fibroblasts on Peripheral Nerve Regeneration in a Rat Sciatic Nerve Model. *PLoS One* **2017**, *12*, No. e0171448.
(299) Zhang, Q.; Nguyen, P. D.; Shi, S.; Burrell, J. C.; Cullen, D. K.; Le, A. D. 3d Bio-Printed Scaffold-Free Nerve Constructs with Human Gingiva-Derived Mesenchymal Stem Cells Promote Rat Facial Nerve Regeneration. *Sci. Rep.* **2018**, *8*, 1.
(300) Zhang, Q.; Nguyen, P.; Xu, Q.; Park, W.; Lee, S.; Furuhashi, A.; Le, A. D. Neural Progenitor-Like Cells Induced from Human Gingiva-Derived Mesenchymal Stem Cells Regulate Myelination of Schwann Cells in Rat Sciatic Nerve Regeneration. *Stem Cells Transl. Med.* **2017**, *6*, 458.
(301) Owens, C. M.; Marga, F.; Forgacs, G.; Heesch, C. M. Biofabrication and Testing of a Fully Cellular Nerve Graft. *Biofabrication* **2013**, *5*, 045007.
(302) Norotte, C.; Marga, F. S.; Niklason, L. E.; Forgacs, G. Scaffold-Free Vascular Tissue Engineering Using Bioprinting. *Biomaterials* **2009**, *30*, 5910.
(303) Koch, D.; Rosoff, W. J.; Jiang, J.; Geller, H. M.; Urbach, J. S. Strength in the Periphery: Growth Cone Biomechanics and Substrate Rigidity Response in Peripheral and Central Nervous System Neurons. *Biophys. J.* **2012**, *102*, 452.
(304) Chan, C. E.; Odde, D. J. Traction Dynamics of Filopodia on Compliant Substrates. *Science* **2008**, *322*, 1687.
(305) Rosso, G.; Young, P.; Shahin, V. Mechanosensitivity of Embryonic Neurites Promotes Their Directional Extension and Schwann Cells Progenitors Migration. *Cell. Physiol. Biochem.* **2017**, *44*, 1263.
(306) Rosso, G.; Liashkovich, I.; Young, P.; Rohr, D.; Shahin, V. Schwann Cells and Neurite Outgrowth from Embryonic Dorsal Root Ganglions Are Highly Mechanosensitive. *Nanomedicine* **2017**, *13*, 493.
(307) McGarvey, M. L.; Baron-Van Evercooren, A.; Kleinman, H. K.; Dubois-Dalcq, M. Synthesis and Effects of Basement Membrane Components in Cultured Rat Schwann Cells. *Dev. Biol.* **1984**, *105*, 18.
(308) Jessen, K. R.; Mirsky, R. The Repair Schwann Cell and Its Function in Regenerating Nerves. *J. Physiol.* **2016**, *594*, 3521.
(309) di Summa, P. G.; Kingham, P. J.; Raffoul, W.; Wiberg, M.; Terenghi, G.; Kalbermatten, D. F. Adipose-Derived Stem Cells Enhance Peripheral Nerve Regeneration. *J. Plast. Reconstr. Aesthet. Surg.* **2010**, *63*, 1544.
(310) Chen, C. J.; Ou, Y. C.; Liao, S. L.; Chen, W. Y.; Chen, S. Y.; Wu, C. W.; Wang, C. C.; Wang, W. Y.; Huang, Y. S.; Hsu, S. H. Transplantation of Bone Marrow Stromal Cells for Peripheral Nerve Repair. *Exp. Neurol.* **2007**, *204*, 443.
(311) Kaewkhaw, R.; Scutt, A. M.; Haycock, J. W. Integrated Culture and Purification of Rat Schwann Cells from Freshly Isolated Adult Tissue. *Nat. Protoc.* **2012**, *7*, 1996.
(312) Jiang, H.; Qu, W.; Han, F.; Liu, D.; Zhang, W. Establishment of Immortalized Schwann Cells Derived from Rat Embryo Dorsal Root Ganglia. *Int. J. Mol. Med.* **2012**, *30*, 480.
(313) Ostrow, K. L.; Donaldson, K.; Blakeley, J.; Belzberg, A.; Hoke, A. Immortalized Human Schwann Cell Lines Derived from Tumors of Schwannomatosis Patients. *PLoS One* **2015**, *10*, No. e0144620.
(314) Navarro, X.; Vivo, M.; Valero-Cabre, A. Neural Plasticity after Peripheral Nerve Injury and Regeneration. *Prog. Neurobiol.* **2007**, *82*, 163.
(315) Labrador, R. O.; Buti, M.; Navarro, X. Influence of Collagen and Laminin Gels Concentration on Nerve Regeneration after Resection and Tube Repair. *Exp. Neurol.* **1998**, *149*, 243.
(316) Ceballos, D.; Navarro, X.; Dubey, N.; Wendelschafer-Crabb, G.; Kennedy, W. R.; Tranquillo, R. T. Magnetically Aligned Collagen Gel Filling a Collagen Nerve Guide Improves Peripheral Nerve Regeneration. *Exp. Neurol.* **1999**, *158*, 290.
(317) Kolesky, D. B.; Truby, R. L.; Gladman, A. S.; Busbee, T. A.; Homan, K. A.; Lewis, J. A. 3d Bioprinting of Vascularized, Heterogeneous Cell-Laden Tissue Constructs. *Adv. Mater.* **2014**, *26*, 3124.
(318) Bertassoni, L. E.; Cecconi, M.; Manoharan, V.; Nikkhah, M.; Hjortnaes, J.; Cristino, A. L.; Barabaschi, G.; Demarchi, D.; Dokmeci, M. R.; Yang, Y.; et al. Hydrogel Bioprinted Microchannel Networks for Vascularization of Tissue Engineering Constructs. *Lab Chip* **2014**, *14*, 2202.
(319) Haigh, J. N.; Chuang, Y. M.; Farrugia, B.; Hoogenboom, R.; Dalton, P. D.; Dargaville, T. R. Hierarchically Structured Porous Poly(2-Oxazoline) Hydrogels. *Macromol. Rapid Commun.* **2016**, *37*, 93.
(320) Miller, J. S.; Stevens, K. R.; Yang, M. T.; Baker, B. M.; Nguyen, D. H.; Cohen, D. M.; Toro, E.; Chen, A. A.; Galie, P. A.; Yu, X.; et al. Rapid Casting of Patterned Vascular Networks for Perfusable Engineered Three-Dimensional Tissues. *Nat. Mater.* **2012**, *11*, 768.
(321) Whalley, K. Neural Development: Finding the Source of Parasympathetic Neurons. *Nat. Rev. Neurosci.* **2014**, *15*, 494.

https://dx.doi.org/10.1021/acs.chemrev.9b00789
Chem. Rev. 2020, 120, 11032−11092

(322) Dyachuk, V.; Furlan, A.; Shahidi, M. K.; Giovenco, M.; Kaukua, N.; Konstantinidou, C.; Pachnis, V.; Memic, F.; Marklund, U.; Muller, T.; et al. Neurodevelopment. Parasympathetic Neurons Originate from Nerve-Associated Peripheral Glial Progenitors. *Science* **2014**, *345*, 82.
(323) Firestein, G. S.; Kelley, W. N. *Kelley's Textbook of Rheumatology*, 8th ed.; Saunders Elsevier, 2009.
(324) Athanasiou, K. A.; Darling, E. M.; DuRaine, G. D.; Hu, J. C.; A.Hari, R. *Articular Cratilage*, CRC Press, 2013.
(325) Camarero-Espinosa, S.; Rothen-Rutishauser, B.; Foster, E. J.; Weder, C. Articular Cartilage: From Formation to Tissue Engineering. *Biomater. Sci.* **2016**, *4*, 734.
(326) Whitesides, T. E. *Orthopaedic Basic Science. Biology and Biomechanics of the Musculoskeletal System*, 2nd ed.; 2001.
(327) Jadin, K. D.; Wong, B. L.; Bae, W. C.; Li, K. W.; Williamson, A. K.; Schumacher, B. L.; Price, J. H.; Sah, R. L. Depth-Varying Density and Organization of Chondrocytes in Immature and Mature Bovine Articular Cartilage Assessed by 3d Imaging and Analysis. *J. Histochem. Cytochem.* **2005**, *53*, 1109.
(328) Williams, G. M.; Klisch, S. M.; Sah, R. L. Bioengineering Cartilage Growth, Maturation, and Form. *Pediatr. Res.* **2008**, *63*, 527.
(329) Athanasiou, K. A.; Darling, E. M.; Hu, J. C. Articular Cartilage Tissue Engineering. *Synth. Lect. Tissue Eng.* **2009**, *1*, 1.
(330) Melrose, J.; Shu, C.; Whitelock, J. M.; Lord, M. S. The Cartilage Extracellular Matrix as a Transient Developmental Scaffold for Growth Plate Maturation. *Matrix Biol.* **2016**, *52*−*54*, 363.
(331) Fujioka, R.; Aoyama, T.; Takakuwa, T. The Layered Structure of the Articular Surface. *Osteoarthr. Cartil.* **2013**, *21*, 1092.
(332) Kumar, P.; Oka, M.; Toguchida, J.; Kobayashi, M.; Uchida, E.; Nakamura, T.; Tanaka, K. Role of Uppermost Superficial Surface Layer of Articular Cartilage in the Lubrication Mechanism of Joints. *J. Anat.* **2001**, *199*, 241.
(333) Eyre, D. R.; Wu, J. J. Collagen Structure and Cartilage Matrix Integrity. *J. Rheumatol. Suppl.* **1995**, *43*, 82.
(334) Eyre, D. Collagen of Articular Cartilage. *Arthritis Res.* **2002**, *4*, 30.
(335) Knudson, C. B.; Knudson, W. Cartilage Proteoglycans. *Semin. Cell Dev. Biol.* **2001**, *12*, 69.
(336) Chen, S. S.; Falcovitz, Y. H.; Schneiderman, R.; Maroudas, A.; Sah, R. L. Depth-Dependent Compressive Properties of Normal Aged Human Femoral Head Articular Cartilage: Relationship to Fixed Charge Density. *Osteoarthr. Cartil.* **2001**, *9*, 561.
(337) Mow, V. C.; Holmes, M. H.; Lai, W. M. Fluid Transport and Mechanical Properties of Articular Cartilage: A Review. *J. Biomech.* **1984**, *17*, 377.
(338) Cohen, N. P.; Foster, R. J.; Mow, V. C. Composition and Dynamics of Articular Cartilage: Structure, Function, and Maintaining Healthy State. *J. Orthop. Sports Phys. Ther.* **1998**, *28*, 203.
(339) Athanasiou, K. A.; Rosenwasser, M. P.; Buckwalter, J. A.; Malinin, T. I.; Mow, V. C. Interspecies Comparisons of in Situ Intrinsic Mechanical Properties of Distal Femoral Cartilage. *J. Orthop. Res.* **1991**, *9*, 330.
(340) Schinagl, R. M.; Gurskis, D.; Chen, A. C.; Sah, R. L. Depth-Dependent Confined Compression Modulus of Full-Thickness Bovine Articular Cartilage. *J. Orthop. Res.* **1997**, *15*, 499.
(341) Kempson, G. E.; Freeman, M. A.; Swanson, S. A. Tensile Properties of Articular Cartilage. *Nature* **1968**, *220*, 1127.
(342) Akizuki, S.; Mow, V. C.; Muller, F.; Pita, J. C.; Howell, D. S.; Manicourt, D. H. Tensile Properties of Human Knee Joint Cartilage: I. Influence of Ionic Conditions, Weight Bearing, and Fibrillation on the Tensile Modulus. *J. Orthop. Res.* **1986**, *4*, 379.
(343) Jurvelin, J. S.; Buschmann, M. D.; Hunziker, E. B. Optical and Mechanical Determination of Poisson's Ratio of Adult Bovine Humeral Articular Cartilage. *J. Biomech.* **1997**, *30*, 235.
(344) Korhonen, R. K.; Laasanen, M. S.; Toyras, J.; Rieppo, J.; Hirvonen, J.; Helminen, H. J.; Jurvelin, J. S. Comparison of the Equilibrium Response of Articular Cartilage in Unconfined Compression, Confined Compression and Indentation. *J. Biomech.* **2002**, *35*, 903.
(345) Woodfield, T. B.; Guggenheim, M.; von Rechenberg, B.; Riesle, J.; van Blitterswijk, C. A.; Wedler, V. Rapid Prototyping of Anatomically Shaped, Tissue-Engineered Implants for Restoring Congruent Articulating Surfaces in Small Joints. *Cell Proliferation* **2009**, *42*, 485.
(346) Hall, B. K.; Miyake, T. The Membranous Skeleton: The Role of Cell Condensations in Vertebrate Skeletogenesis. *Anat. Embryol.* **1992**, *186*, 107.
(347) Pacifici, M.; Koyama, E.; Shibukawa, Y.; Wu, C.; Tamamura, Y.; Enomoto-Iwamoto, M.; Iwamoto, M. In *Skeletal Development and Remodeling in Health, Disease, and Aging*; Zaidi, M., Ed., 2006.
(348) Temenoff, J. S.; Mikos, A. G. Review: Tissue Engineering for Regeneration of Articular Cartilage. *Biomaterials* **2000**, *21*, 431.
(349) Huey, D. J.; Hu, J. C.; Athanasiou, K. A. Unlike Bone, Cartilage Regeneration Remains Elusive. *Science* **2012**, *338*, 917.
(350) Cao, Y.; Vacanti, J. P.; Paige, K. T.; Upton, J.; Vacanti, C. A. Transplantation of Chondrocytes Utilizing a Polymer-Cell Construct to Produce Tissue-Engineered Cartilage in the Shape of a Human Ear. *Plast. Reconstr. Surg.* **1997**, *100*, 297.
(351) Zopf, D. A.; Mitsak, A. G.; Flanagan, C. L.; Wheeler, M.; Green, G. E.; Hollister, S. J. Computer Aided-Designed, 3-Dimensionally Printed Porous Tissue Bioscaffolds for Craniofacial Soft Tissue Reconstruction. *Otolaryngol.–Head Neck Surg.* **2015**, *152*, 57.
(352) Zhou, G.; Jiang, H.; Yin, Z.; Liu, Y.; Zhang, Q.; Zhang, C.; Pan, B.; Zhou, J.; Zhou, X.; Sun, H.; et al. In Vitro Regeneration of Patient-Specific Ear-Shaped Cartilage and Its First Clinical Application for Auricular Reconstruction. *EBioMedicine* **2018**, *28*, 287.
(353) Kronenberg, H. M. Developmental Regulation of the Growth Plate. *Nature* **2003**, *423*, 332.
(354) Kesti, M.; Eberhardt, C.; Pagliccia, G.; Kenkel, D.; Grande, D.; Boss, A.; Zenobi-Wong, M. Bioprinting Complex Cartilaginous Structures with Clinically Compliant Biomaterials. *Adv. Funct. Mater.* **2015**, *25*, 7406.
(355) Olubamiji, A. D.; Izadifar, Z.; Si, J. L.; Cooper, D.; Eames, B. F.; Chen, D. X. B. Modulating Mechanical Behaviour of 3d-Printed Cartilage-Mimetic Pcl Scaffolds: Influence of Molecular Weight and Pore Geometry. *Biofabrication* **2016**, *8*, 025020.
(356) Moncal, K. K.; Heo, D. N.; Godzik, K. P.; Sosnoski, D. M.; Mrowczynski, O. D.; Rizk, E.; Ozbolat, V.; Tucker, S. M.; Gerhard, E. M.; Dey, M.; et al. 3d Printing of Poly(Epsilon-Caprolactone)/Poly(D,L-Lactide-Co-Glycolide)/Hydroxyapatite Composite Constructs for Bone Tissue Engineering. *J. Mater. Res.* **2018**, *33*, 1972.
(357) Malayeri, A.; Gabbott, C.; Reilly, G.; Ghassemieh, E.; Hatton, P. V.; Claeyssens, F. Feasibility of 3d Printing and Stereolithography for Fabrication of Custom-Shaped Poly (Lactic Acid): Hydroxyapatite Composite Biomaterial Scaffolds. *J. Tissue Eng. Regen M* **2012**, *6*, 367.
(358) Lebedev, S. M.; Gefle, O. S.; Amitov, E. T.; Zhuravlev, D. V.; Berchuk, D. Y.; Mikutskiy, E. A. Mechanical Properties of Pla-Based Composites for Fused Deposition Modeling Technology. *International Journal of Advanced Manufacturing Technology* **2018**, *97*, 511.
(359) Poh, P. S. P.; Chhaya, M. P.; Wunner, F. M.; De-Juan-Pardo, E. M.; Schilling, A. F.; Schantz, J. T.; van Griensven, M.; Hutmacher, D. W. Polylactides in Additive Biomanufacturing. *Adv. Drug Delivery Rev.* **2016**, *107*, 228.
(360) Ribeiro, J. F. M.; Oliveira, S. M.; Alves, J. L.; Pedro, A. J.; Reis, R. L.; Fernandes, E. M.; Mano, J. F. Structural Monitoring and Modeling of the Mechanical Deformation of Three-Dimensional Printed Poly(Epsilon-Caprolactone) Scaffolds. *Biofabrication* **2017**, *9*, 025015.
(361) Woods, A.; Wang, G.; Beier, F. Regulation of Chondrocyte Differentiation by the Actin Cytoskeleton and Adhesive Interactions. *J. Cell. Physiol.* **2007**, *213*, 1.
(362) Nurminsky, D.; Magee, C.; Faverman, L.; Nurminskaya, M. Regulation of Chondrocyte Differentiation by Actin-Severing Protein Adseverin. *Dev. Biol.* **2007**, *302*, 427.
(363) Woodfield, T. B. F.; Miot, S.; Martin, I.; van Blitterswijk, C. A.; Riesle, J. The Regulation of Expanded Human Nasal Chondrocyte Re-Differentiation Capacity by Substrate Composition and Gas Plasma Surface Modification. *Biomaterials* **2006**, *27*, 1043.
(364) Hung, K.-C.; Tseng, C.-S.; Dai, L.-G.; Hsu, S.-h. Water-Based Polyurethane 3d Printed Scaffolds with Controlled Release Function

https://dx.doi.org/10.1021/acs.chemrev.9b00789
Chem. Rev. 2020, 120, 11032−11092

for Customized Cartilage Tissue Engineering. *Biomaterials* **2016**, *83*, 156.
(365) Hung, K. C.; Tseng, C. S.; Hsu, S. H. Synthesis and 3d Printing of Biodegradable Polyurethane Elastomer by a Water-Based Process for Cartilage Tissue Engineering Applications. *Adv. Healthcare Mater.* **2014**, *3*, 1578.
(366) Armstrong, C. G.; Bahrani, A. S.; Gardner, D. L. In Vitro Measurement of Articular Cartilage Deformations in the Intact Human Hip Joint under Load. *J. Bone Joint. Surg. Am.* **1979**, *61*, 744.
(367) Mouser, V. H. M.; Abbadessa, A.; Levato, R.; Hennink, W. E.; Vermonden, T.; Gawlitta, D.; Malda, J. Development of a Thermosensitive Hama-Containing Bio-Ink for the Fabrication of Composite Cartilage Repair Constructs. *Biofabrication* **2017**, *9*, 015026.
(368) Abbadessa, A.; Blokzijl, M. M.; Mouser, V. H.; Marica, P.; Malda, J.; Hennink, W. E.; Vermonden, T. A Thermo-Responsive and Photo-Polymerizable Chondroitin Sulfate-Based Hydrogel for 3d Printing Applications. *Carbohydr. Polym.* **2016**, *149*, 163.
(369) Visser, J.; Melchels, F. P.; Jeon, J. E.; van Bussel, E. M.; Kimpton, L. S.; Byrne, H. M.; Dhert, W. J.; Dalton, P. D.; Hutmacher, D. W.; Malda, J. Reinforcement of Hydrogels Using Three-Dimensionally Printed Microfibres. *Nat. Commun.* **2015**, *6*, 6933.
(370) Visser, J.; Gawlitta, D.; Benders, K. E. M.; Toma, S. M. H.; Pouran, B.; van Weeren, P. R.; Dhert, W. J. A.; Malda, J. Endochondral Bone Formation in Gelatin Methacrylamide Hydrogel with Embedded Cartilage-Derived Matrix Particles. *Biomaterials* **2015**, *37*, 174.
(371) Boere, K. W. M.; Blokzijl, M. M.; Visser, J.; Linssen, J. E. A.; Malda, J.; Hennink, W. E.; Vermonden, T. Biofabrication of Reinforced 3d-Scaffolds Using Two-Component Hydrogels. *J. Mater. Chem. B* **2015**, *3*, 9067.
(372) Boere, K. W.; Visser, J.; Seyednejad, H.; Rahimian, S.; Gawlitta, D.; van Steenbergen, M. J.; Dhert, W. J.; Hennink, W. E.; Vermonden, T.; Malda, J. Covalent Attachment of a Three-Dimensionally Printed Thermoplast to a Gelatin Hydrogel for Mechanically Enhanced Cartilage Constructs. *Acta Biomater.* **2014**, *10*, 2602.
(373) Kang, H. W.; Lee, S. J.; Ko, I. K.; Kengla, C.; Yoo, J. J.; Atala, A. A 3d Bioprinting System to Produce Human-Scale Tissue Constructs with Structural Integrity. *Nat. Biotechnol.* **2016**, *34*, 312.
(374) Nowicki, M.; Castro, N. J.; Rao, R.; Plesniak, M.; Zhang, L. G. Integrating Three-Dimensional Printing and Nanotechnology for Musculoskeletal Regeneration. *Nanotechnology* **2017**, *28*, 382001.
(375) Daly, A. C.; Freeman, F. E.; Gonzalez-Fernandez, T.; Critchley, S. E.; Nulty, J.; Kelly, D. J. 3d Bioprinting for Cartilage and Osteochondral Tissue Engineering. *Adv. Healthcare Mater.* **2017**, *6*, 1700298.
(376) Shao, L.; Gao, Q.; Zhao, H.; Xie, C.; Fu, J.; Liu, Z.; Xiang, M.; He, Y. Fiber-Based Mini Tissue with Morphology-Controllable Gelma Microfibers. *Small* **2018**, *14*, No. e1802187.
(377) Kang, H. W.; Lee, S. J.; Ko, I. K.; Kengla, C.; Yoo, J. J.; Atala, A. A 3d Bioprinting System to Produce Human-Scale Tissue Constructs with Structural Integrity. *Nat. Biotechnol.* **2016**, *34*, 312.
(378) Gao, F.; Xu, Z. Y.; Liang, Q. F.; Liu, B.; Li, H. F.; Wu, Y. H.; Zhang, Y. Y.; Lin, Z. F.; Wu, M. M.; Ruan, C. S.; et al. Direct 3d Printing of High Strength Biohybrid Gradient Hydrogel Scaffolds for Efficient Repair of Osteochondral Defect. *Adv. Funct. Mater.* **2018**, *28*, 1706644.
(379) Wang, Y.; Azais, T.; Robin, M.; Vallee, A.; Catania, C.; Legriel, P.; Pehau-Arnaudet, G.; Babonneau, F.; Giraud-Guille, M. M.; Nassif, N. The Predominant Role of Collagen in the Nucleation, Growth, Structure and Orientation of Bone Apatite. *Nat. Mater.* **2012**, *11*, 724.
(380) Fratzl, P.; Fratzl-Zelman, N.; Klaushofer, K.; Vogl, G.; Koller, K. Nucleation and Growth of Mineral Crystals in Bone Studied by Small-Angle X-Ray Scattering. *Calcif. Tissue Int.* **1991**, *48*, 407.
(381) de Melo Pereira, D.; Habibovic, P. Biomineralization-Inspired Material Design for Bone Regeneration. *Adv. Healthcare Mater.* **2018**, *7*, No. e1800700.
(382) Olszta, M. J.; Cheng, X. G.; Jee, S. S.; Kumar, R.; Kim, Y. Y.; Kaufman, M. J.; Douglas, E. P.; Gower, L. B. Bone Structure and Formation: A New Perspective. *Mater. Sci. Eng., R* **2007**, *58*, 77.
(383) Boanini, E.; Gazzano, M.; Bigi, A. Ionic Substitutions in Calcium Phosphates Synthesized at Low Temperature. *Acta Biomater.* **2010**, *6*, 1882.
(384) Gehron Robey, P. In *Principles of Bone Biology*; Bilezikian, J. P., Raisz, L. G., Martin, T. J., Eds.; Academic Press: San Diego, 2008.
(385) Buckwalter, J. A.; Glimcher, M. J.; Cooper, R. R.; Recker, R. Bone Biology. *J. Bone Joint Surg. Am.* **1995**, *77*, 1256.
(386) Florencio-Silva, R.; Sasso, G. R.; Sasso-Cerri, E.; Simoes, M. J.; Cerri, P. S. Biology of Bone Tissue: Structure, Function, and Factors That Influence Bone Cells. *BioMed Res. Int.* **2015**, *2015*, 421746.
(387) Einhorn, T. A.; Gerstenfeld, L. C. Fracture Healing: Mechanisms and Interventions. *Nat. Rev. Rheumatol.* **2015**, *11*, 45.
(388) Byambaa, B.; Annabi, N.; Yue, K.; Trujillo-de Santiago, G.; Alvarez, M. M.; Jia, W.; Kazemzadeh-Narbat, M.; Shin, S. R.; Tamayol, A.; Khademhosseini, A. Bioprinted Osteogenic and Vasculogenic Patterns for Engineering 3d Bone Tissue. *Adv. Healthcare Mater.* **2017**, *6*, 1700015.
(389) Lindsey, R. W.; Gugala, Z.; Milne, E.; Sun, M.; Gannon, F. H.; Latta, L. L. The Efficacy of Cylindrical Titanium Mesh Cage for the Reconstruction of a Critical-Size Canine Segmental Femoral Diaphyseal Defect. *J. Orthop. Res.* **2006**, *24*, 1438.
(390) Gugala, Z.; Lindsey, R. W.; Gogolewski, S. New Approaches in the Treatment of Critical-Size Segmental Defects in Long Bones. *Macromol. Symp.* **2007**, *253*, 147.
(391) Kohli, N.; Ho, S.; Brown, S. J.; Sawadkar, P.; Sharma, V.; Snow, M.; García-Gareta, E. Bone Remodelling in Vitro: Where Are We Headed?: -a Review on the Current Understanding of Physiological Bone Remodelling and Inflammation and the Strategies for Testing Biomaterials in Vitro. *Bone* **2018**, *110*, 38.
(392) Tang, D.; Tare, R. S.; Yang, L. Y.; Williams, D. F.; Ou, K. L.; Oreffo, R. O. C. Biofabrication of Bone Tissue: Approaches, Challenges and Translation for Bone Regeneration. *Biomaterials* **2016**, *83*, 363.
(393) Karageorgiou, V.; Kaplan, D. Porosity of 3d Biomaterial Scaffolds and Osteogenesis. *Biomaterials* **2005**, *26*, 5474.
(394) Almubarak, S.; Nethercott, H.; Freeberg, M.; Beaudon, C.; Jha, A.; Jackson, W.; Marcucio, R.; Miclau, T.; Healy, K.; Bahney, C. Tissue Engineering Strategies for Promoting Vascularized Bone Regeneration. *Bone* **2016**, *83*, 197.
(395) Das, A.; Botchwey, E. Evaluation of Angiogenesis and Osteogenesis. *Tissue Eng., Part B* **2011**, *17*, 403.
(396) Kanczler, J. M.; Oreffo, R. O. Osteogenesis and Angiogenesis: The Potential for Engineering Bone. *Eur. Cell. Mater.* **2008**, *15*, 100.
(397) Ginebra, M. P.; Canal, C.; Espanol, M.; Pastorino, D.; Montufar, E. B. Calcium Phosphate Cements as Drug Delivery Materials. *Adv. Drug Delivery Rev.* **2012**, *64*, 1090.
(398) Samavedi, S.; Whittington, A. R.; Goldstein, A. S. Calcium Phosphate Ceramics in Bone Tissue Engineering: A Review of Properties and Their Influence on Cell Behavior. *Acta Biomater.* **2013**, *9*, 8037.
(399) Malhotra, A.; Habibovic, P. Calcium Phosphates and Angiogenesis: Implications and Advances for Bone Regeneration. *Trends Biotechnol.* **2016**, *34*, 983.
(400) Niinomi, M.; Nakai, M.; Hieda, J. Development of New Metallic Alloys for Biomedical Applications. *Acta Biomater.* **2012**, *8*, 3888.
(401) Wang, X. J.; Xu, S. Q.; Zhou, S. W.; Xu, W.; Leary, M.; Choong, P.; Qian, M.; Brandt, M.; Xie, Y. M. Topological Design and Additive Manufacturing of Porous Metals for Bone Scaffolds and Orthopaedic Implants: A Review. *Biomaterials* **2016**, *83*, 127.
(402) Du, X. Y.; Fu, S. Y.; Zhu, Y. F. 3d Printing of Ceramic-Based Scaffolds for Bone Tissue Engineering: An Overview. *J. Mater. Chem. B* **2018**, *6*, 4397.
(403) Wen, Y.; Xun, S.; Haoye, M.; Baichuan, S.; Peng, C.; Xuejian, L.; Kaihong, Z.; Xuan, Y.; Jiang, P.; Shibi, L. 3d Printed Porous Ceramic Scaffolds for Bone Tissue Engineering: A Review. *Biomater. Sci.* **2017**, *5*, 1690.
(404) Zhang, X. Y.; Fang, G.; Zhou, J. Additively Manufactured Scaffolds for Bone Tissue Engineering and the Prediction of Their Mechanical Behavior: A Review. *Materials* **2017**, *10*, 50.

https://dx.doi.org/10.1021/acs.chemrev.9b00789
Chem. Rev. 2020, 120, 11032−11092

(405) Di Luca, A.; Longoni, A.; Criscenti, G.; Mota, C.; van Blitterswijk, C.; Moroni, L. Toward Mimicking the Bone Structure: Design of Novel Hierarchical Scaffolds with a Tailored Radial Porosity Gradient. *Biofabrication* **2016**, *8*, 045007.
(406) De Giglio, E.; Bonifacio, M. A.; Ferreira, A. M.; Cometa, S.; Ti, Z. Y.; Stanzione, A.; Dalgarno, K.; Gentile, P. Multi-Compartment Scaffold Fabricated Via 3d-Printing as in Vitro Co-Culture Osteogenic Model. *Sci. Rep.* **2018**, *8*, 15130.
(407) Keriquel, V.; Oliveira, H.; Remy, M.; Ziane, S.; Delmond, S.; Rousseau, B.; Rey, S.; Catros, S.; Amedee, J.; Guillemot, F.; et al. In Situ Printing of Mesenchymal Stromal Cells, by Laser-Assisted Bioprinting, for in Vivo Bone Regeneration Applications. *Sci. Rep.* **2017**, *7*, 1778.
(408) Guillemot, F.; Souquet, A.; Catros, S.; Guillotin, B. Laser-Assisted Cell Printing: Principle, Physical Parameters Versus Cell Fate and Perspectives in Tissue Engineering. *Nanomedicine* **2010**, *5*, 507.
(409) Keriquel, V.; Guillemot, F.; Arnault, I.; Guillotin, B.; Miraux, S.; Amedee, J.; Fricain, J. C.; Catros, S. Vivo Bioprinting for Computer- and Robotic-Assisted Medical Intervention: Preliminary Study in Mice. *Biofabrication* **2010**, *2*, 014101.
(410) Pagès, E.; Rémy, M.; Kériquel, V.; Correa, M. M.; Guillotin, B.; Guillemot, F. Creation of Highly Defined Mesenchymal Stem Cell Patterns in Three Dimensions by Laser-Assisted Bioprinting. *J. Nanotechnol. Eng. Med.* **2015**, *6*, 021006.
(411) Chawla, S.; Sharma, A.; Bandyopadhyay, A.; Ghosh, S. Developmental Biology-Inspired Strategies to Engineer 3d Bioprinted Bone Construct. *ACS Biomater. Sci. Eng.* **2018**, *4*, 3545.
(412) Patan, S. Vasculogenesis and Angiogenesis. *Cancer Treat. Res.* **2004**, *117*, 3.
(413) Othman, R.; Morris, E. M.; Shah, D. A.; Hall, S.; Hall, G.; Wells, K.; Shakesheff, K. M.; Dixon, J. E. An Automated Fabrication Strategy to Create Patterned Tubular Architectures at Cell and Tissue Scales. *Biofabrication* **2015**, *7*, 025003.
(414) Patel, A.; Fine, B.; Sandig, M.; Mequanint, K. Elastin Biosynthesis: The Missing Link in Tissue-Engineered Blood Vessels. *Cardiovasc. Res.* **2006**, *71*, 40.
(415) Miri, A. K.; Khalilpour, A.; Cecen, B.; Maharjan, S.; Shin, S. R.; Khademhosseini, A. Multiscale Bioprinting of Vascularized Models. *Biomaterials* **2019**, *198*, 204.
(416) Tan, Y.; Richards, D. J.; Trusk, T. C.; Visconti, R. P.; Yost, M. J.; Kindy, M. S.; Drake, C. J.; Argraves, W. S.; Markwald, R. R.; Mei, Y. 3d Printing Facilitated Scaffold-Free Tissue Unit Fabrication. *Biofabrication* **2014**, *6*, 024111.
(417) Kucukgul, C.; Ozler, S. B.; Inci, I.; Karakas, E.; Irmak, S.; Gozuacik, D.; Taralp, A.; Koc, B. 3d Bioprinting of Biomimetic Aortic Vascular Constructs with Self-Supporting Cells. *Biotechnol. Bioeng.* **2015**, *112*, 811.
(418) Song, K. H.; Highley, C. B.; Rouff, A.; Burdick, J. A. Complex 3d-Printed Microchannels within Cell-Degradable Hydrogels. *Adv. Funct. Mater.* **2018**, *28*, 1801331.
(419) Benning, L.; Gutzweiler, L.; Trondle, K.; Riba, J.; Zengerle, R.; Koltay, P.; Zimmermann, S.; Stark, G. B.; Finkenzeller, G. Assessment of Hydrogels for Bioprinting of Endothelial Cells. *J. Biomed. Mater. Res., Part A* **2018**, *106*, 935.
(420) Kreimendahl, F.; Kopf, M.; Thiebes, A. L.; Duarte Campos, D. F.; Blaeser, A.; Schmitz-Rode, T.; Apel, C.; Jockenhoevel, S.; Fischer, H. Three-Dimensional Printing and Angiogenesis: Tailored Agarose-Type I Collagen Blends Comprise Three-Dimensional Printability and Angiogenesis Potential for Tissue-Engineered Substitutes. *Tissue Eng., Part C* **2017**, *23*, 604.
(421) Schoneberg, J.; De Lorenzi, F.; Theek, B.; Blaeser, A.; Rommel, D.; Kuehne, A. J. C.; Kiessling, F.; Fischer, H. Engineering Biofunctional in Vitro Vessel Models Using a Multilayer Bioprinting Technique. *Sci. Rep.* **2018**, *8*, 10430.
(422) Skardal, A.; Zhang, J.; Prestwich, G. D. Bioprinting Vessel-Like Constructs Using Hyaluronan Hydrogels Crosslinked with Tetrahedral Polyethylene Glycol Tetracrylates. *Biomaterials* **2010**, *31*, 6173.
(423) Meyer, W.; Engelhardt, S.; Novosel, E.; Elling, B.; Wegener, M.; Kruger, H. Soft Polymers for Building up Small and Smallest Blood Supplying Systems by Stereolithography. *J. Funct. Biomater.* **2012**, *3*, 257.
(424) Kang, D.; Ahn, G.; Kim, D.; Kang, H. W.; Yun, S.; Yun, W. S.; Shim, J. H.; Jin, S. Pre-Set Extrusion Bioprinting for Multiscale Heterogeneous Tissue Structure Fabrication. *Biofabrication* **2018**, *10*, 035008.
(425) Miller, J. S.; Stevens, K. R.; Yang, M. T.; Baker, B. M.; Nguyen, D. H.; Cohen, D. M.; Toro, E.; Chen, A. A.; Galie, P. A.; Yu, X.; et al. Rapid Casting of Patterned Vascular Networks for Perfusable Engineered Three-Dimensional Tissues. *Nat. Mater.* **2012**, *11*, 768.
(426) Sooppan, R.; Paulsen, S. J.; Han, J.; Ta, A. H.; Dinh, P.; Gaffey, A. C.; Venkataraman, C.; Trubelja, A.; Hung, G.; Miller, J. S.; et al. In Vivo Anastomosis and Perfusion of a Three-Dimensionally-Printed Construct Containing Microchannel Networks. *Tissue Eng., Part C* **2016**, *22*, 1.
(427) Kolesky, D. B.; Homan, K. A.; Skylar-Scott, M. A.; Lewis, J. A. Three-Dimensional Bioprinting of Thick Vascularized Tissues. *Proc. Natl. Acad. Sci. U. S. A.* **2016**, *113*, 3179.
(428) Xu, Y.; Hu, Y.; Liu, C.; Yao, H.; Liu, B.; Mi, S. A Novel Strategy for Creating Tissue-Engineered Biomimetic Blood Vessels Using 3d Bioprinting Technology. *Materials* **2018**, *11*, 1581.
(429) Pimentel, C. R.; Ko, S. K.; Caviglia, C.; Wolff, A.; Emneus, J.; Keller, S. S.; Dufva, M. Three-Dimensional Fabrication of Thick and Densely Populated Soft Constructs with Complex and Actively Perfused Channel Network. *Acta Biomater.* **2018**, *65*, 174.
(430) Akkineni, A. R.; Ahlfeld, T.; Lode, A.; Gelinsky, M. A Versatile Method for Combining Different Biopolymers in a Core/Shell Fashion by 3d Plotting to Achieve Mechanically Robust Constructs. *Biofabrication* **2016**, *8*, 045001.
(431) Jia, W.; Gungor-Ozkerim, P. S.; Zhang, Y. S.; Yue, K.; Zhu, K.; Liu, W.; Pi, Q.; Byambaa, B.; Dokmeci, M. R.; Shin, S. R.; et al. Direct 3d Bioprinting of Perfusable Vascular Constructs Using a Blend Bioink. *Biomaterials* **2016**, *106*, 58.
(432) Pi, Q.; Maharjan, S.; Yan, X.; Liu, X.; Singh, B.; van Genderen, A. M.; Robledo-Padilla, F.; Parra-Saldivar, R.; Hu, N.; Jia, W.; et al. Digitally Tunable Microfluidic Bioprinting of Multilayered Cannular Tissues. *Adv. Mater.* **2018**, *30*, No. 1706913.
(433) Zhu, W.; Qu, X.; Zhu, J.; Ma, X.; Patel, S.; Liu, J.; Wang, P.; Lai, C. S.; Gou, M.; Xu, Y.; et al. Direct 3d Bioprinting of Prevascularized Tissue Constructs with Complex Microarchitecture. *Biomaterials* **2017**, *124*, 106.
(434) Srivastava, D.; Olson, E. N. A Genetic Blueprint for Cardiac Development. *Nature* **2000**, *407*, 221.
(435) Noor, N.; Shapira, A.; Edri, R.; Gal, I.; Wertheim, L.; Dvir, T. 3d Printing of Personalized Thick and Perfusable Cardiac Patches and Hearts. *Adv. Sci. (Weinh.)* **2019**, *6*, 1900344.
(436) Tirziu, D.; Giordano, F. J.; Simons, M. Cell Communications in the Heart. *Circulation* **2010**, *122*, 928.
(437) Bergmann, O.; Zdunek, S.; Felker, A.; Salehpour, M.; Alkass, K.; Bernard, S.; Sjostrom, S. L.; Szewczykowska, M.; Jackowska, T.; Dos Remedios, C.; et al. Dynamics of Cell Generation and Turnover in the Human Heart. *Cell* **2015**, *161*, 1566.
(438) Lockhart, M.; Wirrig, E.; Phelps, A.; Wessels, A. Extracellular Matrix and Heart Development. *Birth Defects Res., Part A* **2011**, *91*, 535.
(439) Gray, G. A.; Toor, I. S.; Castellan, R.; Crisan, M.; Meloni, M. Resident Cells of the Myocardium: More Than Spectators in Cardiac Injury, Repair and Regeneration. *Curr. Opin. Physiol.* **2018**, *1*, 46.
(440) Rienks, M.; Papageorgiou, A.-P.; Frangogiannis, N. G.; Heymans, S. Myocardial Extracellular Matrix. *Circ. Res.* **2014**, *114*, 872.
(441) Domenech, M.; Polo-Corrales, L.; Ramirez-Vick, J. E.; Freytes, D. O. Tissue Engineering Strategies for Myocardial Regeneration: Acellular Versus Cellular Scaffolds? *Tissue Eng., Part B* **2016**, *22*, 438.
(442) Doppler, S. A.; Deutsch, M.-A.; Lange, R.; Krane, M. Cardiac Regeneration: Current Therapies-Future Concepts. *J. Thorac. Dis.* **2013**, *5*, 683.
(443) Lin, Z.; Pu, W. T. Strategies for Cardiac Regeneration and Repair. *Sci. Transl. Med.* **2014**, *6*, 239rv1.

https://dx.doi.org/10.1021/acs.chemrev.9b00789
Chem. Rev. 2020, 120, 11032−11092

(444) Prabhakaran, M. P.; Venugopal, J.; Kai, D.; Ramakrishna, S. Biomimetic Material Strategies for Cardiac Tissue Engineering. *Mater. Sci. Eng., C* **2011**, *31*, 503.
(445) Jang, J.; Kim, T. G.; Kim, B. S.; Kim, S. W.; Kwon, S. M.; Cho, D. W. Tailoring Mechanical Properties of Decellularized Extracellular Matrix Bioink by Vitamin B2-Induced Photo-Crosslinking. *Acta Biomater.* **2016**, *33*, 88.
(446) Jang, J.; Park, H. J.; Kim, S. W.; Kim, H.; Park, J. Y.; Na, S. J.; Kim, H. J.; Park, M. N.; Choi, S. H.; Park, S. H.; et al. 3d Printed Complex Tissue Construct Using Stem Cell-Laden Decellularized Extracellular Matrix Bioinks for Cardiac Repair. *Biomaterials* **2017**, *112*, 264.
(447) Gaetani, R.; Doevendans, P. A.; Metz, C. H.; Alblas, J.; Messina, E.; Giacomello, A.; Sluijter, J. P. Cardiac Tissue Engineering Using Tissue Printing Technology and Human Cardiac Progenitor Cells. *Biomaterials* **2012**, *33*, 1782.
(448) Gaetani, R.; Feyen, D. A.; Verhage, V.; Slaats, R.; Messina, E.; Christman, K. L.; Giacomello, A.; Doevendans, P. A.; Sluijter, J. P. Epicardial Application of Cardiac Progenitor Cells in a 3d-Printed Gelatin/Hyaluronic Acid Patch Preserves Cardiac Function after Myocardial Infarction. *Biomaterials* **2015**, *61*, 339.
(449) Gaebel, R.; Ma, N.; Liu, J.; Guan, J.; Koch, L.; Klopsch, C.; Gruene, M.; Toelk, A.; Wang, W.; Mark, P.; et al. Patterning Human Stem Cells and Endothelial Cells with Laser Printing for Cardiac Regeneration. *Biomaterials* **2011**, *32*, 9218.
(450) Bejleri, D.; Streeter, B. W.; Nachlas, A. L. Y.; Brown, M. E.; Gaetani, R.; Christman, K. L.; Davis, M. E. A Bioprinted Cardiac Patch Composed of Cardiac-Specific Extracellular Matrix and Progenitor Cells for Heart Repair. *Adv. Healthcare Mater.* **2018**, *7*, No. e1800672.
(451) Gao, L.; Kupfer, M. E.; Jung, J. P.; Yang, L.; Zhang, P.; Da Sie, Y.; Tran, Q.; Ajeti, V.; Freeman, B. T.; Fast, V. G.; et al. Myocardial Tissue Engineering with Cells Derived from Human-Induced Pluripotent Stem Cells and a Native-Like, High-Resolution, 3-Dimensionally Printed Scaffold. *Circ. Res.* **2017**, *120*, 1318.
(452) Duan, B.; Kapetanovic, E.; Hockaday, L. A.; Butcher, J. T. Three-Dimensional Printed Trileaflet Valve Conduits Using Biological Hydrogels and Human Valve Interstitial Cells. *Acta Biomater.* **2014**, *10*, 1836.
(453) Duan, B.; Hockaday, L. A.; Kang, K. H.; Butcher, J. T. 3d Bioprinting of Heterogeneous Aortic Valve Conduits with Alginate/Gelatin Hydrogels. *J. Biomed. Mater. Res., Part A* **2013**, *101*, 1255.
(454) Hinton, R. B.; Yutzey, K. E. Heart Valve Structure and Function in Development and Disease. *Annu. Rev. Physiol.* **2011**, *73*, 29.
(455) Wang, H.; Leinwand, L. A.; Anseth, K. S. Cardiac Valve Cells and Their Microenvironment–Insights from in Vitro Studies. *Nat. Rev. Cardiol.* **2014**, *11*, 715.
(456) Iung, B.; Vahanian, A. Epidemiology of Valvular Heart Disease in the Adult. *Nat. Rev. Cardiol.* **2011**, *8*, 162.
(457) Mylotte, D.; Andalib, A.; Theriault-Lauzier, P.; Dorfmeister, M.; Girgis, M.; Alharbi, W.; Chetrit, M.; Galatas, C.; Mamane, S.; Sebag, I.; et al. Transcatheter Heart Valve Failure: A Systematic Review. *Eur. Heart J.* **2015**, *36*, 1306.
(458) Gunther, T.; Mazzitelli, D.; Schreiber, C.; Wottke, M.; Paek, S. U.; Meisner, H.; Lange, R. Mitral-Valve Replacement in Children under 6 Years of Age. *Eur. J. Cardiothorac. Surg.* **2000**, *17*, 426.
(459) Cheung, D. Y.; Duan, B.; Butcher, J. T. Current Progress in Tissue Engineering of Heart Valves: Multiscale Problems, Multiscale Solutions. *Expert Opin. Biol. Ther.* **2015**, *15*, 1155.
(460) Huang, N. F.; Serpooshan, V.; Morris, V. B.; Sayed, N.; Pardon, G.; Abilez, O. J.; Nakayama, K. H.; Pruitt, B. L.; Wu, S. M.; Yoon, Y. S.; et al. Big Bottlenecks in Cardiovascular Tissue Engineering. *Commun. Biol.* **2018**, *1*, 199.
(461) Palpant, N. J.; Pabon, L.; Friedman, C. E.; Roberts, M.; Hadland, B.; Zaunbrecher, R. J.; Bernstein, I.; Zheng, Y.; Murry, C. E. Generating High-Purity Cardiac and Endothelial Derivatives from Patterned Mesoderm Using Human Pluripotent Stem Cells. *Nat. Protoc.* **2017**, *12*, 15.
(462) Machiraju, P.; Greenway, S. C. Current Methods for the Maturation of Induced Pluripotent Stem Cell-Derived Cardiomyocytes. *World J. Stem Cells* **2019**, *11*, 33.
(463) Kurts, C.; Panzer, U.; Anders, H. J.; Rees, A. J. The Immune System and Kidney Disease: Basic Concepts and Clinical Implications. *Nat. Rev. Immunol.* **2013**, *13*, 738.
(464) Levey, A. S.; Coresh, J. Chronic Kidney Disease. *Lancet* **2012**, *379*, 165.
(465) Short, K. M.; Smyth, I. M. The Contribution of Branching Morphogenesis to Kidney Development and Disease. *Nat. Rev. Nephrol.* **2016**, *12*, 754.
(466) Schell, C.; Wanner, N.; Huber, T. B. Glomerular Development–Shaping the Multi-Cellular Filtration Unit. *Semin. Cell Dev. Biol.* **2014**, *36*, 39.
(467) Miner, J. H. Renal Basement Membrane Components. *Kidney Int.* **1999**, *56*, 2016.
(468) Nagao, R. J.; Xu, J.; Luo, P.; Xue, J.; Wang, Y.; Kotha, S.; Zeng, W.; Fu, X.; Himmelfarb, J.; Zheng, Y. Decellularized Human Kidney Cortex Hydrogels Enhance Kidney Microvascular Endothelial Cell Maturation and Quiescence. *Tissue Eng., Part A* **2016**, *22*, 1140.
(469) Homan, K. A.; Kolesky, D. B.; Skylar-Scott, M. A.; Herrmann, J.; Obuobi, H.; Moisan, A.; Lewis, J. A. Bioprinting of 3d Convoluted Renal Proximal Tubules on Perfusable Chips. *Sci. Rep.* **2016**, *6*, 34845.
(470) Lin, N. Y. C.; Homan, K. A.; Robinson, S. S.; Kolesky, D. B.; Duarte, N.; Moisan, A.; Lewis, J. A. Renal Reabsorption in 3d Vascularized Proximal Tubule Models. *Proc. Natl. Acad. Sci. U. S. A.* **2019**, *116*, 5399.
(471) Homan, K. A.; Gupta, N.; Kroll, K. T.; Kolesky, D. B.; Skylar-Scott, M.; Miyoshi, T.; Mau, D.; Valerius, M. T.; Ferrante, T.; Bonventre, J. V.; et al. Flow-Enhanced Vascularization and Maturation of Kidney Organoids in Vitro. *Nat. Methods* **2019**, *16*, 255.
(472) King, S. M.; Higgins, J. W.; Nino, C. R.; Smith, T. R.; Paffenroth, E. H.; Fairbairn, C. E.; Docuyanan, A.; Shah, V. D.; Chen, A. E.; Presnell, S. C.; et al. 3d Proximal Tubule Tissues Recapitulate Key Aspects of Renal Physiology to Enable Nephrotoxicity Testing. *Front. Physiol.* **2017**, *8*, 123.
(473) Weber, H. M.; Tsurkan, M. V.; Magno, V.; Freudenberg, U.; Werner, C. Heparin-Based Hydrogels Induce Human Renal Tubulogenesis in Vitro. *Acta Biomater.* **2017**, *57*, 59.
(474) Vainio, S.; Lin, Y. Coordinating Early Kidney Development: Lessons from Gene Targeting. *Nat. Rev. Genet.* **2002**, *3*, 533.
(475) Du, B. J.; Yu, M. X.; Zheng, J. Transport and Interactions of Nanoparticles in the Kidneys. *Nat. Rev. Mater.* **2018**, *3*, 358.
(476) Zhang, K.; Fu, Q.; Yoo, J.; Chen, X.; Chandra, P.; Mo, X.; Song, L.; Atala, A.; Zhao, W. 3d Bioprinting of Urethra with Pcl/Plcl Blend and Dual Autologous Cells in Fibrin Hydrogel: An in Vitro Evaluation of Biomimetic Mechanical Property and Cell Growth Environment. *Acta Biomater.* **2017**, *50*, 154.
(477) Sebinger, D. D.; Ofenbauer, A.; Gruber, P.; Malik, S.; Werner, C. Ecm Modulated Early Kidney Development in Embryonic Organ Culture. *Biomaterials* **2013**, *34*, 6670.
(478) Nguyen, D. L. G.; King, S. M.; Presnell, S. C. U. S., US9481868B2, Espacenet, 2016.
(479) Michalopoulos, G. K. Liver Regeneration. *J. Cell. Physiol.* **2007**, *213*, 286.
(480) Nguyen, D. G.; Funk, J.; Robbins, J. B.; Crogan-Grundy, C.; Presnell, S. C.; Singer, T.; Roth, A. B. Bioprinted 3d Primary Liver Tissues Allow Assessment of Organ-Level Response to Clinical Drug Induced Toxicity in Vitro. *PLoS One* **2016**, *11*, 0158674.
(481) Bhise, N. S; Manoharan, V.; Massa, S.; Tamayol, A.; Ghaderi, M.; Miscuglio, M.; Lang, Q.; Shrike Zhang, Y.; Shin, S. R.; Calzone, G.; Annabi, N.; Shupe, T. D; Bishop, C. E; Atala, A.; Dokmeci, M. R; Khademhosseini, A.; et al. A Liver-on-a-Chip Platform with Bioprinted Hepatic Spheroids. *Biofabrication* **2016**, *8*, 014101.
(482) Jeon, H.; Kang, K.; Park, S. A.; Kim, W. D.; Paik, S. S.; Lee, S. H.; Jeong, J.; Choi, D. Generation of Multilayered 3d Structures of Hepg2 Cells Using a Bio-Printing Technique. *Gut Liver* **2017**, *11*, 121.

https://dx.doi.org/10.1021/acs.chemrev.9b00789
Chem. Rev. 2020, 120, 11032−11092

(483) Lee, H.; Cho, D. W. One-Step Fabrication of an Organ-on-a-Chip with Spatial Heterogeneity Using a 3d Bioprinting Technology. *Lab Chip* **2016**, *16*, 2618.
(484) Faulkner-Jones, A.; Fyfe, C.; Cornelissen, D. J.; Gardner, J.; King, J.; Courtney, A.; Shu, W. Bioprinting of Human Pluripotent Stem Cells and Their Directed Differentiation into Hepatocyte-Like Cells for the Generation of Mini-Livers in 3d. *Biofabrication* **2015**, *7*, 044102.
(485) Adams, D. H.; Eksteen, B. Aberrant Homing of Mucosal T Cells and Extra-Intestinal Manifestations of Inflammatory Bowel Disease. *Nat. Rev. Immunol.* **2006**, *6*, 244.
(486) Skardal, A.; Devarasetty, M.; Kang, H. W.; Mead, I.; Bishop, C.; Shupe, T.; Lee, S. J.; Jackson, J.; Yoo, J.; Soker, S.; et al. A Hydrogel Bioink Toolkit for Mimicking Native Tissue Biochemical and Mechanical Properties in Bioprinted Tissue Constructs. *Acta Biomater.* **2015**, *25*, 24.
(487) Kido, T.; Koui, Y.; Suzuki, K.; Kobayashi, A.; Miura, Y.; Chern, E. Y.; Tanaka, M.; Miyajima, A. Cpm Is a Useful Cell Surface Marker to Isolate Expandable Bi-Potential Liver Progenitor Cells Derived from Human Ips Cells. *Stem Cell Rep.* **2015**, *5*, 508.
(488) Kizawa, H.; Nagao, E.; Shimamura, M.; Zhang, G.; Torii, H. Scaffold-Free 3d Bio-Printed Human Liver Tissue Stably Maintains Metabolic Functions Useful for Drug Discovery. *Biochem. Biophys. Rep.* **2017**, *10*, 186.
(489) Lau, J.; Kawahira, H.; Hebrok, M. Hedgehog Signaling in Pancreas Development and Disease. *Cell. Mol. Life Sci.* **2006**, *63*, 642.
(490) Stafford, D.; Hornbruch, A.; Mueller, P. R.; Prince, V. E. A Conserved Role for Retinoid Signaling in Vertebrate Pancreas Development. *Dev. Genes Evol.* **2004**, *214*, 432.
(491) Gu, G.; Dubauskaite, J.; Melton, D. A. Direct Evidence for the Pancreatic Lineage: Ngn3+ Cells Are Islet Progenitors and Are Distinct from Duct Progenitors. *Development* **2002**, *129*, 2447.
(492) Wilson, M. E.; Scheel, D.; German, M. S. Gene Expression Cascades in Pancreatic Development. *Mech. Dev.* **2003**, *120*, 65.
(493) Sakula, A. Paul Langerhans (1847−1888): A Centenary Tribute. *J. R. Soc. Med.* **1988**, *81*, 414.
(494) Ahlqvist, E.; Storm, P.; Karajamaki, A.; Martinell, M.; Dorkhan, M.; Carlsson, A.; Vikman, P.; Prasad, R. B.; Aly, D. M.; Almgren, P.; et al. Novel Subgroups of Adult-Onset Diabetes and Their Association with Outcomes: A Data-Driven Cluster Analysis of Six Variables. *Lancet Diabetes Endocrinol.* **2018**, *6*, 361.
(495) Hering, B. J.; Clarke, W. R.; Bridges, N. D.; Eggerman, T. L.; Alejandro, R.; Bellin, M. D.; Chaloner, K.; Czarniecki, C. W.; Goldstein, J. S.; Hunsicker, L. G.; et al. Phase 3 Trial of Transplantation of Human Islets in Type 1 Diabetes Complicated by Severe Hypoglycemia. *Diabetes Care* **2016**, *39*, 1230.
(496) Shapiro, A. M.; Ricordi, C.; Hering, B. J.; Auchincloss, H.; Lindblad, R.; Robertson, R. P.; Secchi, A.; Brendel, M. D.; Berney, T.; Brennan, D. C.; et al. International Trial of the Edmonton Protocol for Islet Transplantation. *N. Engl. J. Med.* **2006**, *355*, 1318.
(497) Ravnic, D. J.; Leberfinger, A. N.; Ozbolat, I. T. Bioprinting and Cellular Therapies for Type 1 Diabetes. *Trends Biotechnol.* **2017**, *35*, 1025.
(498) Marchioli, G.; van Gurp, L.; van Krieken, P. P.; Stamatialis, D.; Engelse, M.; van Blitterswijk, C. A.; Karperien, M. B.; de Koning, E.; Alblas, J.; Moroni, L.; et al. Fabrication of Three-Dimensional Bioplotted Hydrogel Scaffolds for Islets of Langerhans Transplantation. *Biofabrication* **2015**, *7*, 025009.
(499) Ellis, C.; Ramzy, A.; Kieffer, T. J. Regenerative Medicine and Cell-Based Approaches to Restore Pancreatic Function. *Nat. Rev. Gastroenterol. Hepatol.* **2017**, *14*, 612.
(500) Duin, S.; Schutz, K.; Ahlfeld, T.; Lehmann, S.; Lode, A.; Ludwig, B.; Gelinsky, M. 3d Bioprinting of Functional Islets of Langerhans in an Alginate/Methylcellulose Hydrogel Blend. *Adv. Healthcare Mater.* **2019**, *8*, No. e1801631.
(501) Schutz, K.; Placht, A. M.; Paul, B.; Bruggemeier, S.; Gelinsky, M.; Lode, A. Three-Dimensional Plotting of a Cell-Laden Alginate/Methylcellulose Blend: Towards Biofabrication of Tissue Engineering Constructs with Clinically Relevant Dimensions. *J. Tissue Eng. Regener. Med.* **2017**, *11*, 1574.
(502) Liu, X.; Carter, S. D.; Renes, M. J.; Kim, J.; Rojas-Canales, D. M.; Penko, D.; Angus, C.; Beirne, S.; Drogemuller, C. J.; Yue, Z.; et al. Development of a Coaxial 3d Printing Platform for Biofabrication of Implantable Islet-Containing Constructs. *Adv. Healthcare Mater.* **2019**, *8*, No. e1801181.
(503) Sears, R.; Allen-Petersen, B.; Langer, E., U.S., US20160040132A1, Espacenet, 2016.
(504) Kroon, E.; Martinson, L. A.; Kadoya, K.; Bang, A. G.; Kelly, O. G.; Eliazer, S.; Young, H.; Richardson, M.; Smart, N. G.; Cunningham, J.; et al. Pancreatic Endoderm Derived from Human Embryonic Stem Cells Generates Glucose-Responsive Insulin-Secreting Cells in Vivo. *Nat. Biotechnol.* **2008**, *26*, 443.
(505) Alipio, Z.; Liao, W.; Roemer, E. J.; Waner, M.; Fink, L. M.; Ward, D. C.; Ma, Y. Reversal of Hyperglycemia in Diabetic Mouse Models Using Induced-Pluripotent Stem (Ips)-Derived Pancreatic Beta-Like Cells. *Proc. Natl. Acad. Sci. U. S. A.* **2010**, *107*, 13426.
(506) Huang, S.; Yao, B.; Xie, J.; Fu, X. 3d Bioprinted Extracellular Matrix Mimics Facilitate Directed Differentiation of Epithelial Progenitors for Sweat Gland Regeneration. *Acta Biomater.* **2016**, *32*, 170.
(507) Liu, N.; Huang, S.; Yao, B.; Xie, J.; Wu, X.; Fu, X. 3d Bioprinting Matrices with Controlled Pore Structure and Release Function Guide in Vitro Self-Organization of Sweat Gland. *Sci. Rep.* **2016**, *6*, 34410.
(508) Adine, C.; Ng, K. K.; Rungarunlert, S.; Souza, G. R.; Ferreira, J. N. Engineering Innervated Secretory Epithelial Organoids by Magnetic Three-Dimensional Bioprinting for Stimulating Epithelial Growth in Salivary Glands. *Biomaterials* **2018**, *180*, 52.
(509) Bulanova, E. A.; Koudan, E. V.; Degosserie, J.; Heymans, C.; Pereira, F. D.; Parfenov, V. A.; Sun, Y.; Wang, Q.; Akhmedova, S. A.; Sviridova, I. K.; et al. Bioprinting of a Functional Vascularized Mouse Thyroid Gland Construct. *Biofabrication* **2017**, *9*, 034105.
(510) Wu, Z.; Su, X.; Xu, Y.; Kong, B.; Sun, W.; Mi, S. Bioprinting Three-Dimensional Cell-Laden Tissue Constructs with Controllable Degradation. *Sci. Rep.* **2016**, *6*, 24474.
(511) Isaacson, A.; Swioklo, S.; Connon, C. J. 3d Bioprinting of a Corneal Stroma Equivalent. *Exp. Eye Res.* **2018**, *173*, 188.
(512) Shi, P.; Tan, Y. S. E.; Yeong, W. Y.; Li, H. Y.; Laude, A. A Bilayer Photoreceptor-Retinal Tissue Model with Gradient Cell Density Design: A Study of Microvalve-Based Bioprinting. *J. Tissue Eng. Regener. Med.* **2018**, *12*, 1297.
(513) Garcia-Lizarribar, A.; Fernandez-Garibay, X.; Velasco-Mallorqui, F.; Castano, A. G.; Samitier, J.; Ramon-Azcon, J. Composite Biomaterials as Long-Lasting Scaffolds for 3d Bioprinting of Highly Aligned Muscle Tissue. *Macromol. Biosci.* **2018**, *18*, No. e1800167.
(514) Mozetic, P.; Giannitelli, S. M.; Gori, M.; Trombetta, M.; Rainer, A. Engineering Muscle Cell Alignment through 3d Bioprinting. *J. Biomed. Mater. Res., Part A* **2017**, *105*, 2582.
(515) Yeo, M.; Lee, H.; Kim, G. H. Combining a Micro/Nano-Hierarchical Scaffold with Cell-Printing of Myoblasts Induces Cell Alignment and Differentiation Favorable to Skeletal Muscle Tissue Regeneration. *Biofabrication* **2016**, *8*, 035021.
(516) Kim, J. H.; Seol, Y. J.; Ko, I. K.; Kang, H. W.; Lee, Y. K.; Yoo, J. J.; Atala, A.; Lee, S. J. 3d Bioprinted Human Skeletal Muscle Constructs for Muscle Function Restoration. *Sci. Rep.* **2018**, *8*, 12307.
(517) Laternser, S.; Keller, H.; Leupin, O.; Rausch, M.; Graf-Hausner, U.; Rimann, M. A Novel Microplate 3d Bioprinting Platform for the Engineering of Muscle and Tendon Tissues. *SLAS Technol.* **2018**, *23*, 599.
(518) Laronda, M. M.; Rutz, A. L.; Xiao, S.; Whelan, K. A.; Duncan, F. E.; Roth, E. W.; Woodruff, T. K.; Shah, R. N. A Bioprosthetic Ovary Created Using 3d Printed Microporous Scaffolds Restores Ovarian Function in Sterilized Mice. *Nat. Commun.* **2017**, *8*, 15261.
(519) Rutz, A. L.; Hyland, K. E.; Jakus, A. E.; Burghardt, W. R.; Shah, R. N. A Multimaterial Bioink Method for 3d Printing Tunable, Cell-Compatible Hydrogels. *Adv. Mater.* **2015**, *27*, 1607.
(520) Gjorevski, N.; Sachs, N.; Manfrin, A.; Giger, S.; Bragina, M. E.; Ordonez-Moran, P.; Clevers, H.; Lutolf, M. P. Designer Matrices for Intestinal Stem Cell and Organoid Culture. *Nature* **2016**, *539*, 560.

https://dx.doi.org/10.1021/acs.chemrev.9b00789
Chem. Rev. 2020, 120, 11032−11092

(521) Vrij, E. J.; Espinoza, S.; Heilig, M.; Kolew, A.; Schneider, M.; van Blitterswijk, C. A.; Truckenmuller, R. K.; Rivron, N. C. 3d High Throughput Screening and Profiling of Embryoid Bodies in Thermoformed Microwell Plates. *Lab Chip* **2016**, *16*, 734.
(522) Vrij, E.; Rouwkema, J.; LaPointe, V.; van Blitterswijk, C.; Truckenmuller, R.; Rivron, N. Directed Assembly and Development of Material-Free Tissues with Complex Architectures. *Adv. Mater.* **2016**, *28*, 4032.
(523) Jung, J. P.; Bhuiyan, D. B.; Ogle, B. M. Solid Organ Fabrication: Comparison of Decellularization to 3d Bioprinting. *Biomater. Res.* **2016**, *20*, 27.
(524) Simoes, I. N.; Vale, P.; Soker, S.; Atala, A.; Keller, D.; Noiva, R.; Carvalho, S.; Peleteiro, C.; Cabral, J. M. S.; Eberli, D.; da Silva, C. L.; Baptista, P. M.; et al. Acellular Urethra Bioscaffold: Decellularization of Whole Urethras for Tissue Engineering Applications. *Sci. Rep.* **2017**, *7*, 41934.
(525) Abolbashari, M.; Agcaoili, S. M.; Lee, M. K.; Ko, I. K.; Aboushwareb, T.; Jackson, J. D.; Yoo, J. J.; Atala, A. Repopulation of Porcine Kidney Scaffold Using Porcine Primary Renal Cells. *Acta Biomater.* **2016**, *29*, 52.
(526) Hubbell, J. A.; Thomas, S. N.; Swartz, M. A. Materials Engineering for Immunomodulation. *Nature* **2009**, *462*, 449.
(527) Chan, G.; Mooney, D. J. New Materials for Tissue Engineering: Towards Greater Control over the Biological Response. *Trends Biotechnol.* **2008**, *26*, 382.

https://dx.doi.org/10.1021/acs.chemrev.9b00789
Chem. Rev. 2020, 120, 11032−11092